MOLECULAR MECHANISMS OF ALLOSTERIC MODULATION OF NICOTINIC
ACETYLCHOLINE RECEPTORS

Sean Christopher Barron

A dissertation submitted to the faculty of the University of North Carolina at Chapel
Hill in partial fulfillment of the requirements for the degree of Doctor of Philosophy in
the Curriculum of Neurobiology.

Chapel Hill
2010

Approved by:

Robert L. Rosenberg, Ph.D. (Advisor)

Paul B. Manis, Ph.D. (Chair)

Jerrel L. Yakel, Ph.D.

T. Kendall Harden, Ph.D.

Ken D. McCarthy, Ph.D.

ABSTRACT

Sean Christopher Barron: Molecular Mechanisms of Allosteric Modulation of
Nicotinic Acetylcholine Receptors
(under the direction of Dr. Robert L. Rosenberg)

Nicotinic acetylcholine receptors (nAChR) are part of the Cys-loop family of ligand-gated ion channels, and are implicated in a wide variety of neurological disorders such as nicotine addiction, schizophrenia, and cognitive dysfunction. Therefore, they represent a critical molecular target for drug development and targeted therapeutic intervention. Positive allosteric modulators (PAMs) of ligand-gated ion channels have a unique therapeutic potential because they enhance synaptic transmission without disrupting the endogenous timing mechanisms. This research focused on the neuronal α7 nicotinic receptor because they are located both pre- and postsynaptically and can modulate glutamatergic and dopaminergic release in the brain regions involved in drug-seeking behaviors. Understanding the molecular mechanisms by which allosteric modulators enhance activation of neuronal nicotinic acetylcholine receptors is therefore critically important to the development of new drugs for research and therapeutics.

Experiments with the Substituted Cysteine Accessibility Method indicate that two chemically different positive allosteric modulators, PNU-120596 and permeable divalent cations, cause structural transitions (or changes in local electrostatic potential) in the extracellular ligand binding domain of the α7 nicotinic receptor that

are similar but not identical to those caused by the agonist, acetylcholine. These results suggest that positive allosteric modulators share a conserved mechanism to enhance receptor gating that is unrelated to the chemical structure of the molecule.

As an additional approach to study gating of the nicotinic receptors, I developed homology models derived from the structures of bacterial Cys-loop receptors in the closed and open states. A comparison of electrophysiological MTSEA modification data against *in silico* calculations of solvent accessibility and electrostatic potential showed that electrostatic potential in the extracellular ligand-binding domain of the α7 nAChR is a better predictor of receptor gating from the closed to open states.

Overall, this body of work has shown that positive allosteric modulators and agonists of the α7 nAChR induce similar conformational changes in the extracellular-ligand binding domain of the receptor by reducing the large electronegative potential energy along the ion-permeation pathway. A unifying model of receptor gating (electrostatic compensation) and future experiments designed to test this model are discussed.

This body of work is dedicated to my wife, Andréa Michelle Barron, for her constant love, support, and patience. To my grandfather, Samuel (Harry) Kasinowitz, who taught me that an education is not fancy titles and degrees but what you choose to do with it. Finally, to my two cats, Garfield and Swee'pea, who have provided company, entertainment, and relaxation while writing my dissertation.

ACKNOWLEDGEMENTS

TABLE OF CONTENTS

LIST OF TABLES

LIST OF FIGURES

LIST OF ABBREVIATIONS

5-HT$_{2C}$R	Serotonin Receptor, type 2C
5-HT$_3$R	Serotonin Receptor, type 3
α-Bgtx	α-Bungarotoxin
ACh	acetylcholine
AChBP	acetylcholine Binding Protein
ADHD	Attention-deficit hyperactivity disorder
AMF	Anamolous Mole Fraction
ASD	Autism Spectrum Disorders
Ba^{2+}	Barium Ion
C^x	x-Carbon (where x = α, β, γ, etc.)
Ca^{2+}	Calcium Ion
Cl$^-$	Chloride Ion
CCh	Carbamylcholine
CNS	Central Nervous System
cryo-EM	Cryo-electron Microscopy
DMSO	Dimethyl Sulfoxide
DTNB	5,5'-dithiobis-(2-nitrobenzoic acid); Ellman's Reagent
EC$_{50}$	Half Maximal Excitatory Concentration
ELIC	*Erwinia chrysanthemi* ligand-gated ion channel
EtOH	Ethanol
GABA$_A$R	γ-Aminobutyric Acid Receptor, type A
GLIC	*Gloeobacter violaceus* ligand-gated ion channel

GlyR	Glycine Receptor
GPCR	G-protein coupled receptor
IC_{50}	Half Maximal Inhibitory Concentration
ICD	Intracellular Domain
Imax	Peak Current Amplitude
K^+	Potassium Ion
K_{eq}	Equilibrium Rate Constant
K_i	Equilibrium Dissociation Constant
β	Rate of channel opening
α	Rate of channel closing
K_v	Voltage-gated Potassium Channel
LBD	Extracellular Ligand Binding Domain
Mg^{2+}	Magnesium Ion
MMTS	Methyl Methanethiosulfonate
M_r	Molecular Weight
MTS	Methanethiosulfonate
MTSBn	Benzyl Methanethiosulfonate
MTSCE	2-Carboxyethyl Methanethiosulfonate
MTSEA	2-Aminoethyl Methanethiosulfonate
MTSEA-biotin	N-Biotinylaminoethyl Methanethiosulfonate
MTSES	2-Sulfonatoethyl Methanethiosulfonate
MWC	Monod, Wymann and Changeux (model of allosteric transitions)

Na$^+$	Sodium Ion
nAChR	Nicotinic acetylcholine Receptor
NS 1738	N-(5-Chloro-2-hydroxyphenyl)-N'-[2-chloro-5 (trifluoromethyl)phenyl]urea
PAM(s)	Positive Allosteric Modulator(s)
PCP	Phencyclidine
PNU-120596	N-(5-Chloro-2,4-dimethoxyphenyl)-N'- (5-methyl-3-isoxazolyl)-urea
REFER	Rate-Equilibrium Free Energy Relationships
RIC-3	Resistant to Inhibitors of Cholinesterase
RMSD	Root Mean Squared Deviation
SCAM	Substituted cysteine Accessibility Method
TMD	Transmembrane Domain
TNF	Tumor Necrosis Factor
TZ	Transition Zone
VTA	Ventral Tegmental Area

CHAPTER 1

INTRODUCTION

Nicotinic acetylcholine receptors are the prototypical member of the Cys-loop family of ligand-gated ion channels, which also includes GABA$_A$, serotonin type 3 (5-HT$_3$), and glycine receptors. These ligands bind to their respective ionotropic receptor, inducing a conformational change in the receptor that allows for ion permeation through the channel. Seventeen genes encoding for different nAChR subunits have been identified and classified into the alpha subfamily (α1-α10), beta subfamily (β1-β4), and muscle-specific (γ, δ, ε) subfamily [Gotti et al. 2007]. As a family, the nAChRs share a conserved molecular architecture with other Cys-loop ionotropic receptors and assemble as heteromeric or homomeric pentamers around a central pore within the plasma membrane [Raftery et al. 1980; Anand et al. 1991].

In vertebrates, nAChRs are cation-selective channels (Na$^+$/K$^+$) with variation in Ca^{2+} permeability among different subtypes. Nicotinic acetylcholine receptors have a complex stoichiometry of assembly that influences the pharmacology and biophysical properties of the assembled receptors, and they are divided into three broad categories. **Alpha-bungarotoxin-sensitive (α-Bgtx) nAChRs** consist of homomeric α7 receptors and α8, α9, and α10-containing receptors. The α7 receptors have nanomolar affinity for the competitive inhibitor α-Bgtx, micromolar affinity for nicotine, rapidly desensitize, and are highly permeable to Ca^{2+} [Couturier *et al.* 1990; Mulle *et al.* 1992]. **Muscle nAChRs** consist of (α1)$_2$β1δγ/ε subunits, have low but significant permeability to calcium, and bind irreversibly to α-Bgtx [Leprince et al. 1981; Vernino et al. 1994]. **Non-α-Bgtx nAChRs** consist of any combination of the other heteromeric, neuronal nAChRs (α2-α6, β2-β4). These receptors do not bind α-Bgtx, have nanomolar affinity for nicotine, slowly desensitize,

and are relatively impermeable to Ca^{2+} [Vernino *et al.* 1992; Fucile 2004; Gotti and Clementi 2004]. All nAChRs show strong inward rectification at positive membrane potentials due to intracellular block of the receptor by Mg^{2+} [Ifune and Steinbach 1990; Ifune and Steinbach 1991; Briggs *et al.* 1995; Wu *et al.* 2006].

nAChR pharmacology

The pharmacological properties of the nicotinic acetylcholine receptors have been extensively characterized, due to the large variety of agonists, competitive and non-competitive antagonists that occur naturally. Historically, the classification of receptor subtype was determined by pharmacology before the individual genes were identified and cloned.

The history of acetylcholine and its significance in neurotransmission dates back to the past century. Sir Henry Dale isolated and determined the structure of acetylcholine in the early 1900's. By the early 1920's, Otto Loewi had discovered that acetylcholine and epinephrine acted as chemical messengers of the nervous system, which we now define as a "neurotransmitter." Both compounds were found to be secreted from the vagus nerve after electrical stimulation, and Dale and Loewi shared the Nobel Prize in Physiology or Medicine for their pioneering work. Additionally, Sir Henry Dale first determined the two classes of acetylcholine receptors, based on the differential response of cells to nicotine and muscarine [Dale 1914; Dale 1954]. We now know that nicotinic acetylcholine receptors are ligand-gated ion channels that mediate fast neurotransmission, while muscarinic acetylcholine receptors mediate slow neurotransmission via G-protein coupled

receptors [Daly 2005]. This body of work focuses on the nicotinic acetylcholine receptors.

Pyridine alkaloid agonists, such as *(-)*-nicotine, *(-)*-nornicotine, and anabasine (**Figure 1.1**), are found in the leaves of tobacco plants (genus *Nicotinana*) and are presumed to act as herbivore deterrents at non-toxic doses [Metcalf 1992; Glendinning and Gonzalez 1995]. Analogously, the potent agonist epibatidine and a wide variety of alkaloid non-competitive antagonists are secreted on the skin of phantasmal poison frog (*Epipedobates tricolor)* as a predatory deterrent [Daly 1995; Daly 2005]. The potent competitive antagonist, (+)-tubocurarine, is the main component of the poison curare used by South American tribes to paralyze the respiratory muscles of prey [Wintersteiner and Dutcher 1943]. Finally, predatory animals utilize nicotinic receptor peptide antagonists as paralytics, such as α-bungarotoxin from the Taiwanese Banded Krait (*Bungarus multicinctus*) or the α-conotoxins from the marine cone snails (genus *Conus)* [Nicke et al. 2004; Chu 2005].

Agonists and Partial Agonists

Acetylcholine
29/520/2200

(α4β2/α3β4/α7)

Carbamylcholine
61/1300/22000

(-)-Nicotine
1.0/73/1600

(-)-Nornicotine
26/610/>10000

Anabasine
65/35/58

Epibatidine
0.058/0.51/21

(-)-Cytisine*
0.12/54/160

Varenicline* (EC$_{50}$, %Efficacy)
[Mihalak et al. 2006]
2.3μM,13% = α4β2
55μM,75% = α3β4
18μM,93% = α7

ABT-248 [Arneric et al. 1994]
α4β2 >> α7 = α1β1$\gamma$$\delta$

GTS-21
α7 selective

Competitive Antagonists

Dihydro-β-Erythroidine
35/50/9000

Morphine [Lioudyno et al. 2000]
α9α10 selective

(+)-Tubocurarine
α1$_{(2)}$$\beta$1$\gamma$$\delta$ selective

Methyllycaconitine
1300/1600/1.0

Non-competitive Antagonists

Cocaine (IC$_{50}$)
-/15μM/6μM/-
(α4β2/α3β4/α7/α1$_{(2)}$$\beta$1$\gamma$$\delta$)

Serotonin (IC$_{50}$) [Arias 1998]
269μM/-/40μM/57μM

Figure 1.1: Agonists and antagonists of the nAChR. Unless otherwise stated, the numbers underneath each compound are the equilibrium dissociation constant (K_i, in nM) and are from [Daly 2005]. Only the physiologically relevant enantiomers are shown where applicable, and K_i values are reported in the same order: α4β2/α3β4/α7/α1$_{(2)}$$\beta$1$\gamma$$\delta$. A smaller value corresponds to a higher binding affinity and higher specificity for that nAChR isoform with the exception of GTS-21, which has a higher affinity for α4β2* but the primary effect is full agonism of α7 receptors. Relative selectivity is shown for ABT-418. "*" denotes partial agonism is the primary effect for those compounds (cytisine and varenicline at α4β2* receptors), and "–" denotes no measurable binding or effect at that nAChR isoform. All compounds occur naturally except varenicline, ABT-418, and GTS-21.

5

The naturally occurring, small molecule drugs that target nicotinic

acetylcholine receptors have served as templates for structure-activity relationships,

in order to discover subunit-selective compounds (α7 vs. α4β2*, etc.)[1] for research

and clinical applications (**Figure 1.1**). It is important to note that selectivity of an

agonist, antagonist, or allosteric modulator can be defined in multiple ways including

binding affinity (K_i) or potency (EC_{50}/IC_{50}) using *in vitro* electrophysiological or

calcium flux assays. An extensive review of the important natural compounds and

their synthetic derivatives can be found elsewhere using K_i as a basis for

comparison [Daly 2005].   From the structures and binding affinities of these

compounds, we observe that the α4β2* receptors generally have a higher affinity

and selectivity for agonists than both the α7 and $α1_{(2)}β1γδ$ isoforms. Nicotine,

cytisine, morphine, and anabasine have served as important structural templates for

the development of selective agonists of the α4β2* and α7 receptors. ABT-418

(α4β2* agonist) and GTS-21 (α7 agonist) are representative compounds from this

group. GTS-21 is unique because it acts as a competitive antagonist at α4β2*

isoforms, but is a full agonist at the α7 isoform [Briggs *et al.* 1995; de Fiebre *et al.*

1995; Briggs *et al.* 1997]. Therefore, this anabaseine derivative may serve as a

useful template for additional α7-selective agonists. The most successful compound

of this group is varenicline (Chantix[©]), which a partial agonist of $α_4β_2$* receptors and

full agonist of the α7 receptors and is FDA-approved for smoking cessation [Mihalak

et al. 2006]. Selective competitive antagonists, such as dihydro-β-erythoidine

---

[1] For heteromeric nicotinic receptors, an asterisk is used refer to all possible subunit combinations and is a standard naming convention [Gotti *et al.* 2009]. For example, α4β2 nicotinic receptors can exist as either low affinity $\{(α4)_3(β2)_2\}$or high affinity $\{(α4)_2(β2)_3\}$ for nicotine and acetycholine [Zwart and Vijverberg 1998; Nelson *et al.* 2003].

(α4β2*) and methyllycaconitine (α7), are important tools to determine agonist-selectivity between neuronal nicotinic receptors.

The development of positive allosteric modulators for the nicotinic receptors has been based on a variety of chemical templates (**Figure 1.2**). Ivermectin was the first generation positive allosteric modulator of the homomeric α7 receptor [Krause et al. 1998], and is characterized as a macrocyclic lactone and an anti-parasitic compound that activates invertebrate glutamate-gated chloride channels [McCavera et al. 2007]. Ivermectin is also an allosteric modulator of the P2X4 receptor [Khakh et al. 1999], and an agonist of γ2-GABA$_A$ receptors [Adelsberger et al. 2000; Dawson et al. 2000]. Other important, but less selective modulators of the α7 receptor include 5-hydroxyindole and genistein [Bertrand and Gopalakrishnan 2007]. The first breakthrough came with the discovery of PNU-120596 as the first selective α7 receptor positive allosteric modulator. This compound was developed from a urea/carbamide chemical library and exerts dramatic effects on macroscopic desensitization [Hurst et al. 2005; Piotrowski DW 2005]. Positive allosteric modulators that slow macroscopic kinetics and receptor desensitization are classified as type II [Gronlien et al. 2007]. In contrast, NS 1738 is also derived from a urea/carbamide library but does not exert any effect on macroscopic kinetics [Timmermann et al. 2007]. These modulators are classified as type I [Gronlien et al. 2007]. Chemotypes that have been associated with GABA$_A$R modulators and 5-HT$_{2C}$R antagonists have been shown to enhance function of the α7 nicotinic receptor [Ng et al. 2007; Dunlop et al. 2008]. Finally, while most of the existing positive allosteric modulators are selective for homomeric α7 receptors, indolic alkaloids

have recently described as a chemotype selective for α4β2* receptors [Kim et al. 2007].
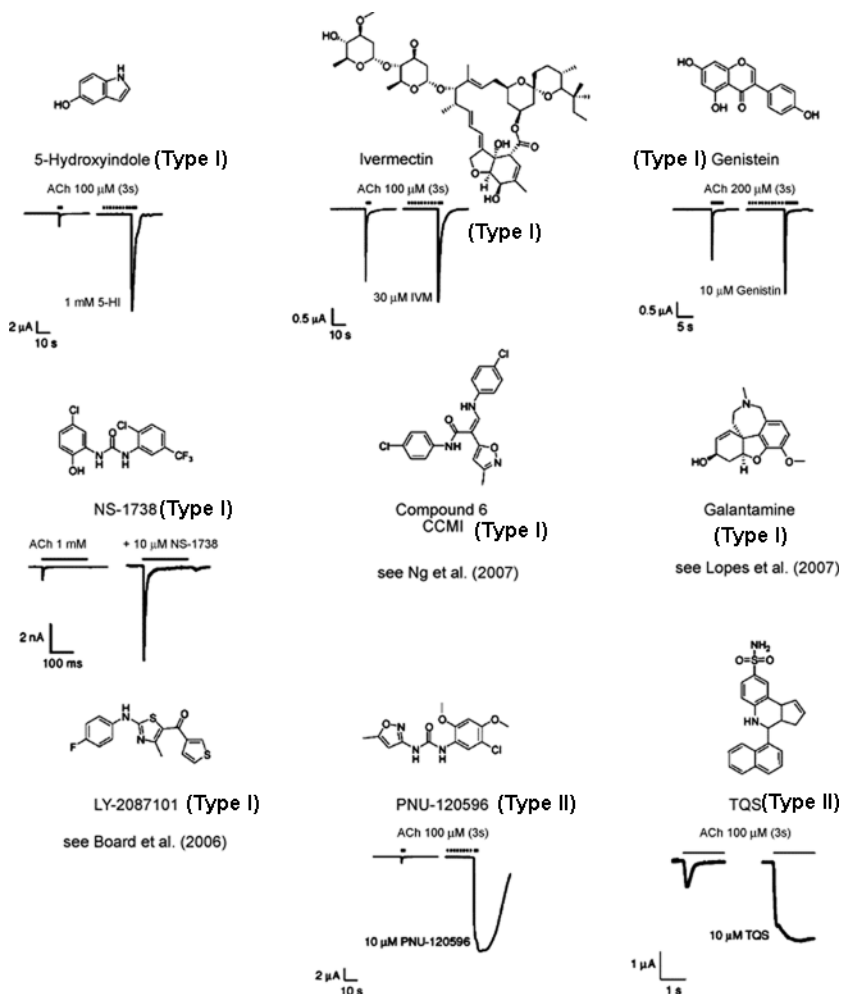
Figure 1.2: Allosteric Modulators of the α7 nicotinic receptor.
Structures and differential profiles of PAMs at the α7 nAChR. Structures of prototypical positive allosteric modulators of nAChRs and their effects at α7 nAChRs measured in *Xenopus* oocytes or in a cell lines. Note the difference in time course of the agonist-evoked currents observed following exposure to type I or type II modulators. Data for NS-1738 and TQS adapted from [Timmermann *et al.* 2007]and [Gronlien *et al.* 2007] respectively. For details of allosteric modulator profiles of compound **6**, galantamine and LY-2087101, please see cited references. Figure and text adapted from [Bertrand and Gopalakrishnan 2007].

Cholinergic neurotransmission

The development of selective compounds and existence of natural compounds that target the nicotinic receptors has been critical elucidating the mechanisms of nicotinic cholinergic neurotransmission. In particular, the peripheral nervous system and neuromuscular junction have been important models to study the basic properties of fast synaptic neurotransmission. Pioneering work by Hodgkin and Huxley utilized the giant squid axon and determined that Na_V and K_V channels underlie action potentials [Hodgkin and Huxley 1952d; Hodgkin and Huxley 1952c; Hodgkin and Huxley 1952b; Hodgkin and Huxley 1952a; Hodgkin *et al.* 1952]. Shortly thereafter, Del Castillo and Katz utilized the neuromuscular junction and characterized the quantal nature of neurotransmitter release [Del Castillo and Katz 1954].

Neuronal nAChRs (α2-α10 and β2-β4) are diffusely expressed throughout most of the central nervous system (CNS), with α4β2* and α7 receptors showing the highest levels of expression in experiments of radioligand binding to brain slices [Orr-Urtreger et al. 1997; Perry et al. 2002; Gotti and Clementi 2004]. In the peripheral nervous system, α3β4-containing and α7 receptors predominate in autonomic ganglion cells and $(α1)_2β1δγ/ε$ receptors are expressed exclusively at the neuromuscular junction.

In the CNS, the cholinergic system has a unique architecture compared to the excitatory glutamatergic neurotransmission of the somato-cortical system. The somatosensory system is characterized by a columnar/modular organization and

bidirectional flow of information between the sensory cortices (feedforward), higher cognitive processing centers (feedback), and motor output regions along dedicated circuits [Gilbert and Sigman 2007]. In contrast, the cholinergic neurons show a large amount of interconnection at distal dendrites, receive sparse inputs that sample every cortical area, and form reentrant circuits between different brain regins [Woolf 1991]. This diffuse yet interconnected architecture allows the cholinergic system to sample the internal state of the brain, and modulate both feedback and feedforward processes to effect behavior and cognition. The complex spatiotemporal integration of sensory information depends on the internal state of the system, which can be behaviorally defined as "attention." At the molecular level, the internal state depends on the combination and strength of excitatory and inhibitory input any individual neuron receives over time [Buonomano and Maass 2009].

While cholinergic neurons regulate the sensory-cortical network, nicotinic receptors are expressed on cholinergic and non-cholinergic terminals and can directly modulate other neurotransmitter systems [Dani 2001]. For example, nicotinic receptors have been shown to modulate glutamate, GABA and norepinephrine release in the hippocampus, and glutamate release in the medial habenula [Radcliffe et al. 1999; Girod and Role 2001; Azam and McIntosh 2006]. Many other drugs of abuse including ethanol, cocaine, and PCP antagonize multiple nAChR subtypes [Arias 1998; Dopico and Lovinger 2009]. Nicotinic AChRs also affect cocaine-induced dopamine release in the ventral tegmental area (VTA). The VTA projects to the nucleus accumbens that ultimately leads to motor output, and so nAChRs can modulate the pathways that are important in drug addiction and drug-

seeking behavior [Zanetti et al. 2007]. The α4β2* and α7 subtypes are implicated in a wide variety of neurological diseases such as nicotine addiction, schizophrenia, autism spectrum disorders, ADHD, Parkinson's disease, epilepsy, depression, and anxiety disorders. [Fryer and Lukas 1999a; Fryer and Lukas 1999b; Rezvani and Levin 2001; Gotti and Clementi 2004; Hajos *et al.* 2005; Rabenstein *et al.* 2006; Mineur and Picciotto 2008]. The α7 receptor is also required to inhibit TNF release from macrophages, indicating its importance in non-neuronal systems as well [Wang et al. 2003].

The interconnectivity of the cholinergic system with multiple brain regions combined with the broad expression of multiple nAChR subtypes provides a framework for understanding the role of the cholinergic system in neurological diseases and the promise of nicotinic receptor compounds as a therapeutic option for treatment. In order to understand how different nAChR subtypes contribute to disease states, it is critical to understand the molecular mechanisms by which these receptors couple the binding of agonists and positive allosteric modulators to opening of the channel.

Structural models of nAChRs

Most of our working knowledge of the agonist-binding site of the Cys-loop receptor family comes from the work Brejc et al. [Brejc et al. 2001] and Hansen et al. [Hansen et al. 2005], who have solved the crystal structure of the Acetylcholine Binding Protein from *Lymnaea stagnalis and Aplysia californica*, respectively. The AChBP is a glial protein that is unique to several species of mollusks and other

invertebrates, and is secreted into the synaptic cleft to bind acetylcholine and sequester it away from the post-synaptic receptors [Smit et al. 2001]. These high-resolution structures of AChBPs have been used to model the ligand-binding domain of the nAChRs because they provide a structural rationalization for decades of biochemical and binding studies. For example, the structure shows well-defined agonist binding sites that are lined by the residues previously shown to be essential for ligand binding. It also explains the requirement for at least two subunits because the binding sites are formed at the interfaces between subunits [Sine and Engel 2006]. With this high-resolution structure, Unwin has refined his cryo-EM images of the *Torpedo marmorata* muscle-type nAChR down to a 4Å resolution to provide the first structural model of a full-length nAChR [Brejc et al. 2001; Unwin 2005]. More recently, high resolution and full-length *de novo* structures have been solved of bacterial Cys-loop receptors in the closed and open states [Chen 2009].

There are four major structural regions of the Cys-loop receptor family: the extracellular ligand-binding domain (LBD), the transition zone (TZ), the transmembrane domain (TMD), and the intracellular domain (ICD) **(Figure 1.3)** [Brejc et al. 2001; Unwin 2005]. In the LBD, the major structural feature consists of two arrays of β-sheets oriented in a β-sandwich. The agonist-binding site exists at the interface between two subunits in a pocket of aromatic and hydrophobic residues. The agonist binding site contains a C-loop that defines the principal subunit of the interface and moves to cover the bound agonist, acting as a cap or cover or the agonist-binding site. At the agonist-binding site, the C-loop is always part of an α subunit in full-length receptors. [Celie et al. 2005; Gao et al. 2005;

Hansen et al. 2005]. The C-loop of nicotinic receptors also contains aromatic residues and two cysteine residues that are important for agonist binding. The other subunit that contributes to agonist binding is called the complimentary subunit, and can be either an α or non-α (β, γ/ε, δ) subunit. The TMD consists of four α-helices; the M2 helix lines the pore of the channel [Oblatt-Montal et al. 1993; Akabas et al. 1994; Unwin 2005], and the other helices (M1, M3, and M4) come into contact with the plasma membrane [Barrantes 2002]. The TZ is composed of loops from the LBD and the TMD that serve to link these structurally different regions. Finally, the ICD is a partial α-helical structure linking the M3 and M4 helices. The ICD is involved in receptor trafficking, insertion, and single-channel conductance [Williams et al. 1998; Kelley et al. 2003; Xu et al. 2006].
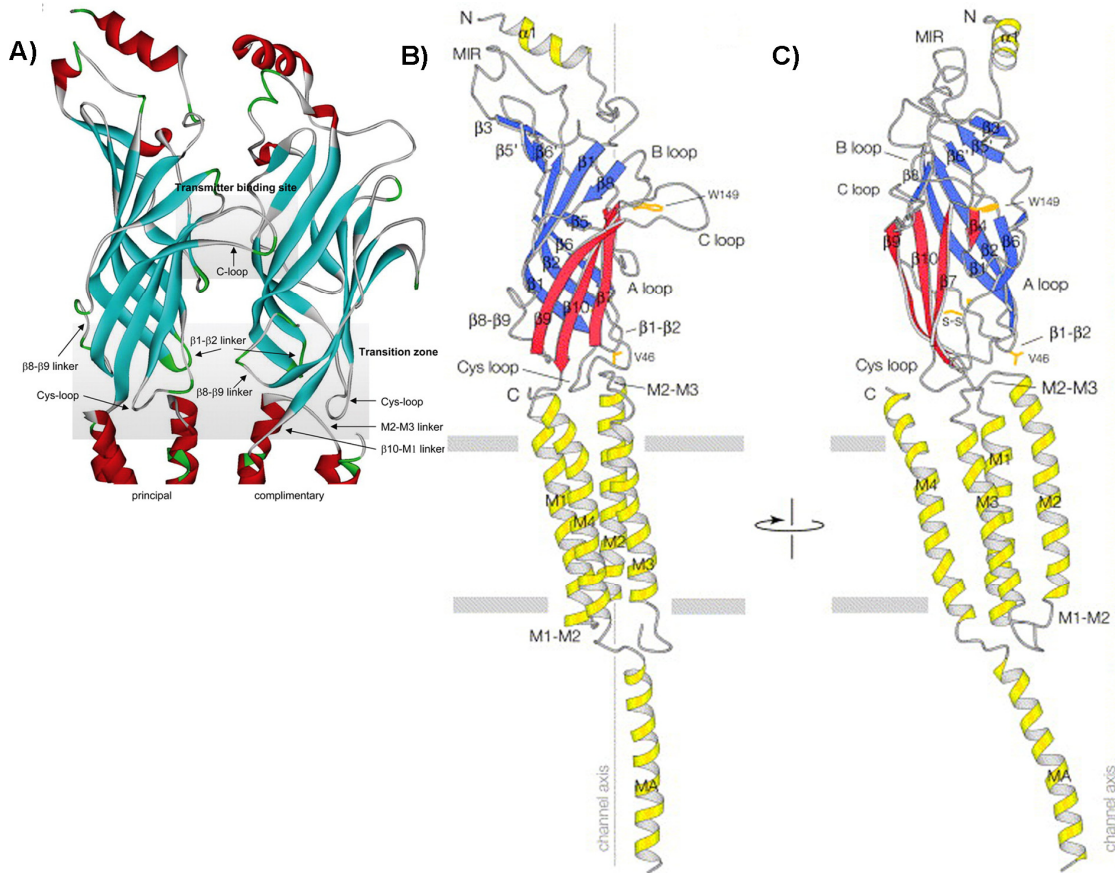
Figure 1.3: Ribbon diagrams of the *Torpedo* nAChR (PDB:2BG9)
1.1A) Only two of five subunits are displayed. Two major structural elements of the LBD are shown for two of the five subunits: the transmitter-binding site and the transition zone. The transmitter-binding site is composed of a cluster of aromatic residues from both the principal and complimentary subunits and is capped by the C-loop. The transition domain consists of several loops including: Cys-loop, β1–β2 linker, β8–β9 linker, β10–M1 linker and the M2–M3 linker. These loops are involved in converting structural changes at the transmitter-binding site down to the pore domain and inducing channel gating. *1.1B and 1.1C)* Ribbon diagram of a single subunit, rotated 90° relative to each other. The secondary structural elements are labeled and numbered accordingly; the outer beta sheet is colored red (β7, β9, β10), the inner beta sheet (β1, β2, β6) and other beta sheets are colored in blue, and the transmembrane helices are colored in yellow. Part of the M3–M4 loop (connecting MA to M3) is missing. 1.1A and text are adapted from [Gay and Yakel 2007]. 1.1B and 1.1C are adapted from [Unwin 2005].

Ion permeation and selectivity of Cys-loop receptors

The primary function of the receptor channel is to reduce the energy barrier to ion translocation through the hydrophobic core of the cellular membrane, to discriminate between ions, and open and close when exposed to endogenous agonists. Early mutagenesis studies of the *Torpedo* nAChR revealed the importance of three rings of negative charge along the pore-lining M2 helix at positions -5', -2', and 20' (D238, E241, and E262 for the mouse α1 subunit respectively) (**Figure 1.4**) [Karlin 2002][2]. Mutating the glutamates/aspartates at these positions to positively charged amino acids reduced single channel conduction of movovalent cations, and the effect was additive when mutations were introduced into multiple subunits [Imoto *et al.* 1988]. Reducing the negative charge at the -2' position has a more dramatic effect on channel conductance than the other two positions, and can eliminate Ca^{2+} permeation of α7 receptor [Bertrand *et al.* 1993]. The 19' position in anion-selective receptors (20' in cation-selective receptors) has a more prominent role in rectification, and regulates ion concentration in the extracellular vestibule [Moorhouse *et al.* 2002]. An additional ring of charge was identified in the LBD in Loop A (α1-D97) using a similar experimental design, and α1-N47 and α1-E86 have also been proposed as putative sites that determine both ion conduction and selectivity [Hansen *et al.* 2008; Sine *et al.* 2009]. The local charge provided by these negative residues over the axial length of the receptor channel would serve as a funnel to attract cations into the vestibular space in the closed state and counteract the low dielectric environment of the lipid bilayer during ion transport in the open

---

[2] See [Miller 1989] for a review of the prime numbering system. For nAChRs, -5' represents the far intracellular end of the pore-lining M2 helix, while 20' is at the extracellular end of the pore.

state. It is important to note that a conformational effect of the mutagenesis in the

charged rings cannot be completely ruled out [Kienker *et al.* 1994].
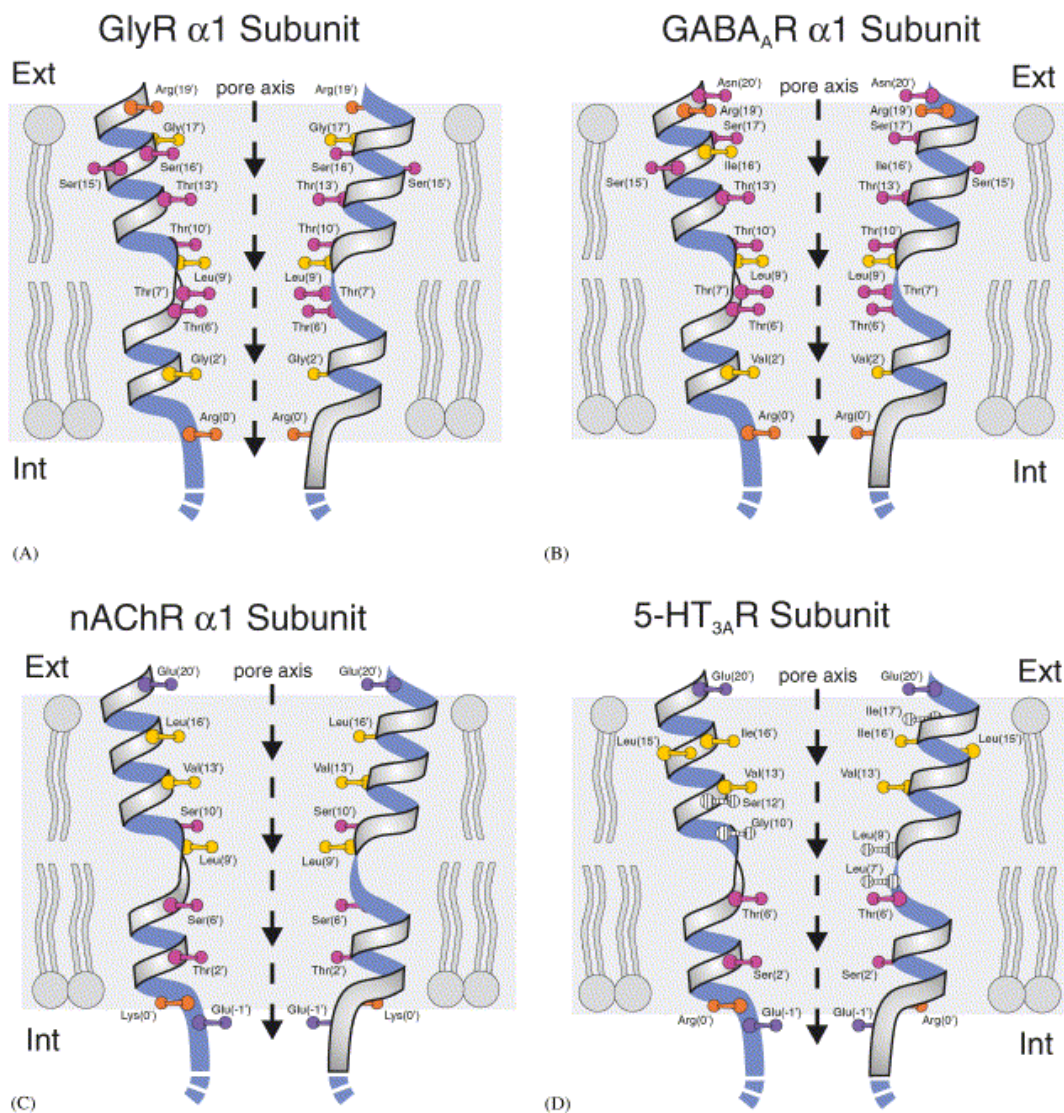
Fig. 1.4: Schematic representation of the pore-lining (M2) helicies. Open state conformations of two M2 segments of the α1 subunits of the anion-selective GlyR **(A)**, GABA$_A$R **(B)** and the cation-selective nAChR (C) and the 5-HT$_{3A}$R subunits **(D)**. Note the tapering of the pores to a constriction at their intracellular end, the charged residues flanking the intra- and extracellular mouths of the channels and the abundance of polar residues within the channels, especially in the GlyR and GABA$_A$R. Residues believed to be projecting their side chains towards the channel pore are shown, labeled with the amino acid three letter code and with the generalized LGIC nomenclature for M2 domains [Lester 1992]. In addition, the lysine residue (K0′) in the cation-selective nAChR, the arginine (R0′) and leucine (L15′) residues in the 5-HT$_{3A}$R and the serine residue (S15′) in the anion-selective GABA$_A$R and GlyR are depicted as facing away from the channel axis. Note the predominantly hydrophobic (non-polar) extracellular part of the cation-selective LGICs contrasting with the anion-selective LGICs, and the predominantly hydrophilic (polar) intracellular part of all of these channels. Figure and text modified from [Keramidas *et al.* 2004].

The dimensions of the ion-conducting pore of the Cys-loop receptor family appear to vary between receptor subtypes. In the closed-state structure of *Erwinia* Cys-loop receptor, the pore narrows to less than 3 Å at the 2' position, which is too small for passage of a hydrated ion [Hilf and Dutzler 2008]. The open-state structures of the *Gleobacter* Cys-loop receptor suggest a pore diameter of about 5Å, which would suggest that increasing the pore diameter is an important receptor gating mechanism [Bocquet *et al.* 2009; Hilf and Dutzler 2009]. However, cryo-EM studies of the *nAChR* identifiy a pore diameter of 20Å [Unwin 2005]. Ion permeability studies suggest that the pore diameter of anion-selective receptors ($GABA_AR$, GlyR) ranges from 5-6 Å, whereas cation-selective receptors (nAChR, $5-HT_3R$) range from 7.4-8.4 Å [Keramidas *et al.* 2004]. Because an ion would need to partially dehydrate at diameters below approximately 8Å to pass through the channel [Hille 2001], the similarities in pore diameter from the structural and functional studies argue for related (if not identical) gating mechanisms for the Cys-loop receptors.

Several important differences exist in ion permeation between cation-selective (nAChR, $5-HT_3R$) and anion-selective ($GABA_AR$, GlyR) Cys-loop receptor channels. Substituted cysteine accessibility studies (SCAM) on the M2 helix have revealed a pattern of similar, but non-identical accessibilities to permeating ions in cation-selective vs. anion-selective receptors (**Figure 1.4**). In general, the solvent accessible residues in the anionic receptors are hydrophilic over the entire length of the M2 helix, while solvent accessible residues in the cationic receptors are more hydrophobic towards the top of the M2 helix and hydrophilic towards the bottom. Energetically, the presence of extra polar residues in the anionic receptors could

contribute to additional ion binding sites within these receptors that would not be present in the cationic receptors. This important difference is supported by the anomalous mole fraction effect in GlyR and GABA$_A$ receptors, which is not observed in nAChRs [Bormann *et al.* 1987; Lester and Dougherty 1998][3].

While there are a few examples of anion-selective nAChRs in invertebrates, the vast majority of nAChRs are cation-selective as are the 5-HT$_3$ receptors. In the α7 nAChR, three mutations in the M2 helix were found to convert the ion selectivity from cations to anions: V13'T (see **Figure 1.4**), E-1'A, and the insertion of a proline between the -1' and -2' positions (-2'P) [Galzi *et al.* 1992]. The rationale for these mutations came from a sequence alignment of the M2 helix of the cation-selective α7 nAChR with the anion-selective α1 GlyR. Follow up studies from the same lab showed that the proline insertion was required to convert from cationic to anionic selectivity in the V13'T/E-1'A background α7 nAChR, but the proline insertion by itself or in combination with the V13'T mutation led to non-functional channels [Corringer *et al.* 1999]. The authors concluded that the proline insertion caused a structural rearrangement at the bottom of the M2 helix, which was compensated by a reduction of hydrophobicity at V13' and charge neutralization at E-1'. The role of these three positions are conserved among the Cys-loop receptor family, as the equivalent mutations also result in an anion-selective 5-HT$_3$R, and the inverse mutations (T13'V, A-1'E', P-2'Δ) resulted in a cation-selective α1 GlyR [Keramidas *et al.* 2000; Gunthorpe and Lummis 2001]. Interestingly, the E-1'A mutation by itself eliminates Ca^{2+} permeability in α7 nAChRs, and the inverse A-1'E mutation confers Ca^{2+} permeability in the α1 GlyR [Keramidas *et al.* 2004]. These studies

---

[3] See [Lester 1991] for a review of the AMF effect and applications to ion channel research.

demonstrate that the 13' position, -1' position, and the conformation at the intracellular end of the pore (proline insertion/deletion) are necessary and sufficient to determine ion selectivity in the Cys-loop receptor family. While these data are from homomeric receptors, they illustrate that determinants of ion selectivity are largely conserved within the Cys-loop receptor family.

Gating of Nicotinic Receptors

For the nicotinic receptor subfamily, acetylcholine and other agonists interact with aromatic residues in the binding pocket through π-cation interactions [Meyer et al. 2003; Xiu et al. 2009]. The critical aromatic residues are part of the C-loop, the principal side, and the complementary side of the agonist-binding site. Agonist-binding leads to a closure of the C-loop over the binding pocket [Hansen et al. 2005], which dramatically increases the probability of a transition into the open, ion-conducting state. The position of the C-loop is highly variable due to thermal motion, which is probably responsible for the low probability of receptors to open in the absence of agonist [Venkatachalan and Czajkowski 2008; Wang *et al.* 2009b]. After agonist binding, a series of structural transitions are allosterically transmitted to the activation gate at the -3' to 2' positions in the M2 helix [Imoto *et al.* 1988; Lester 1992; Wilson and Karlin 2001].

The first kinetic description of the closed-open isomerization of muscle nAChRs was described by Neher and Sakmann, who won the Nobel Prize in 1991 for their development of the patch clamp technique [Neher and Sakmann 1976; Neher et al. 1978; Sakmann et al. 1980; Colquhoun and Sakmann 1981]. This

permitted a detailed analysis of the kinetics of activation, de-activation, and

desensitization at the single-channel level. The kinetics of the muscle nAChR are

best described by a multi-state mechanism **(Figure 1.5),** where the receptor can

transition into multiple open states from the unliganded, mono-, or di-liganded

conformations [Colquhoun 1998]. Under physiological conditions, gating of the

muscle-type nicotinic receptors is an "all-or-none" event. A high concentration of

acetylcholine is needed to enter the diliganded-closed state, which than quickly

isomerizes to the diliganded-open state. Ion permeation then rapidly terminates by

when the receptor enters diliganded-desensitized state. Rapid onset and termination

of ion permeation is critically important for synaptic function of the nAChRs, as

mutations that enhance or inhibit channel gating have been linked to congenital

myasthenia syndromes and epilepsy [Steinlein 2007]. The significance of single

channel events are observable in recordings from *in vitro* brain slices, where

activation of single or small populations of the α7 nAChRs can enhance neuronal

excitability and trigger voltage-gated ion channels in the CNS [Gusev and Uteshev

2009]. Therefore, understanding the mechanisms by which nAChRs transition

between kinetic states is important for understanding physiological function.

From the agonist-bound ion conducting state(s), the nicotinic receptors can

isomerize back to one of multiple closed states or desensitized states [Elenes and

Auerbach 2002], which show higher affinity for agonists but no ion conduction [Boyd

and Cohen 1980; Sine and Taylor 1982]. The rate of desensitization depends on the

status of the activation gate, as faster rates are observed in the diliganded-open

state than other open or closed states [Auerbach and Akk 1998]. However, the rate

of desensitization is directly proportional to the number of agonist-binding sites, as inactivation of individual binding sites on an α7 nAChR/5HT$_3$ chimeric ion channel slows the rate of desensitization [Rayes et al. 2009]. In this respect, desensitization represents a complex allosteric interaction between the agonist-binding sites and activation gate.

One such approach to study the energetic relationships between the closed and open states is rate-equilibrium free energy relationships (REFER). The equilibrium rate constant (K_{eq}) for ion channels is defined as the rate of channel opening (k_o) divided by the rate of channel closing (k_c): $K_{eq} = k_o/k_c$. In REFER analysis, k_o and K_{eq} are determined using single channel recordings for receptors carrying at 3-4 mutations at a single residue using single channel recordings, and are plotted as log k_o vs. log K_{eq} (**Figure 1.5**). If there is a linear relationship between log k_o and log K_{eq}, the slope of the fit is defined as Φ. Phi values always exist between 0 and 1, and sample the energy landscape between the closed and open states. While there are several biophysical interpretations of Φ, Auerbach and colleagues have used a temporal interpretation of the resulting Φ-values to suggest blocks of coordinated motion within the muscle-type nAChR [Auerbach 2007]. In the temporal interpretation of Φ-values, phi values close to 1 suggest the residue mutated affects early transitions (closer to the closed state) and phi values closer to 0 suggest that the residue mutated affects later transitions. Their extensive work suggests coordinated motion (Φ-blocks) starting with the agonist-binding site (C-loop, β4-β5 loop, and β7-β8 loop) and then moving through the transition zone (Cys-loop and β1-β2 loop) and the pore region (M2 helix) to the gate of the channel

[Grosman *et al.* 2000; Chakrapani *et al.* 2004; Chakrapani and Auerbach 2005; Jha *et al.* 2007; Purohit and Auerbach 2007a; Purohit and Auerbach 2007b]. This proposed "conformational wave" propagates throughout the receptor in approximately 1 µs [Grosman et al. 2000]. Although REFER analysis provides a comprehensive view of the kinetics of the transition from the closed to open state, it does not provide any information about the specific structural rearrangements that occur.

(A)

$$C\ (A + R) \underset{\alpha}{\overset{\beta}{\rightleftharpoons}} O\ (AR^*)$$

$$D\ (AD)$$

(B) $K_{eq} = \dfrac{\beta}{\alpha}$

(C) $\log(\beta) = \phi * \log(K_{eq})$

(D)

$$C\ (2A + R) \underset{k_{-1}}{\overset{k_1}{\rightleftharpoons}} C_1\ (A + AR) \underset{k_{-2}}{\overset{k_2}{\rightleftharpoons}} C_2\ (A_2R)$$

$$\alpha \Big\Updownarrow \beta$$

$$O\ (2A + R^*) \rightleftharpoons O_1\ (A + AR^*) \rightleftharpoons O_2\ (A_2R^*)$$

$$k_{-3} \Big\Updownarrow k_3$$

$$D_1\ (A + AD) \rightleftharpoons D_2\ (A_2D)$$
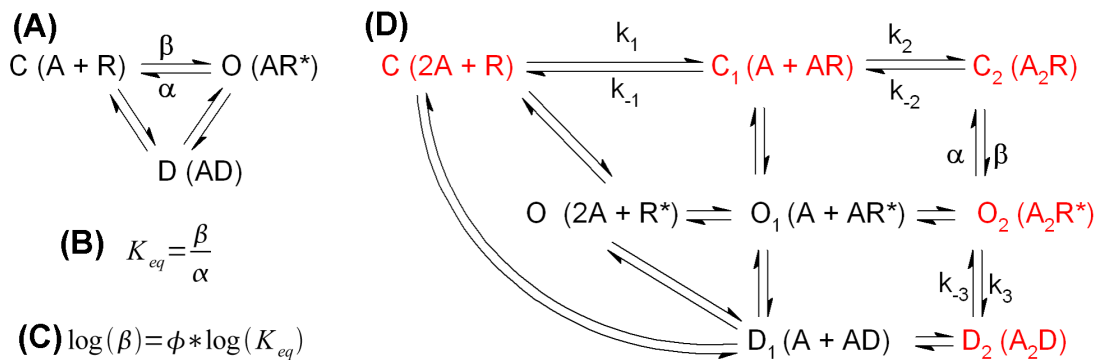
Figure 1.5: Single channel kinetic scheme for the muscle nAChR.
(A) shows a generalized cyclic three-state kinetic scheme for any desensitizing ion channel. **[C]** is the closed state where the agonist **[A]** has not yet bound to the receptor **[R]**, and is non-conducting. **[O]** is the open state, where agonist has bound to the receptor and the receptor is in the ion-conducting state **[AR*]. [D]** is the desensitized state, which has higher affinity for agonists and the agonist remains bound **[AD]** but is non-conducting. The agonist must dissociate from the desensitized receptor to return to the closed state **[AD → A + R]**. Each isomerization **(C↔O, O↔D,** or **D↔C)** can occur bi-directionally, and depends on the equilibrium constant (forward reaction divided by reverse reaction). The kinetic isomerization that leads to the highest open probability of the receptor is defined as the equilibrium gating constant **[K_{eq}]**, which is calculated from the opening rate **[β]** divided by the closing rate **[α]** and is shown in (B). (C) shows the mathematical relationship between **β** and K_{eq}, where the linear slope equals **Φ** in the rate-equilibrium free energy relationship (REFER) [Auerbach 2007]. (D) shows multi-state kinetic scheme for the muscle (α1$_{(2)}$β1γδ/ε) nAChR. The pathway outlined in red represents a well-validated simplification of this reaction scheme, This is probably an oversimplification of the continuous wave of conformational changes that occurs during activation. [Colquhoun and Hawkes 1981; Sine and Steinbach 1986; Sine and Steinbach 1987; Auerbach and Akk 1998; Purohit *et al.* 2007; Purohit and Auerbach 2007a; Purohit and Auerbach 2007b]. Under physiological conditions, the high synaptic concentration of ACh shifts the equilibrium in the forward direction; sequential binding of two agonist molecules to each receptor **(C→C$_1$→C$_2$)** dramatically increases the open probability of the receptor **(β>>>k$_{-2}$)**, which leads to a gating transition **(C$_2$→O$_2$).** From the primary open state, the receptor then transitions to the desensitized state **(C$_2$→D$_2$, k$_3$>>>α)**. Degradation of ACh in the synaptic cleft by acetylcholine esterase dramatically lowers the ACh concentration, and leads to the ultimate transition of the desensitized state back to the unliganded closed state **(D$_2$→C).**

Structural transitions during nAChR gating

The structures of the different AChBPs and the AChBP/*Torpedo* chimeric model of a full-length nicotinic acetylcholine receptor serve as a template to generate homology models for other nAChRs and Cys-loop family receptors. These structural models provide a starting point to test hypothetical mechanisms of conformational changes resulting from agonist binding that lead to channel opening. From these models, Unwin originally proposed that a rigid-body rotation of the alpha-subunits was the predominant molecular movement that coupled agonist binding to channel gating [Horenstein et al. 2001; Unwin 2005]. Subsequent work utilizing SCAM [Lyford et al. 2003; McLaughlin et al. 2007] and proton binding-unbinding reactions of ionizable residues [Cymes et al. 2005] argue against a rigid-body subunit rotation as the sole mechanism of agonist-induced conformational change. Overall, subtle rearrangements around the agonist binding site are thought to propagate through the rigid β-sheets to induce conformational changes in the transition zone, which then propagate towards the M2 helix and the channel gate [Wilson and Karlin 2001; Mukhtasimova et al. 2005; Sine and Engel 2006; Gay and Yakel 2007].

The "conformational wave" model of receptor gating proposes that structural rearrangments occur in discrete groups. One of the first structural movements of the Cys-loop receptor family is that of the C-loop (**Figure 1.3**). The C-loop occupies distinct conformations when bound to agonists vs. competitive antagonists, demonstrating that movement of the C-loop is one of the first conformational changes associated with receptor gating [Hansen *et al.* 2005]. Disulfide trapping

experiments have shown that the C-loop is a highly flexible structure and may move upwards of 5Å from the closed to open state of the GABA$_A$R [Venkatachalan and Czajkowski 2008]. Induced closure of the C-loop over the agonist-binding site (using targeted molecular dynamics) correlates with ion flooding of the receptor pore, further suggesting C-loop closure is necessary and sufficient to induce the "conformational wave" that leads to an open (ion-conducting) receptor [Wang *et al.* 2009b].

      After closure of the C-loop, normal mode analysis of a α7 nAChR homology model suggests that a quaternary twist is the predominant structural rearrangement [Taly et al. 2005; Taly et al. 2006]. In this motion, the ligand-binding domain rotates counterclockwise while the transmembrane domain rotates clockwise (as viewed looking down the ion-conduction path from the extracellular side) [Taly et al. 2005; Taly et al. 2006][4]. Other simulations of the α7 and muscle-type nAChRs that include the intracellular domain suggest that the predominant structural transitions also contain asymmetric motions, where one subunit moves before the other four subunits of the assembled receptor independent of the type of motion [Szarecka *et al.* 2007; Yi *et al.* 2008]. Within a subunit, the capping of the C-loop propagates a conformational change along the outer beta sheet (β7, β9, β10) towards the Cys-loop and M2-M3 linker, while the transmembrane domains undergoes a combination of twisting and tilting motions [Cheng et al. 2007; Szarecka et al. 2007]. Tilting of the M2 helices was also observed in a comparison of x-ray crystallography structures in the closed and open state of bacterial Cys-loop receptors [Hilf and Dutzler 2008; Hilf

---

[4] Supplemental videos demonstrate this motion [Taly *et al.* 2005].

and Dutzler 2009]. Conformational changes of the M2 helices are thought to relax

the open channel gate between the -3' and 2' positions.

In cation-selective Cys-loop receptors, another structural feature important for

gating is the presence of a hydrophobic girdle between the 9' and 17' positions

(**Figure 1.4**),which is large enough to fill with water molecules but excludes

permeable cations in closed-state receptor models [Keramidas *et al.* 2004;

Beckstein and Sansom 2006].   This model only applies to nAChRs (and likely 5-

HT$_3$Rs), as the anion-selective Cys-loop receptors lack the solvent exposed

hydrophobic residues that contribute to the girdle. Simulations of Cl$^-$ translocation in

α1 GlyR suggest a more variable energy barrier in the M2 helix [Ivanov *et al.* 2007]

For cation-selective Cys-loop receptors, the "conformational wave" would converge

on both the hydrophobic girdle and the channel gate (further down the M2 helices) to

allow ion-permeation as a result from the binding of agonists.

While there is compelling evidence for C-loop movement during receptor

gating, the specific conformational changes that occur downstream of the agonist-

binding site remain a mystery. The substituted cysteine accessibility method

(SCAM) provides a powerful approach to study conformational change in ion

channels, and complements models of receptor gating dervied from structural and

computational studies [Akabas et al. 1992; McLaughlin et al. 2007]. This

methodology takes advantage of the fact that cysteines introduced at specific

positions in the protein have a very specific chemical reactivity to

methanethiosulfonate (MTS) reagents. Hydrophillic MTS chemicals preferentially

modify the introduced cysteine at the surface of the protein, exposed to the aqueous

environment. The advantage of SCAM is that it can also be used to measure the reactivity of MTS reagents in the presence or absence of various agonists, antagonists, or modulators. Differences in the rate of MTS modification are interpreted as being caused by conformational changes of the protein that move the introduced thiol or by change in the local electrostatic environment that surrounds the introduced thiol. By using SCAM to probe the rates of accessibility in the closed, open and desensitized states, the gating domain has been localized to the bottom third of the M2 helix of muscle nAChRs [Wilson and Karlin 2001]. Work from our laboratory using SCAM has shown that the LBD of the α7 nAChR undergoes agonist-dependent conformational changes in the inner β-sheet (β1, β2, and β6), the outer β-sheet (β7, β9, and β10) and the β8-β9 loop [Lyford et al. 2003; McLaughlin et al. 2006; McLaughlin et al. 2007].

Because of its critical location between the LBD and TMD, mutagenesis studies in transition zone (TZ) have been an active area of research to understand nAChR gating. Fusion of the AChBP to the transmembrane domain of the 5-HT$_{3A}$ receptor (AChBP/5-HT$_3$) produced a protein that was properly trafficked to the cell surface but was non-functional [Bouzat *et al.* 2004]. However, receptor function was restored to the AChBP/5HT$_{3A}$ chimera when all residues from the AChBP in the transition zone (β1-β2, Cys loop, β8-β9) were replaced with those of the 5-HT$_{3A}$ receptor. These results demonstrated that functional coupling between agonist binding and channel gating requires specific structural compatibility in the TZ [Bouzat et al. 2004]. While specific residue interactions for channel gating are known for different Cys-loop receptors, they are not necessarily conserved. For example,

Lee and Sine [Lee and Sine 2005] argue that a salt bridge between residues in the β1-β2 loop and the pre-M1 region in muscle nAChR (E45-R209) is critical for gating of muscle-type nAChRs, as shown by charge reversing mutations (E45R/R209E) and REFER analysis. However, subsequent work has argued against a salt-bridge at the E45-R209 position in muscle-type nAChRs. First, charge-reversing mutations argue for a salt bridge in $GABA_c$ receptors, but they are not formed in $5\text{-}HT_3$ receptors [Price et al. 2007]. Second, extensive mutagenesis using natural and unnatural amino acids argues that the balance of positive and negative charges in the TZ controls gating rather than pairwise residue interactions [Xiu et al. 2005]. Third, the E45L/R209A double mutation has a nearly identical K_{eq} value and multiple double mutations at these positions are functional, arguing against a salt bridge mechanism [Purohit and Auerbach 2007a]. Another example of a specific residue interaction is a cis-trans isomerization of a highly conserved proline in the M2-M3 loop of $5\text{-}HT_{3A}$ receptors (P307) and α7 nAChRs (P261) [Lummis et al. 2005]. However, there is no proline at the equivalent position in either $GABA_A$ (lysine for β1 $GABA_AR$, threonine for α1 $GABA_AR$) or glycine receptors (lysine for α1 GlyR) [Bera *et al.* 2002]. Proline has a cyclic (*cis*), hydrophobic R group which leads to a non-variable Ψ angle[5] and conformational rigidity. In contrast, lysine is positively charged at physiological pH and threonine has a polar –OH side chain and both of these amino acids are conformationally flexible. The differences in the sequence alignment and amino acid chemistry for the *cis-trans* isomerization of proline demonstrate that there is no single, conserved transduction mechanism from agonist binding to

---

[5] The Ψ dihedral angle describes the rotation around the $C^{\alpha}\text{-}C(O)$ bond.

28

channel gating. Rather, each Cys-loop receptor may employ a unique transduction

mechanism that depends upon the charge profile of the transition zone.

Positive allosteric modulation

In 1965, Monod, Wymann and Changeux (MWC) introduced a model of

allosteric transition in which a protein can exist in multiple conformational states and

that the binding of small molecules can stabilize it in a preferred conformational state

[Monod et al. 1965]. While this model was originally developed for enzymes, the

same principles can be applied to ligand-gated ion channels and other membrane

proteins [Changeux and Edelstein 2005]. The main principles of the MWC model as

applied to nAChRs are that: **1)** the receptor can thermodynamically transition

between conformational states (**Figure 1.5**), **2)** binding of an agonist at the agonist-

binding (orthosteric) site causes a conformational change in a distal region of the

protein. One important difference in applying the original MWC model to ligand-

gated ion channels is that competitive and non-competitive antagonists do not have

a higher affinity for the resting/closed state, arguing against the postulate that ligand-

binding stabilizes the channel in a preferred conformational state (also called the

"concerted" state model) [Krauss et al. 2000]. Each class of ligand (agonist,

antagonist, modulator, etc.) does not alter a preexisting equilibrium between the

closed and open states for the Cys-loop receptor family, and supports the conclusion

that there is no unifying mechanism for ligand-induced conformational changes. By

definition, nAChR agonists and competitive antagonists bind at the orthosteric site,

but a sequential mechanism best fits radioligand binding and single channel REFER

data from the muscle type nAChR [Koshland et al. 1966; Auerbach and Sachs 1983; Krauss et al. 2000]. In this model, binding of agonists induces specific conformational changes that lead to receptor gating. Competitive and non-competitive antagonists may simply occlude specific conformational changes along the gating transition, or induce different conformational changes to block the gating transition.

In contrast, positive allosteric modulators (PAMs) bind away from the orthosteric site and lower the energy required to transition between conformational states [Bertrand and Gopalakrishnan 2007]. For ligand-gated ion channels, PAMs enhance agonist-evoked currents by increasing the peak current amplitude and/or lowering the EC_{50} for agonist. Mechanistically, PAMs could enhance agonist-evoked currents by: 1) increasing the binding affinity for agonists, 2) increasing the opening rate (β) of the receptor, 3) reducing receptor desensitization (which could reflect changes in agonist binding and/or gating), or 4) a combination of all of the above. Ultimately, the binding of PAMs to their target receptor would add additional energy to the agonist - receptor complex (**Figure 1.2**), allowing more of the energy associated with agonist-binding to drive the C-O gating isomerization [Jackson 1989].

The specific mechanisms of positive allosteric modulation are slowly emerging for the Cys-loop family of ligand-gated ion channels. At the single channel level, PAMs can increase the mean open time but their mechanism of action in the absence of agonist is not well-defined [Hurst et al. 2005]. By definition, PAMs can only enhance channel function in the presence of an agonist. The best known

example of positive allosteric modulation is benzodiazepine acting on $GABA_A$

receptors [Greenblatt et al. 1981; McKernan et al. 2000]. These compounds bind at

the interface of the α1 and γ2 subunits at a non-functional agonist-binding site (at the

interface between two subunits that is homologous to the orthosteric site), making it

an allosteric binding site [Kucken et al. 2000; Atack 2003]. With the success of

benzodiazepines, there is a growing interest in developing PAMs for the nAChRs.

Positive allosteric modulators targeting the α7 nAChR have shown better specificity

for this isoform compared to natural and synthetic agonists. [Daly 2005; Bertrand

and Gopalakrishnan 2007].. Because allosteric modulators require the presence of

the neurotransmitter agonist, the timing of endogenous synaptic transmission is not

disrupted and PAMs can also enhance the activity of endogenous partial agonists,

such as choline activation of the α7 nAChR [Gusev and Uteshev 2009]. This last

point is crucial; by enhancing the **amplitude** of neurotransmission without disrupting

the **frequency and synchrony** of signaling between different regions of the brain,

PAMs should have reduced occurance and severity of side effects compared to

orthosteric ligands. Academic and pharmaceutical industry researchers are actively

developing allosteric modulators for ligand-gated ion channels (α7 and α4β2*

nAChRs) and GPCRs (mAChR and mGluR subtypes) [Conn *et al.* 2009; Taly *et al.*

2009].

Positive allosteric modulation of α7 nAChRs

Over the last several years there has been great success in developing synthetic PAMs for the α7 nAChRs from diverse chemical templates (**Figure 1.2**) [Bertrand and Gopalakrishnan 2007]. The discovery that two PAMs, PNU-120596 and TQS, not only enhance peak current amplitudes but also eliminate macroscopic desensitization during continuous application of these compounds with agonists led to a classification system based on the presence or absence of the desensitization "phenotype.". PAMs that reduce or eliminate desensitization of the α7 nAChR are classified as Type II modulators, while PAMs that do not alter receptor desensitization are classified as Type I modulators [Gronlien *et al.* 2007].

The chemotype of the different positive allosteric modulators does not correlate with effects on receptor desensitization; for example, PNU-120596 and NS-1738 are very similar in structure (amide linker flanked by 5/6 carbon rings) but act as Type II and Type I modulators, respectively [Gronlien *et al.* 2007]. However, the important difference between Type I vs. Type II modulators may be the location of the binding sites for these compounds. The putative PNU-120596 binding site lies in the intrahelical space of the four transmembrane helices, but the binding sites for NS-1738 and galanthamine (Type I modulators) are in the extracellular ligand-binding domain [Hansen and Taylor 2007; Bertrand *et al.* 2008; Young *et al.* 2008]. In our model, PNU-120596 would stabilize the open state and lower the energy barrier to transition to the open state from either the closed state or the desensitized state in part because of its close proximity to the receptor gate.

In additional to small organic molecules, physiological concentrations of Ca^{2+} allosterically modulate the α7 nAChR [Mulle et al. 1992; Vernino et al. 1992]. Under the current Type I/Type II nomenclature, Ca^{2+} and other permeable divalent cations behave as Type I PAMS, which do not have any effect on macroscopic desensitization [Sands et al. 1993; Eddins et al. 2002a; McLaughlin et al. 2006]. Changes in extracellular Ca^{2+} are well documented in the brain and can range anywhere from 1-3 mM under physiological conditions, with total available calcium (bound and free) decreasing with age [Jones and Keep 1988; Cohen and Fields 2004]. The exact EC_{50} for Ca^{2+} modulation of wildtype α7 nAChRs is unknown, but reductions in extracellular Ca^{2+} are likely to reduce ACh-evoked currents through the α7 nAChR. This could have implications for the Ca^{2+}-dependent processes such as vesicle fusion and synaptic plasticity Furthermore, the mechanisms of modulation by Ca^{2+} are unknown, as increases in extracellular Ca^{2+} decreases single channel amplitude but increase receptor gating [Mulle *et al.* 1992; Vernino *et al.* 1992].

The conformational changes induced by PAMs for the Cys-loop receptor family are just emerging. Based on the work of Pless et al. [Pless et al. 2007], it is likely that PAMs cause a combination of similar and different conformational changes than agonists. Since PAMs do not directly activate their target receptor, conformational changes that are similar to agonists would likely induce a subsection (but not all) of the gating conformational wave. Benzodiazepines induce a conformational change at their binding site of $GABA_A$ receptors [Teissere and Czajkowski 2001; Kloda and Czajkowski 2007], but the conformational changes induced by binding of PAMs to nAChRs are unknown.

To date, several α7 nAChR PAMs have shown promise in pre-clinical models of neuropsychiatric diseases including Alzheimers Disease and schizophrenia [Hurst *et al.* 2005; Timmermann *et al.* 2007]. Impairment of sensorimotor gating is a common symptom in human patients suffering from schizophrenia, and is thought to contribute to the cognitive symptoms (impaired attention and memory, poor decision-making) by imparing the patient's ability to filter out irrelevant stimuli from the external environment [McGhie and Chapman 1961; Braff *et al.* 1992]. Assays for sensorimotor gating include prepulse inhibition (auditory or visual stimuli,) EEG of human patients measuring the P50 wave, and hippocampal EPSP recordings to evoked auditory potentials in anestheized or free-behaving animals. These different techniques are related, in that subject/animal is exposed to a conditioning stimulus, followed by a test stimulus. In healthy subjects/animals, the amplitude of the test stimulus should be smaller than the amplitude of the conditioning stimulus; the test stimulus is effectively filtered by the reduction in amplitude. In schizophrenic patients and animal models of impaired sensorimotor gating, there is no reduction in amplitude between stimuli; the test stimulus is not filtered. The involvement of the nAChRs in schizophrenia is well-established, as patients self-medicate with nicotine products and the expression of the α7 nAChR is reduced in the hippocampus and prefrontal cortex. [Hughes *et al.* 1986; Freedman *et al.* 1995; Guan *et al.* 1999]. The Type II modulator PNU-120596 can partially restore auditory gating deficits in *D-*amphetamine treated rodents, demonstrating that this class of drug could be effective as an anti-schizophrenic agent in humans.

While these previous studies have demonstrated that PNU-120596 and permeable divalent cations are PAMs of the α7 nAChR and synthetic PAMs have therapeutic potential, more work is needed to understand how these compounds enhance receptor gating. The mechanisms that determine type I vs. type II modulation are unknown; it is also unclear how changes in macroscopic desensitization affect physiological systems. Prolonged activation of α7 nAChRs is predicted to cause Ca^{2+}-induced cellular toxicity, as a gain-of-function mutation (L9'T) that increases receptor open probability, neuronal apoptosis, and is lethal by post-natal day one in mouse models when two copies are present [Orr-Urtreger *et al.* 2000]. However, a recent study showed that PNU-120596 has no cytotoxic effects in heterologous and primary neuronal cell cultures [Hu *et al.* 2009]. These results[6] suggest that allosteric modulation by PNU-120596 (and likely other type II PAMs) is attenuated *in vivo,* underlying the importance for a mechanistic understanding of positive allosteric modulation.

The following work will investigate how Type I versus Type II PAMs induce conformational changes in the α7 nAChR, and how those structural transitions compare to those of the agonist acetylcholine. In addition, I developed homology models of α7 receptors from the structures of bacterial Cys-loop receptors and I experimentally tested the ability of these models to predict conformational changes associated with receptor gating.

---

[6] It is unknown how Type I vs Type II PAMs would effect nAChRs on non-neuronal cells; the α7 nAChR is important in the cholinergic anti-inflammatory pathway but the role of PAMs and receptor desensitization in non-neuronal systems has not yet been investigated [Wang *et al.* 2009a].

CHAPTER 2

MATERIALS AND METHODS

Reagents and Molecular Biology

Female *Xenopus laevis* frogs were obtained from Xenopus One (Dexter, MI, USA) or Xenopus Express (Brooksville, FL, USA). Methanethiosulfonate chemicals were obtained from Toronto Research Chemicals (Toronto, ON, Canada). PNU-120596 was obtained from Tocris Bioscience (Ellisville, MO, USA). Quikchange® site-directed mutagenesis kit was obtained from Stratagene (La Jolla, CA, USA) and the mMessage mMachine® *in vitro* RNA transcription kit was obtained from Ambion (Austin, TX, USA). All other reagents for molecular biology, oocyte dissection, and electrophysiological recordings were obtained from Sigma-Aldrich (St. Louis, MO, USA) or Fisher Scientific (Pittsburgh, PA, USA).

The chick α7 nAChR was expressed in the pAMV vector under the control of the T7 promoter. Mutations were introduced into C115A/L247T receptors using the Quikchange site-directed mutagenesis kit according to the manufacturer's instructions, and were verified by DNA sequencing. All receptors contained a cysteine-to-alanine mutation at position 115. C115 is the only unpaired cysteine in the LBD , and the C115A mutation simplifies the interpretation of thiol modification experiments without affecting responses to ACh [McLaughlin *et al.* 2006] or PNU-120596. The utility of the L247T mutation is described below (in Chapter 3). Capped cRNA transcripts were made as previously described [Lyford et al. 2003].

Construct expression in Xenopus oocytes

Xenopus laevis oocytes were surgically removed as described [Lyford et al. 2003]. The oocytes were injected with 20 ng of α7 nAChR cRNA and were incubated

for 2-7 days in ND96 (96 mM NaCl, 2 mM KCl, 1 mM $MgCl_2$, 1.8 mM $CaCl_2$, 5 mM Na-HEPES, pH 7.5) plus 50 mg/ml gentamicin and 0.55 mg/ml sodium pyruvate.

Some cysteine mutants, displaying a peak current response to maximal ACh of less than 100 nA, were coexpressed with human RIC-3 protein (resistant to inhibitors of cholinesterase) in a 1:1 (w/w) cRNA ratio [Lansdell et al. 2005]. Dose-response curves from several mutant α7 receptors were generated with and without coexpression of RIC-3. The data suggest that RIC-3 substantially increased the peak current amplitude without major effects on the ACh EC_{50} values (**Table 3.3**).

Two-electrode voltage clamp of Xenopus oocytes

Oocytes were superfused with ESLC (in mM: 96 NaCl, 2 KCl 1 $MgCl_2$, 0.1 $CaCl_2$, 10 HEPES-NaOH, pH 7.5), a low-Ca^{2+} solution that minimizes currents through Ca^{2+}-activated Cl^- channels. For each mutant α7 nAChR, a 5-7 point dose-response curve was generated to ACh alone or with the addition of 1 µM PNU-120596 or 10 mM $BaCl_2$ (in ESLC). Dose responses for ACh with and without PNU were obtained from the same oocytes. Unless otherwise noted, PNU-12096 was preapplied for 30 seconds, and than coapplied with ACh. $BaCl_2$ was coapplied with ACh. This experimental design maximized the effect of these two modulators on the rate of modification of MTSEA with introduced cysteines and on the efficacy of ACh-evoked currents. For some mutant receptors, a dose response curve was generated for the allosteric modulator in the presence of an EC_{30-50} dose of ACh. All dose response curves were fit to a three-parameter Hill equation using SigmaPlot 9.0 (Systat Software, San Jose, CA, USA). Data were reported as the average ± S.E.M.

Two-electrode voltage clamp was performed as described [McLaughlin et al. 2007]. Solutions were applied by gravity perfusion with a 3-5 ml/min flow rate. Oocytes were superfused with ESLC for at least two minutes between all drug applications, and current amplitudes returned to baseline.

To eliminate complications of run-up and run-down of current over the course of an experiment, all oocytes were initially treated with a maximal ACh dose 3-4 times consecutively. Oocytes were discarded if the response to the maximal ACh dose varied by more than ± 10%, or corrected for run-down/run-up.

Substituted Cysteine Accessibility Method

Charged MTS reagents were made fresh daily in distilled H_2O and stored on ice, whereas neutral MTS reagents were dissolved in either DMSO or 95% EtOH and stored in aliquots at -20°C. Just prior to use, the cysteine-modifying reagents were diluted to the appropriate concentration in ESLC and were applied immediately to the oocytes. MTSEA was our primary test compound to screen for reactivity at introduced thiols, but MTSEA-biotin, MTSBn, and DTNB were also used at select residues.

We compared the ACh dose response curves of each mutant before and after application of a high concentration of MTSEA (0.5-10 mM for 0.5-4 minutes). For mutants that showed a functional effect of MTSEA, a limiting concentration of MTSEA (0.1-100 µM), yielding 20-50% of the maximal MTSEA effect, was determined empirically. To measure modification rates, the limiting concentration of MTSEA was applied repeatedly for 15-30 sec. In experiments with PNU-120596, 1 µM of this compound was pre-applied for 30 seconds and then co-applied with the

limiting concentration of MTSEA. In experiments with agonists, an EC_{100} dose (which yields maximal peak current amplitudes) was coapplied with the limiting concentration of MTSEA. In all experimental conditions, the functional effect of MTSEA modification was tested with a $\sim EC_{50}$ concentration of ACh. Each application of ACh was applied until a peak current amplitude was obtained (~15 s), and than the perfusion was switched back to ESLC (wash buffer). At the end of each experiment, a maximal dose of MTSEA was applied (0.5-10 mM) to measure the effect when all accessible thiols were modified.

Normalized current amplitudes $(I_t - I_\infty)/(I_{zero} - I_\infty)$, where I_t is the current amplitude after the cumulative time of MTSEA exposure, I_∞ is the current amplitude after the final maximal dose of MTSEA, and I_{zero} is the initial current amplitude before modification, were fit to a single exponential decay [Pascual and Karlin 1998] using SigmaPlot 9.0. The pseudo first-order rate constant was determined and was divided by the MTSEA concentration to give the second-order rate constant ($M^{-1}sec^{-1}$).

To test for the presence of a vestibular constriction, the ACh dose response of each introduced cysteine was measured before and after a fixed application of a neutral cysteine-modifying reagent (2mM of MTSBn, MTSEA-biotin, or DTNB for 60 seconds) with or without a maximally activating concentration (EC_{100}) of acetylcholine. The rationale and use of MTS reagents to probe the diameter of an ion channel domain is described elsewhere [del Camino and Yellen 2001].

Statistical Analysis

Hill equation parameters and second order rate constants were analyzed by one-way or two-way analysis of variance (ANOVA) with Tukey's post-hoc test (SigmaStat 3.0, Systat Software, San Jose, CA, USA). P values of <0.05 were interpreted to indicate significant differences.

Structural models of the α7 nicotinic receptor

A model of the chick α7 nicotinic receptor extracellular domain, based on the coordinates of the *Lymnaea* ACh Binding Protein [Brejc et al. 2001] was constructed as described previously [Lyford et al. 2003; McLaughlin et al. 2006]. For reference, L247 is located in the transmembrane domain, in the pore-lining M2 helix, approximately 1/3 of the pore's length from the intracellular end [Revah et al. 1991; Unwin 2005].

Homology Modeling and Refinement

Coordinates from ELIC [Hilf and Dutzler 2008] (PDB accession number = 2vl0) and GLIC [Bocquet et al. 2009] (PDB accession number = 3eam) were used to generate homology models of the chick α7 nicotinic receptor (NCBI accession number: NP_989512) in the closed and open state, respectively. The GLIC coordinates from Bocquet *et al.* 2009 were chosen because they were obtained at higher resolution, and had fewer outliers in a Ramachadran Plot than the Hilf and Dutzler 2009 coordinates. A truncated α7 receptor sequence, with non-crystallographic sequence removed, was aligned using HHPred2 [Soding 2005;

Soding et al. 2005] and than manually refined for both models to chooses sites of insertions and deletions. The non-crystallographic sequence removed from the a7 receptor corresponds to the N-terminus prior to the inner beta sheet, and the large cytoplasmic loop (M3-M4 loop) for both models. The coordinates of the ELIC and GLIC structures were fit using five-fold non-crystallographic symmetry, rendering each subunit identical in the final structural models[7]. Therefore, we used the same approach in designing our homology models; only one subunit was modeled using InsightII 2005 (Accelrys Inc, San Diego, CA) and was assembled as a homopentamer prior to model refinement. Both homology models were generated in the absence of ligand.

For the closed and open models of the α7 receptor, energy minimization was carried out using the Discover module of Insight II 2005 using Consistent Valence Forcefield (CVFF) parameters *in vacuo* [Ponder and Case 2003]. Energy minimization was performed using steepest descent gradient for 500 iterations or until the maximum derivative ≤ 10 kcal/(mol * Å), followed by conjugate gradient minimization for 500 iterations or until the maximum derivative ≤ 0.5 kcal/(mol * Å) [Allwright 1976]. After energy minimization, the closed and open state models converged to a final r.m.s. deviation of 0.26 kcal/(mol * Å). After each run, the models were manually inspected for distortion with their respective starting structure.

---

[7] Non-crystallographic symmetry (NCS) refers to multiple copies of a molecule with the asymmetric unit of the crystal, and the number of folds refers to the number of copies. So, a five-fold NCS would refer to a protein that assembles as a pentamer. NCS also refers to refinement calculations where the electron density is averaged over the entire oligomeric assembly; each subunit of the oligomeric protein will be identical in the final structural model. NCS refinement calculations are usually necessary for protein structures of lower resolution (≈ >2Å) [Kleywegt 1996].

Models were validated *in silico* using Procheck and Profiles 3D [Luthy et al. 1992; Morris et al. 1992; Laskowski et al. 1993].

Solvent accessibility and continuum electrostatics

Calculations were carried out on local computing resources utilizing Pentium IV processors and either the Ubuntu 9.04 or Red Hat Enterprise Linux operating systems. Solvent accessibility calculations were performed using nAccess, which utilizes the "rolling ball" model of solvent accessible surface area (ASA) (Hubbard and Thornton 1993, [Lee and Richards 1971; Shrake and Rupley 1973]. In brief, the solvent is reduced to a sphere of equal radius to the starting three-dimensional structure (1.4Å for water). The sphere of solvent is the rolled along the surface of the protein, where ASA is calculated as $Å^2$. Relative surface accessibility (RSA) is reported as the percentage of accessibility in comparison to a tri-amino acid peptide of the following structure: ala-X-ala, where "X" is the amino acid being probed [Hubbard et al. 1991]. *In silico* mutagenesis was carried out after energy minimization, and the introduced cysteines were manually inspected for distortions in the χ1 and χ2 bond angles.

For continuum electrostatics calculations, PDB2PQR was used to convert PDB files to PQR files using the Parse forcefield and to generate an instruction file for APBS [Sitkoff et al. 1994; Dolinsky et al. 2004]. APBS was used to calculate the local electrostatic potential using a linearized form of the Poisson-Boltzmann equation [Baker et al. 2001]. A derivation and detailed explanation of this equation can be found elsewhere [Fogolari et al. 2002]. APBS parameters were as follows:

protein dielectric of 2.0, solvent dielectric of 78.54, solvent radius 1.4 Å, temperature

of 298.15 K, and grid spacing set to 0.5 Å. Ionic salt concentration was set to that of

ESLC, which yields an ionic strength of 0.129 M [8] and a Debye length of 8.8 Å[9].

Atomic radii were defined as described [Shannon 1976]. The local electrostatic

potential is reported as kT/e, where k = Boltzmann's Constant ($1.3806504 \times 10^{-23}$

Joules/Kelvins), T = Temperature (Kelvins), and e = elementary charge (1.60217646

$\times 10^{-19}$ Coulombs) [Mohr et al. 2008].

Model Visualization

   Chemical structures (found at http://www.pubchem.gov) and ion channel

kinetic schemes were generated using the freeware version of ACD/Chemsketch

12.01. Images of x-ray crystallography data and homology models were generated

with PyMOL 0.99 (DeLano Scientific, South San Francisco, CA) and edited using

Adobe Photoshop 7.0 (Adobe Systems Inc, San Jose, CA). The results from APBS

were visualized in PyMOL using an included plug-in. MOLE was used to generate

Voronoi mesh diagrams of ion-conducting pores, as an included plug-in for PyMOL

[Petrek et al. 2007].

---

[8] Ionic Strength (I) = 0.5 * [Σ ($c_i z^2$)], where c_i = Molar concentration of ion, z = valence of ion.
[9] Debye Length in an electrolyte (κ^{-1}) ≈ 100/$\sqrt{I}$, where I = Ionic Strength in mM. This simplification is valid for conditions at room temperature (T = 300 K) and a solvent dielectric constant of 80 [Russel 1989].

CHAPTER 3

PNU-120596 AND ACETYLCHOLINE CAUSE SIMILAR GATING TRANSITIONS IN THE EXTRACELLULAR LIGAND-BINDING DOMAIN OF THE α7 NICOTINIC RECEPTOR

Introduction

Nicotinic acetylcholine receptors are the prototypical member of the Cys-loop family of ligand-gated ion channels that also includes $GABA_A$, serotonin type 3 (5-HT_3), and glycine receptors. This family of receptors are assembled as heteromeric or homomeric pentamers around a central pore [Karlin 2002]. Each subunit contains an extracellular ligand-binding domain (LBD), an α-helical transmembrane domain (TMD), a transition zone that couples the LBD to the TMD, and an intracellular domain [Gay and Yakel 2007].

Neuronal nAChRs are expressed diffusely throughout most of the central nervous system (CNS), with α4β2* and α7-containing receptors showing the highest levels of expression [Orr-Urtreger et al. 1997]. Of the neuronal nicotinic receptors, the homomeric α7 receptor is implicated in neurological diseases such as schizophrenia, Alzheimer's Disease, and anxiety disorders [Gotti and Clementi 2004]. Therefore, the α7 nicotinic receptor potentially represents an important therapeutic target.

Over the last several years there has been success in developing synthetic PAMs for α7 nAChRs, including PNU-120596 [Bertrand and Gopalakrishnan 2007]. These compounds are predicted to bind away from the orthosteric agonist binding sites and enhance gating of the receptor in the presence of agonists. PNU-120596 is part of a growing class of PAMs that can reopen α7 receptors from the desensitized state and slow additional desensitization, designated as Type II modulators [Gronlien et al. 2007]. By eliminating transitions into the desensitized state, Type II

PAMs exert a much greater effect on α7 receptor activation than agonists or PAMs that do not alter desensitization (Type I modulators).

In animal models, PNU-120596 can partially restore auditory gating deficits [Hurst et al. 2005], a common symptom of schizophrenia. Understanding the molecular mechanisms and structural determinants of PAM action could lead to the development of drugs for the treatment of a wide variety of neuropsychiatric disorders. For example, structural elements from cytisine and morphine guided the development of varenicline, a α4β2 partial agonist and α7 agonist that reduces drug-seeking behavior and consumption of nicotine [Mihalak et al. 2006].

To understand how different nAChR subtypes contribute to disease states, it is crucial to understand the molecular mechanisms by which these receptors couple the binding of agonists and PAMs to opening of the channel. Benzodiazepines, the archetypal positive allosteric modulators of GABA$_A$ receptors, induce conformational changes in the ligand-binding domain of GABA$_A$ receptors [Sharkey and Czajkowski 2008]. We have found that agonists of α7 receptors also induce structural transitions in the LBD, as measured by the substituted cysteine accessibility method (SCAM) [Lyford et al. 2003; McLaughlin et al. 2006; McLaughlin et al. 2007]. Based on the existing data, we hypothesize that PAMs and agonists cause similar but non-identical conformational changes.

Here, we used SCAM to compare changes in cysteine accessibility caused by PNU-120596 and ACh. We found that PNU-120596 induced conformational changes in the inner beta sheet, transition zone, and orthosteric site that were similar to those induced by ACh. These results show that PAMs and agonists share a conserved

47

molecular mechanism regardless of their action on receptor gating and independent of their initial binding sites. We have identified mutations that either eliminate or enhance allosteric modulation to the point of full agonism. Finally, we present evidence that PNU-120596 does not bind at the agonist-binding site.

Results

Figure 3.1 shows our homology model of the α7 nAChR derived from the structure of the *Lymnaea* AChBP [Brejc et al. 2001] and the regions of interest targeted in this study. W148 and W54 are located in the agonist-binding "pocket" (the orthosteric site). M37, N52, and M40 are located at the interface between subunits (the inner beta sheet), "below" the agonist binding pocket. These residues were previously shown to be good reporters of agonist-induced conformational changes [McLaughlin et al. 2007]. E44, N170, and E172 are located in the "transition zone" that couples the LBD to the TMD.

All mutants in this study contained the well-characterized leucine 247 to threonine (L247T or L9'T) mutation. L247T-containing α7 receptors have conductance and ion selectivity that are similar to the wildtype receptor, but are more sensitive to acetylcholine and exhibit slower macroscopic desensitization [Revah et al. 1991]. L247T is a good model system for our studies because its large current amplitudes allow us to measure modification rates for cysteine substitutions with decreased functional expression levels. All mutants also contained the C115A mutation, in which the single unpaired cysteine in the LBD is mutated to an alanine. This mutation, which has no effect on activation kinetics, ligand sensitivity, or ion

permeation, simplifies interpretation of cysteine modification experiments

[McLaughlin et al. 2006].
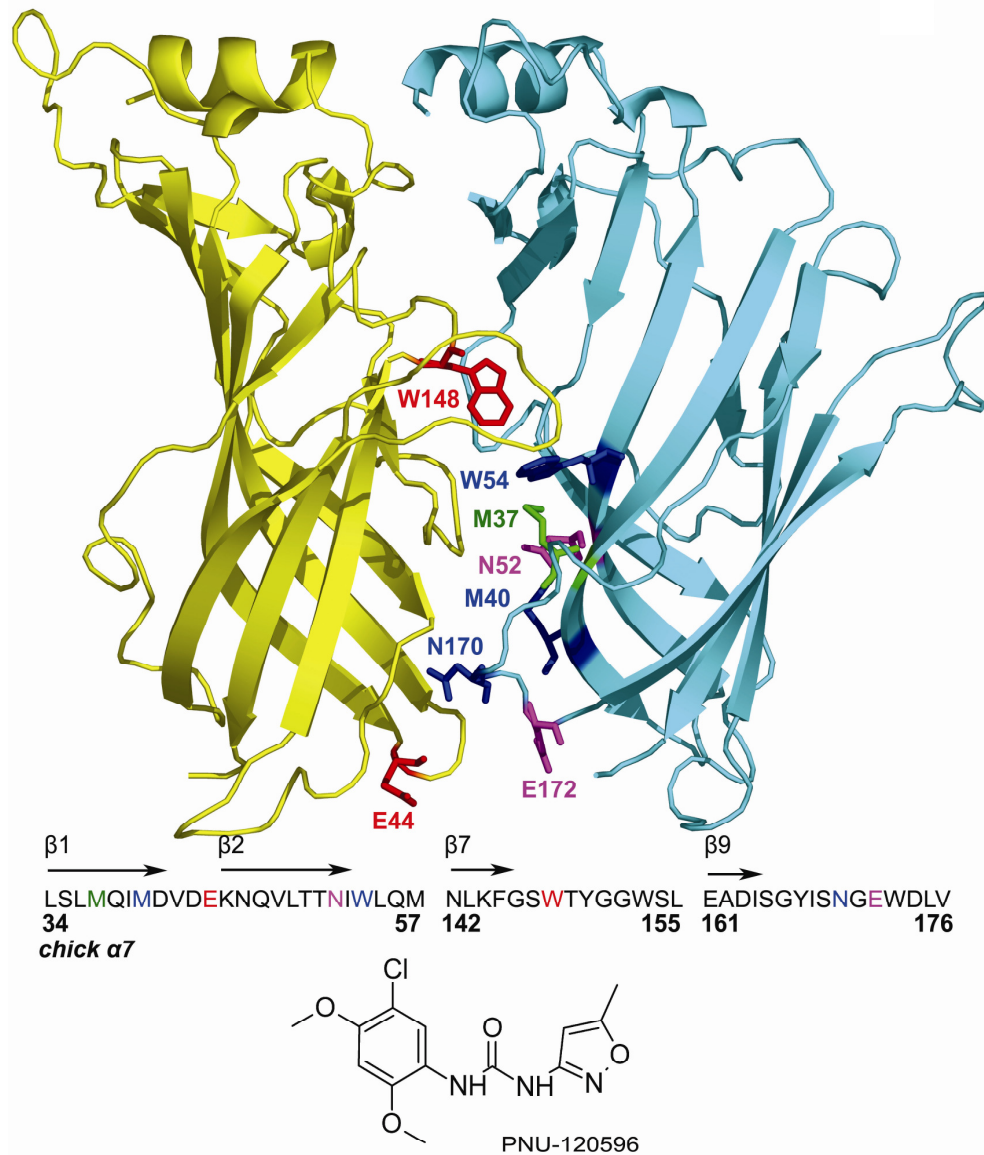
Figure 3.1: Homology model of the extracellular domain of α7 nAChR. A ribbon cartoon displaying two subunits of the pentameric receptor, viewed from the outside. The primary ACh-binding subunit is shown in yellow and the complimentary subunit is in cyan. Residues of interest are shown as sticks and are labeled on one of the two subunits for clarity. M37, M40, and N52 are part of the inner beta sheet (β1, β2, β6). E44, N170, and E172 are part of the transition zone (loop 2 and loop 9). W54 and W148 are part of the orthosteric (agonist-binding) site (β6, and behind the C loop). The residues of interest and the surrounding amino acid sequence is shown beneath the cartoon. The structure of PNU-120596 is shown below the chick α7 nAChR amino acid sequence.

We first examined if PNU-120596 acts as a positive allosteric modulator of C115A/L247T α7 receptors. PNU-120596 retained its modulatory effect in the C115A/L247T background, as measured by the ability to enhance ACh-evoked currents in a dose-dependent manner (**Figure 3.2A**). The concentration of PNU-120596 that elicited a half-maximal modulation (when applied with an EC_{30-50} concentration of ACh) was 257 ± 22 nM (**Figure 3.2A**), a value that is similar to that reported for wildtype α7 receptors (216 ± 64 nM; Hurst *et al.* 2005). This suggests that the C115A/L247T mutations do not significantly alter the affinity of PNU-120596 for the α7 nicotinic receptor.

PNU-120596 (1 μM) caused a left-shift of the ACh dose-response curve of C115A/L247T α7 receptors and a significant decrease in the EC_{50} for ACh (**Figure 3.2B, Table 3.1**). In contrast to the responses of wildtype α7 receptors [Hurst et al. 2005], PNU-120596 did not cause a significant change in the current amplitudes of C115A/L247T α7 receptors evoked at maximal ACh concentrations. We speculate that the L247T mutation increased the equilibrium gating constant of the receptors($K_{eq} = β/α$; **Figure 1.2**) [Colquhoun 1998], lowering the ACh EC_{50} compared to wild-type receptors. For receptors with a low gating constant (α >> β), such as wild-type α7 receptors, a PAM could increase the maximal response, decrease the EC_{50}, or both. In contrast, for receptors with a high gating constant (β >> α,) such as L247T-containing α7 receptors, we expect PAMs to affect EC_{50} alone, since the maximal response to agonist is already near 1 [Colquhoun 1998].
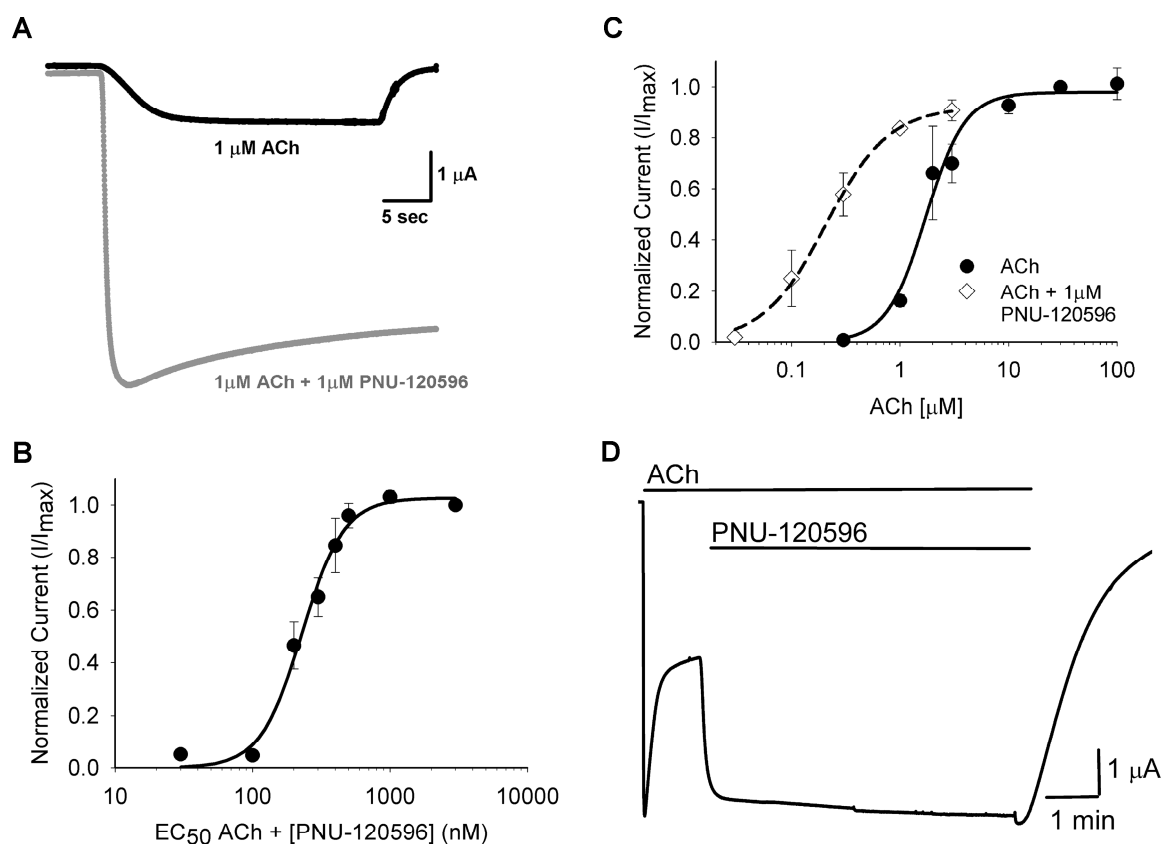
Figure 3.2: PNU-120596 is a positive allosteric modulator of C115A/L247T α7 receptor and elicits opening from a partially desensitized state. (A) A maximal dose of PNU-120596 (1μM) enhances ACh-evoked currents. Peak current amplitude increases approximately 81% with the addition of PNU-120596 to a fixed dose of ACh (1μM). Traces are from the same oocyte. (B) PNU-120596, at the concentrations shown, was applied with an ~EC_{50} dose of ACh (2-3 μM). Positive allosteric modulation was observed as a significant enhancement of ACh-evoked current (189 ± 18%, n=5). The EC_{50} for PNU-120596 was 257 ± 22 nM (n=5). (D) ACh was applied with an EC_{100} dose of PNU-120596 (1 μM). Positive allosteric modulation was observed as a significant reduction in the EC_{50} for ACh. (**Table 3.1**). Data are fit to the Hill equation and are the mean value ± S.E.M, normalized to the maximal value of the Hill equation fit of each data set. (D) A representative trace showing that an EC_{100} dose of PNU-120596 (1 μM) is sufficient to reactivate partially desensitized C115A/L247T receptors (n=5). Coapplication of ACh and PNU-120596 is also sufficient to completely inhibit desensitization, and responses are reversible when both compounds are washed out.

51

Table 3.1 - Summary of ACh dose response data

Mutant	ACh EC_{50} (µM)			I_{max} (µA)			Hill Coefficient			n	ACh EC_{50} + 1 µM PNU-120596 (µM)			n	Effect[+]
C115A/L247T background	2.4	±	0.23	6.4	±	0.64	2.8	±	0.25	10	0.22	±	0.09	(3)	PAM
Inner Beta Sheet															
M37C	4.5	±	1.30	0.4	±	0.12	1.3	±	0.10	10	1.6	±	0.18	(7)	No effect
M40C	6.7	±	0.70	2.2	±	0.47	1.4	±	0.11	16	0.58	±	0.17	(4)	PAM
N52C	0.79	±	0.20	0.31	±	0.08	0.68	±	0.07	13	N.D[‡]				
Transition Zone															
E44C	7.2	±	0.56	4.6	±	0.39	2.6	±	0.31	10	2.5	±	0.37	(3)	PAM
N170C[†]	12	±	1.4	1.3	±	0.24	1.6	±	0.12	15	2.6	±	0.56	(3)	PAM
E172C[†]	30	±	2.0	0.74	±	0.11	2.4	±	0.10	16	41	±	5.3	(3)	No effect
Agonist-Binding Site															
W54C	88	±	9.7	2.3	±	0.40	1.6	±	0.04	12	15	±	5.1	(5)	PAM
W148C[†]	205	±	28	3.5	±	0.52	1.5	±	0.06	11	N.D[‡]				

+ = based on statistically significant differences between ACh EC_{50} with and without 1 µM PNU-120596 (P<0.05)
† = denotes co-expression with human RIC-3 (see Methods)
‡ = value not determined because of agonism observed with PNU-120596

A unique feature of PNU-120596 is the ability to reactivate desensitized α7 receptors in the presence of agonist, a feature defined as Type II modulation [Hurst et al. 2005; Gronlien et al. 2007]. Therefore, we determined if PNU-120596 could reactivate C115A/L247T α7 receptors following slow desensitization. A representative trace is shown in **Figure 3.2C**. As expected, C115A/L247T receptors showed partial desensitization during continuous application of an EC_{100} concentration of ACh (100 µM, a maximally effective concentration), plateauing at $48.2 \pm 0.02\%$ desensitization by 87.5 ± 7.0 seconds (n=5). Then, application of an EC_{100} concentration of PNU-120596 (1 µM) after partial desensitization reactivated the C115A/L247T receptors (n=5), consistent with Type II modulation. The continuous application of ACh and PNU-120596 completely blocked slow desensitization of C115A/L247T receptors, as observed in wildtype α7 receptors [Gronlien et al. 2007]. The ability of PNU-120596 to reactivate partially desensitized C115A/L247T receptors and prevent subsequent desensitization did not depend on the ACh concentration, and the subsequent introduction of cysteine mutants into this background also did not alter the Type II modulation properties of PNU-120596 (data not shown). Furthermore, the reduction in receptor desensitization caused by the L247T mutation was not dramatically altered by the introduction of our cysteine mutations into this background (data not shown).We conclude that the C115A/L247T mutations do not alter the affinity or kinetics of PNU-120596 (**Figure 3.2A and 3.2C**), only the ability to enhance peak current amplitude (**Figure 3.2B**), which we attribute to enhanced gating of the C115A/L247T receptors. This interpretation is

supported by macroscopic and single-channel analysis, showing that effects on apparent desensitization by mutations at L9' in other Cys-loop receptors can be explained by increases in mean open time alone [Filatov and White 1995; Bianchi and Macdonald 2001]. Therefore, α7 receptors containing the C115A/L247T mutation are a reasonable model to examine conformational transitions underlying allosteric modulation by PNU.

For all of the cysteine mutations used in this study, we generated ACh concentration-response curves to probe for possible deleterious effects of the individually introduced cysteines on channel function. Most cysteine mutations generated ACh EC_{50} values that were not significantly different from the parent C115A/L247T receptor **(Table 3.1)**, suggesting that the introduced mutations were well tolerated. Two mutations at the orthosteric site (W54C and W148C), significantly increased the ACh EC_{50} compared to the parent C115A/L247T receptor, as expected for residues required for the binding of agonists or in close proximity to the binding site [Brejc et al. 2001]. Unexpectedly, we found that two mutants (N52C and W148C) were activated by PNU-120596 alone. The EC_{50} values for PNU-120596 activation were 340 ± 20 nM (n=3) and 450 ± 10 nM (n=3) for N52C and W148C mutant receptors, respectively. Our interpretation is that the N52C and W148C mutations enhance the ability of PNU-120596 to induce conformational changes such that it can directly gate these mutant receptors.

Because a binding site for divalent cation modulators has been proposed in the transition zone [Galzi et al. 1996], we also introduced mutations at positions E44 and E172 to test if the putative divalent cation binding site is required for modulation

54

by PNU-120596. We found that one mutation in the transition zone (E172C), and one mutation in the inner beta sheet (M37C), eliminated positive allosteric modulation by PNU-120596 (**Table 3.1**). These data provide evidence that M37 and E172 are required for binding of PNU-120596 and/or PNU-120596-induced changes in gating.

To explore conformational changes in α7 receptors evoked by PNU-120596, we examined PNU-120596-dependent changes in the rate of MTSEA modification of cysteines introduced in the LBD. The ability of ligands to alter the rate of MTS modification of introduced thiols is interpreted as (1) steric interference between the ligand and the MTS reagent, (2) a conformational change of the introduced thiol induced by that ligand that changes the surface accessibility of the thiol, and/or (3) a conformational change induced by the ligand in the environment near the introduced thiol that alters its local electrostatic environment [Akabas et al. 1992; McLaughlin et al. 2007].

It is important to note that SCAM measures the time-averaged conformational transition of the receptor, including closed, open, desensitized, and multiple intermediate states. Because the L9'T mutation increases the open time of α7 receptors [Revah et al. 1991; Filatov and White 1995], we assume that the conformational changes measured in the presence of ACh are dominated by those relating to activation over those relating to desensitization. However, we cannot rule the effects of our introduced cysteines and L247T on the conformational pathways associated with desensitization.

Figure 3.3 shows an example of the protocol used to measure the thiol

modification rate (E44C). **Figure 3.3A** shows an experiment from a single oocyte in

which a sub-maximal concentration of MTSEA (1 µM) was applied between test

applications of ACh (see Methods). The effect of covalent modification was a

decrease in ACh-evoked currents. **Figure 3.3B** shows an experiment in which 1 µM

PNU-120596 was preapplied and than coapplied with MTSEA (1 µM) between test

applications of ACh. For clarity, only the ACh-evoked currents that were used to

determine the rate of modification are shown. For each experiment, peak ACh-

evoked current amplitudes were plotted versus the cumulative time of exposure to

MTSEA (**Figure 3.3C**). Pseudo first-order rate constants obtained from the fits of the

data to a single exponential equation were divided by the concentration of MTSEA to

yield the second order rate constants (k_2) shown in **Table 3.2**.
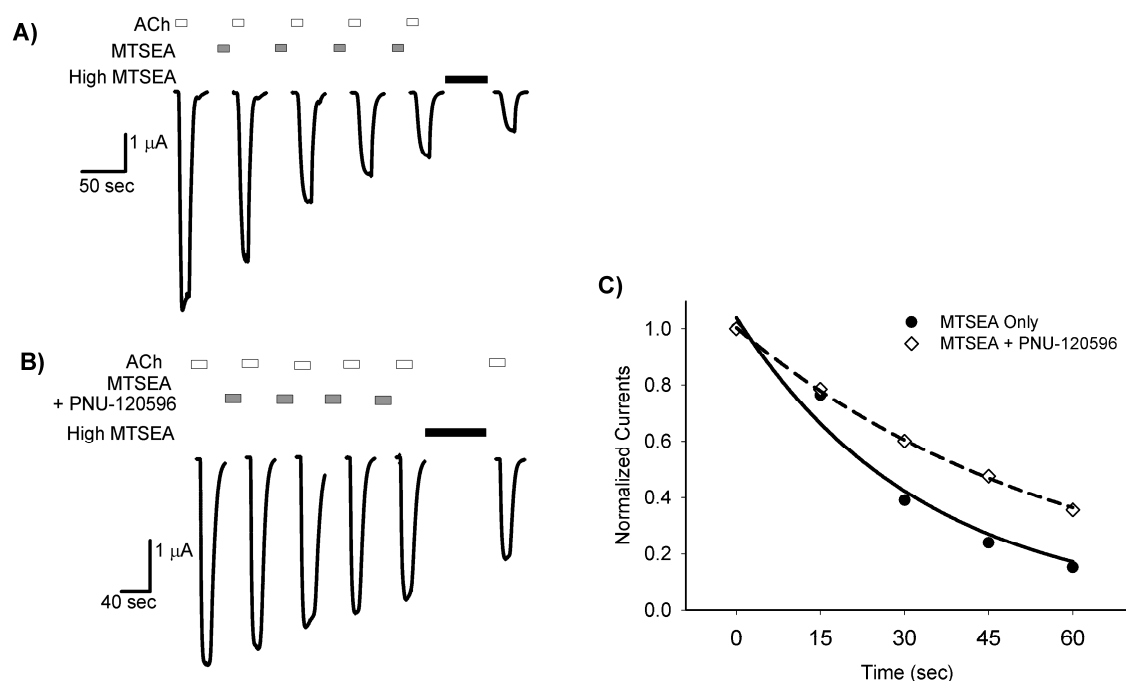
Figure 3.3: PNU-120596 slows the rate of MTSEA modification at E44C. (A) Successive ACh-evoked currents before and after the addition of a submaximal concentration of MTSEA (1 µM, 15 second exposures). After four successive applications, the endpoint of MTSEA modification was determined by a prolonged application of 500 µM MTSEA for 60 seconds. Washes of 1-2 minutes between drug applications are not shown. (B) The same protocol as (A), with a 30 second pre-exposure to 1 µM PNU-120596 followed by co-application of 1 µM PNU-120596 with MTSEA. (C). Normalized peak current amplitudes from a single experiment are plotted against cumulative MTSEA exposure. The calculated pseudo first-order rate constants from these experiments are 0.0299 sec^{-1} for control (A), and 0.0169 sec^{-1} in the presence of PNU-120596 (B). Second order rate constants (k_2) are calculated from these values and are displayed in **Table 3.2.**

Using this protocol, we determined the second order rate constants for

modification of three residues in the inner beta sheet (M37C, M40C, N52C). **Figure**

3.4A shows the mean second order rate constants measured in the presence of

MTSEA alone (control), MTSEA plus ACh, and MTSEA plus PNU-120596. PNU-

120596 and ACh each caused a 7-9 fold reduction in the modification rate of M37C

and a 5-7 fold reduction in the modification rate of M40C (**Figure 3.4B**). The

modification rates in the presence of ACh or PNU-120596 were significantly different

57

from control but were not significantly different from each other. Thus, without activating these receptors, PNU-120596 caused changes in the accessibility or electrostatic environment of M37C and M40C that were similar to those caused by ACh [McLaughlin et al. 2007]. PNU-120596 decreased the rate of modification of M37C, even though receptors containing this mutation were not positively modulated by PNU-120596 (**Table 3.1**). This result demonstrates that PNU-120596 can elicit conformational changes in the inner beta sheet in the absence of a modulatory effect. Because M37 or M40 are not part of the agonist-binding site, it is unlikely that steric interference between ligand and MTSEA is responsible for the decreased modification rates observed at these positions. In contrast, PNU-120596 did not cause a difference in the rate of modification of N52C (**Figure 3.4A and B**). Although ACh increased the rate of MTSEA modification of N52C [McLaughlin et al. 2007], PNU-120596 did not cause a significant change. Thus, PNU120596 caused some but not all of the changes in thiol accessibility in the inner beta-sheet caused by ACh. To verify that the conformational changes studied in L247T α7 receptors were similar to those in fast-desensitizing α7 receptors, we also studied cysteine accessibility of M40C constructed in the C115A background. This mutation was included because position C115 is the only solvent accessible cysteine in the LBD; mutation of this residue to alanine allows us to conclude that our rates of chemical modification are due ONLY to a reaction at the introduced cysteine. The rates of MTSEA modification of M40C/WT, with and without ACh, were similar as those measured in the C115A/L247T background (**Figure 3.8**). This suggests that the changes in accessibility we measure are independent of the C115A/L247T mutation.
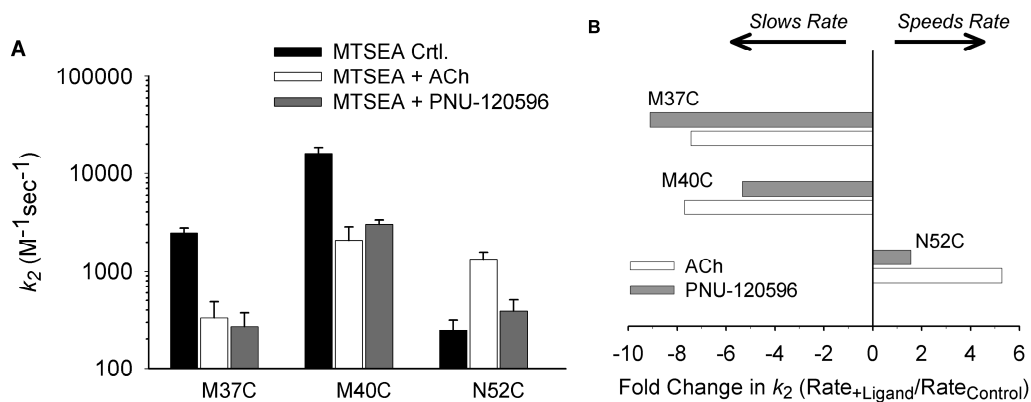
Figure 3.4: PNU-120596 differentially alters the rate of MTSEA modification at inner β sheet residues. (A) Mean second-order modification rate constants (k_2), calculated using the protocol outlined in **Figure 3**, at three residues in the inner beta sheet, M37C, M40C, and N52C. Mean values for MTSEA alone (control), MTSEA plus ACh, and MTSEA plus PNU-120596 are shown, plotted on a log scale. PNU-120596 slows the rate of modification at M37C and M40C compared to control but has no effect at N52C . * = Rate was significantly different from control (P<0.05). (B) A plot of the second order rate constant ratios. The average rate from each experimental condition is divided by the average control rate for each residue. Positive values represent an acceleration of the rate of modification and negative values represent a reduction in the rate of modification.

Table 3.2 - Second order rate constants for MTSEA modification of receptors carrying Cys substitutions in the extracellular domain of α7 nAChR.

Mutant	Control ($M^{-1}sec^{-1}$)			MTSEA + ACh ($M^{-1}sec^{-1}$)				MTSEA + PNU-120596 ($M^{-1}sec^{-1}$)				MTSEA + ACh + PNU-120596 ($M^{-1}sec^{-1}$)			
Inner Beta Sheet															
M37C	2470 ± 310		(12)	333 ± 152	*	(6)		271 ± 104	*	(7)					
M40C	16100 ± 2370		(15)	2090 ± 748	*	(5)		3030 ± 313	*	(5)					
N52C	250 ± 68		(8)	1320 ± 238	*	(9)		390 ± 118	‡	(4)					
Transition Zone															
E44C	33700 ± 6540		(8)	1460 ± 505	*	(8)		4180 ± 637	*	(5)		312 ± 19	*	(5)	
N170C	3160 ± 392		(7)	5730 ± 682	*	(7)		818 ± 114	*,‡	(10)		3660 ± 115		(4)	
E172C	12900 ± 1560		(9)	3450 ± 470	*	(6)		2830 ± 410	*	(7)		1710 ± 310	*	(7)	
Agonist-Binding Site															
W54C	9500 ± 1330		(6)	4030 ± 770	*	(5)		6080 ± 920		(4)					
W148C	45900 ± 7640		(9)	3010 ± 1100	*	(6)		8830 ± 1320	*	(6)					

* = Statistically different from Control (P<0.05).
‡ = Statistically different from + ACh (P<0.05)

Next, we determined the second order rate constants for the modification of three residues in the transition zone (E44C, N170C, and E172C). **Figure 3.5A** shows the mean second order rate constants measured in the presence of MTSEA alone (control), MTSEA plus ACh, and MTSEA plus PNU-120596. We observed differential effects of PNU-120596 in all three mutant receptors. PNU-120596 and ACh each decreased the rate of MTSEA modification of E44C by ~8-fold and ~21-fold, respectively (**Figure 3.5A and B**). PNU-120596 and ACh both decreased the rate of modification of E172C by 2-5 fold, even though receptors containing this mutation were not positively modulated by PNU-120596 (**Table 3.1**). This result demonstrates that PNU can elicit conformational changes in the transition zone without enhancing agonist-evoked currents. The rate of MTSEA modification of N170C was altered differently by PNU-120596 and ACh. PNU-120596 significantly decreased the rate of modification while ACh increased the rate of modification. Overall, these data show that PNU-120596 induces conformational changes at E44 and E172 that are similar to those induced by ACh, but PNU-120596-induced changes at N170 are different from those induced by ACh.

We also measured the combined effects of ACh plus PNU-120596 on MTSEA modification at introduced cysteines in the transition zone (E44C, N170C, and E172C). At E44C and E172C, the combination of PNU-120596 and ACh caused a larger effect than that caused by either ACh or PNU-120596 alone (**Figure 3.5, Table 3.2**). At N170C, PNU-120596 and ACh had opposite effects on the rate of MTSEA modification. The simultaneous application both reagents gave a rate of

MTSEA modification was not significantly different from control. In this respect,

combined effects of PNU-120596 and ACh lead to a net cancelation of each

individual effect.
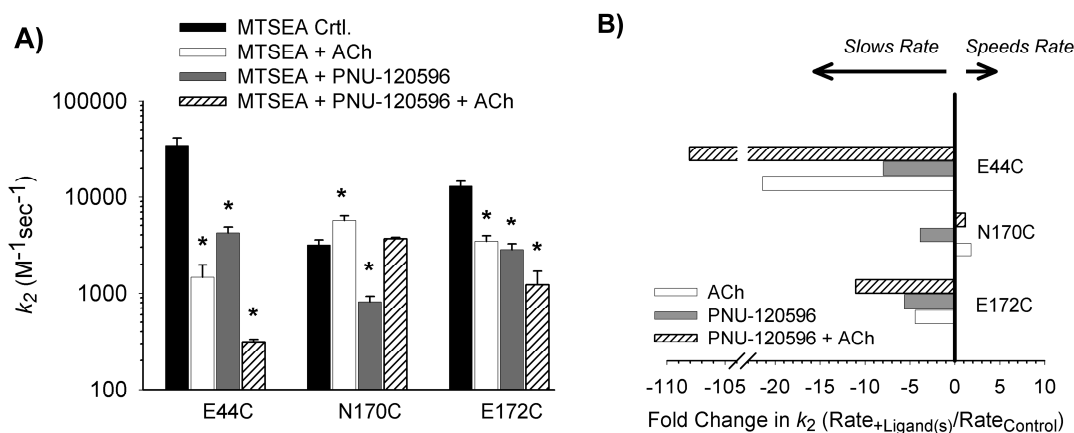
Figure 3.5: PNU-120596 differentially alters the rate of MTSEA modification at residues in the transition zone. (A) Mean second-order modification rate constants (k_2) of at three residues in the transition zone, E44C, N170C, and E172C. PNU-120596 significantly reduces the rate of modification at E44C and N170C. PNU-120596 significantly reduces the rate of modification at E172C, despite the lack of positive allosteric modulation at this residue (**Table 3.1**). At N170C, the rate of modification in the presence of PNU-120596 is significantly slower than in the presence of ACh. * = Rate was significantly different from control (P<0.05). (B) A plot of the second order rate constant ratios. Note that PNU-120596 slows the rate of modification of N170C while ACh increases the rate of modification.

Because the vestibule of the LBD of nicotinic receptors is predicted to be

highly electronegative [Unwin 2005], we also examined the rates of MTS

modification using anionic MTS reagents (**Figures 3.9-3.11**). We found that MTSEA

modified E44C much faster than MTSCE and MTSES (**Figure 3.10**), even after

accounting for the lower intrinsic rates of reaction by MTSCE and MTSES (**Figure

3.9**). In addition, the effect of ACh on the rate of MTSEA modification was much

greater than the effect of ACh on the rate of MTSCE modification. Modification of

M40C by either MTSES or MTSCE was too slow to measure (**Figure 3.11**). These

results provide additional evidence for a highly negative electrostatic environment lining the vestibule of nAChRs, and suggest that changes in the electrostatic environment affect modification rates at residues in the inner beta sheet and transition zone. This highly electronegative environment could serve to focus cations along the ion-permeation path of the inner vestibule. Additional "rings of charge" have been proposed at D97 (conserved in all nAChRs except α3/α6) [Hansen *et al.* 2008], and four negatively charged residues specific for the α7 nAChR (D41, D43, E44, and E172) in the transition zone could act as an α7-specific feature to enhance ion conductance.

Figure 3.6 shows second order rate constants of MTSEA modification of two residues in the orthosteric agonist-binding site (W54C and W148C). ACh slowed the rate of modification of W54C, which agrees with previously published results on wildtype α7 receptors [Gay et al. 2008]. However, PNU-120596 did not significantly reduce the rate of modification at W54C (**Figure 3.6A**). ACh and PNU-120596, acting as agonists (**Table 3.1**), both significantly slowed the rate of modification of W148C (**Figure 3.6A**). Since the aromatic side chains of W54 and W148 are both known to be part of the ligand-binding site, it is likely that steric occlusion by ACh is at least partially responsible for the slowing of modification of these Cys mutants. Slowing of modification of W148C by PNU-120596 could also be explained by steric hindrance, if PNU-120596 binds at unoccupied agonist binding sites, analogous to the binding site for benzodiazepines at the α-γ subunit interface of $GABA_A$ receptors [Gunther et al. 1995; Amin et al. 1997]. Acetylcholine (M_r=146) contains a positively charged choline group that makes π-cation interactions with the agonist-binding site

63

[Zhong *et al.* 1998]. PNU-120596 (M_r=312) is a amide analog flanked by isoxazole and chloro,dimethoxyphenyl groups [Hurst et al. 2005]. Recent evidence, however, suggests that PAMs of α7 receptors bind to sites in the TMD [Bertrand et al. 2008; Young et al. 2008], and thus slowing of W148C modification by PNU-120596 could be explained by an allosteric effect at the ligand-binding pocket, perhaps including partial closure of loop C.
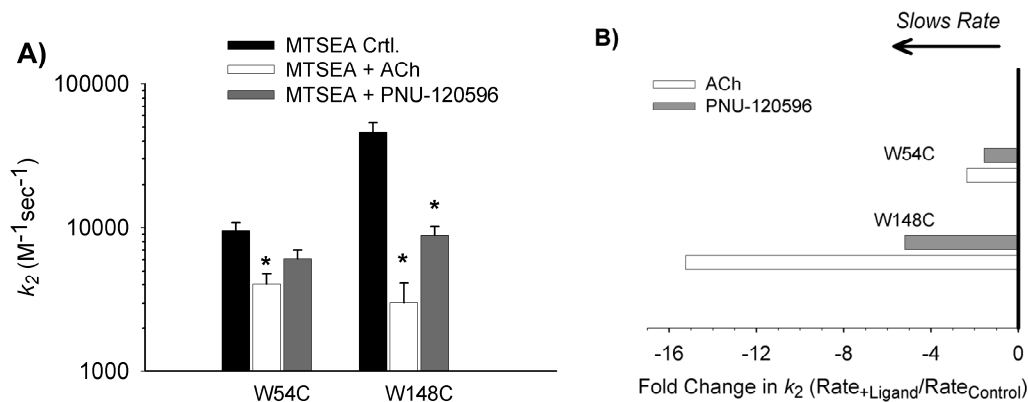
Figure 3.6: PNU-120596 slows the rate of MTSEA modification at W148C, but not W54C in the orthosteric site. (A) Mean second order rate constants (k_2) were calculated at two residues in the transition zone; W54C and W148C. * = Rate was significantly different from control (P<0.05). (B) A plot of the second order rate constant ratios.

To distinguish between these possibilities we took advantage of an unexpected observation: Introduction of W148C in the C115A/L247T parent receptor converted PNU-120596 from a positive allosteric modulator to a full agonist **(Table 3.1 and Figure 3.7A)**. The phenotype of this receptor is useful because it allows us to compare the effects of covalent modification with MTS reagents on either ACh- or PNU-120596-evoked gating at the well-defined agonist-binding site. If PNU-120596 activates the receptors via binding to the orthosteric agonist binding site, we expect that covalent modification of W148C in the agonist binding pocket to disrupt

64

activation by both ACh and PNU-120596 similarly via steric effects on ligand binding. If PNU does not activate W148C mutants by binding at the agonist binding site than PNU-evoked currents should be less sensitive to covalent modification of W148C then ACh-evoked currents. For these experiments, we used two MTS reagents of different size and charge to determine moiety-dependent affects on ACh and PNU-evoked current at W148C. MTSEA adds a positively charged ethyl amine to thiols at physiological pH, and is comparatively small. MTSEA-biotin adds a neutral, bulky ring structure to thiols and is comparatively large.

Figure 3.7B shows representative ACh- and PNU-120596-evoked currents before and after modification of W148C by MTSEA (100 µM for 60 seconds). This exposure to MTSEA was sufficient to completely eliminate ACh-evoked current, but it had no effect on currents evoked by PNU-120596. If we assume that modification of a binding site residue interferes with activation by steric interference with ligand, than this result implies that PNU-120596 activates receptors via a site distinct from the orthosteric site. However, an alternative explanation is that the two ligands interact with a different set of "contact points" in the binding pocket, and those for PNU-120596 are removed from the ethyl amine adduct at W148. To test this, we examined the effect of MTSEA-biotin, which modifies the thiol with a bulky ring structure. **Figure 3.7C** shows representative ACh- and PNU-120596-evoked currents before and after modification of W148C by MTSEA-biotin (4 µM for 60 seconds). This exposure of MTSEA-biotin was sufficient to reduce ACh-evoked current by 70%, but had no significant effect on the magnitude of currents evoked by PNU-120596. Modification of the agonist binding site by MTSEA-biotin slowed the

kinetics of PNU-120596-dependent activation (**Figure 3.7C**), suggesting that there

are allosteric conformational changes at the agonist binding site during activation by

PNU-120596. The results from multiple experiments are summarized in **Figure**

3.7D. Covalent modification of W148C by MTSEA and MTSEA-biotin had a

significantly greater effect on ACh-evoked current than on PNU-120596-evoked

currents ($P<0.01$). This observation provides evidence that, while behaving as an

agonist, PNU-120596 does not interact with the agonist-binding site of α7 receptors.

Our interpretation is that PNU-120596 induces conformational changes at the

agonist-binding site through allosteric mechanisms, rather than steric occlusion,

because occlusion is predicted to impair both ACh and PNU-evoked currents

similarly.
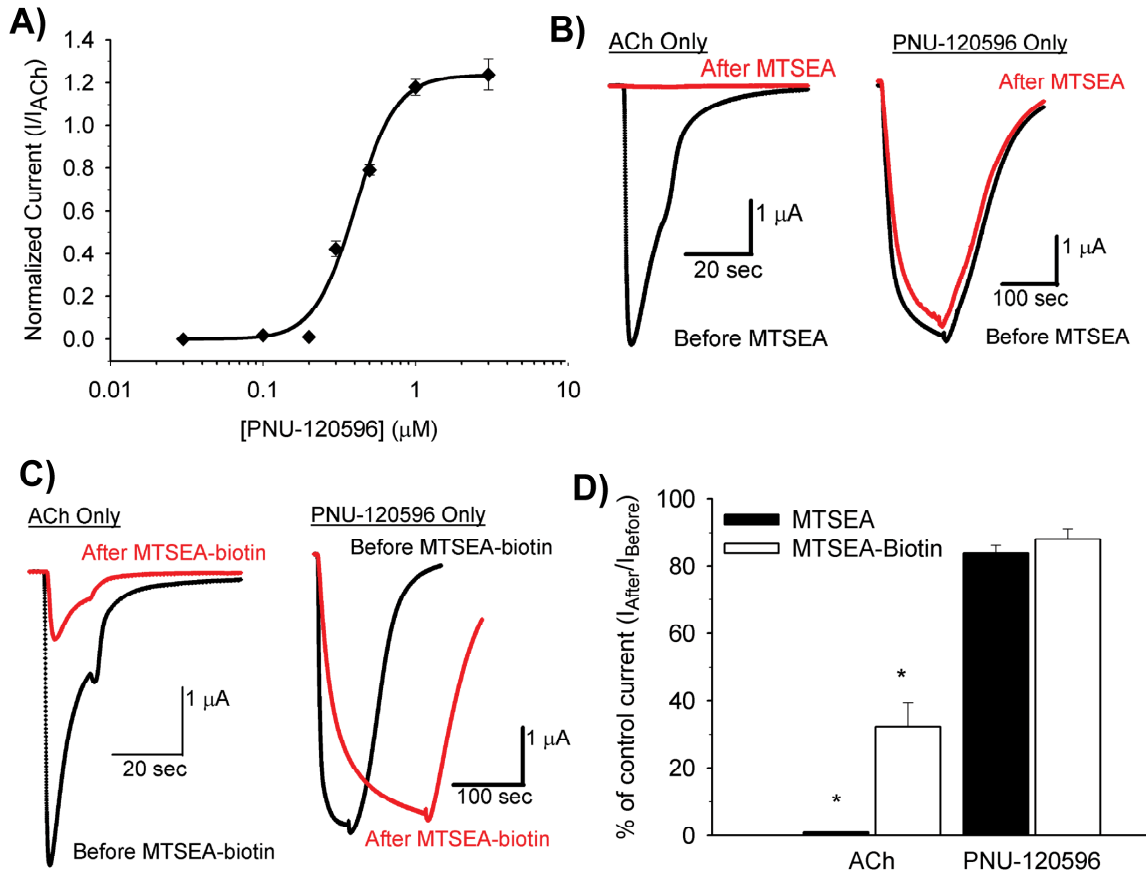
Figure 3.7: Covalent modification of W148C in the orthosteric site does not affect agonism by PNU-120596. (A) PNU-120596 acts as a full agonist of W148C/C115A/L247T α7 receptors. Hill parameter fits for activation by ACh are in **Table 3.1**. For PNU-120596, the EC_{50} is 0.45 ± 0.01 μM, Imax is 3.87 ± 0.65 μA, and Hill Coefficient = 6.79 ± 0.81 (n=3). PNU-evoked currents are normalized to peak ACh-evoked current (I/I_{ACh}).(B) Representative traces for 3 mM ACh and 3 μM PNU-120596 shown before (black) and after (red) application of 100 μM MTSEA for 60 seconds. (C) Representative traces for 3 mM ACh and 3 μM PNU-120596 shown before (black) and after (red) application 4 μM MTSEA-biotin for 60 seconds. (D) Summary data for the effects of covalent modification of W148C with MTSEA (n=8) and MTSEA-biotin (n=10) on ACh and PNU-evoked currents. Bars represent the percentage of ACh or PNU-evoked current after MTS modification relative to the control currents before modification (I_{after}/I_{before}). Both MTSEA and MTSEA–biotin caused a significantly greater reduction in ACh-evoked currents than PNU-evoked currents (* P<0.01).

Discussion

In this study, we provide evidence that the positive allosteric modulator PNU-120596 causes conformational changes in the LBD of α7 nicotinic receptors that partially overlap with those caused by ACh. We focused on mapping the structural transitions of PAMs in three regions of the LBD: 1) The inner beta sheet, 2) the transition zone, and 3) the orthosteric site (**Figure 3.1**). A homology model of the LBD of the α7 receptor, based on the structure of AChBP, was used to guide our experiments [Brejc et al. 2001; Lyford et al. 2003].
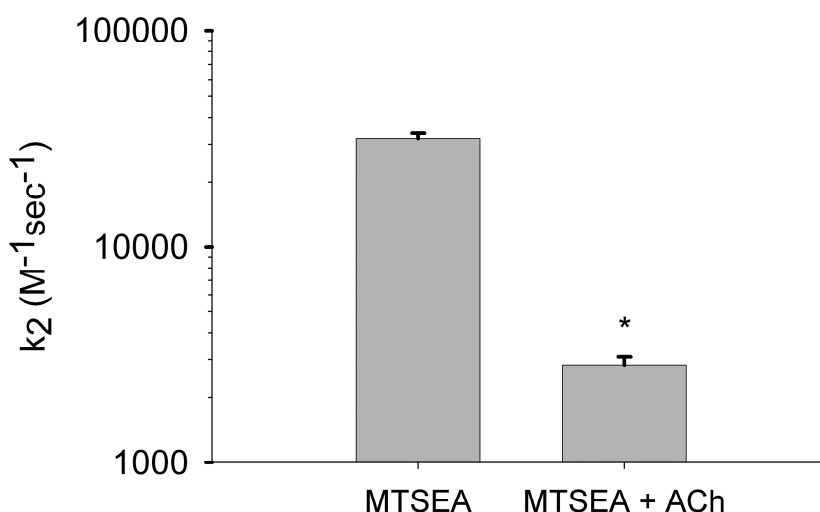
Figure 3.8: ACh reduces the rate of MTSEA modification in M40C/C115A α7 receptors. MTSEA modification experiments were performed as described in the Methods section. The rate of MTSEA modification of M40C/C115A in the absence of ACh was 31900 ± 2830 M^{-1}s^{-1} (n = 5), and the rate of modification in the presence of ACh was 1830 ± 261 M^{-1}s^{-1} (n = 4). ACh significantly reduces the rate of MTSEA modification by approximately 18-fold (P < 0.001), similar to M40C/C115A/L247T receptors (Table 2).

The inner beta sheet, comprised of the β1, β2, and β6 strands, resides at the interface between two subunits (**Figure 3.1**). In this study, we found that PNU-120596 caused reductions in the rate of modification of M37C and M40C that were similar to those caused by ACh (**Figure 3.4, Table 3.2,** [McLaughlin et al. 2007]).

68

The similarity in the effects on cysteine modification at M37C and M40C suggests that PAMs and agonists induce similar conformational changes in the LBD of α7 receptors. We have provided the first evidence that PAMs of α7 receptors enhance gating by causing some of the same structural transitions in the LBD as ACh.
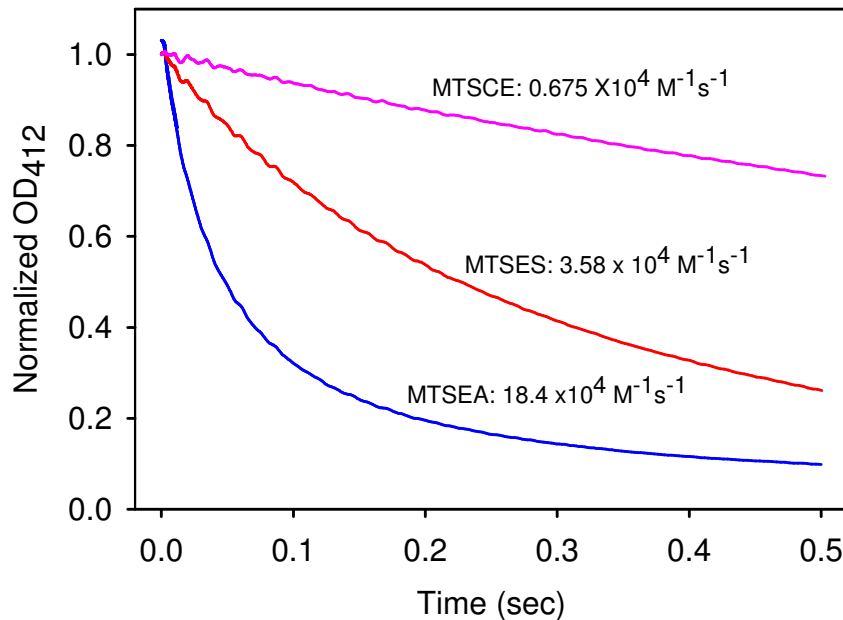
Figure 3.9: Intrinsic reaction rates of charged MTS reagents. Comparison of the rates of modification of 5-Thio-(2-nitrobenzoic acid) (TNB) by MTSEA, MTSES, and MTSCE. 5,5'-Dithio-bis(2-nitrobenzoic acid) (DTNB) was dissolved in Tris buffer (100 mM Tris HCl, pH 8.0) and was reduced to TNB with DTT immediately before the MTS modification assay (0.5 mol DTT per mol DTNB). Modification of TNB by MTS reagents was measured as a decrease in OD_{412} with a stopped-flow spectrophotometer as described (Karlin and Akabas, 1998, Meth. Enzymol 293, 123-145). The intrinsic rate of modification of NTB by MTSEA was 5-fold faster than by MTSES and was 27-fold faster than by MTSCE.

The transition zone, comprised of loops from the LBD (loop 2, loop 9, and the Cys loop) and the TMD (pre-M1 sequence and M2-M3 linker), is positioned to convey structural rearrangements caused by agonist binding in the LBD to the channel gate in the TMD [Bouzat et al. 2004]. Therefore, we examined the effect of PNU-120596 on the rate of MTSEA modification at three reporter residues within the transition zone (E44C, N170C, and E172C), which is also a proposed site of

modulation by divalent cations [Galzi et al. 1996]. PNU-120596 reduced the rate of

MTSEA modification at all three positions (**Figure 3.5, Table 3.2**). At N170C, PNU-

120596 decreased the accessibility of the substituted cysteine whereas ACh caused

an increase. The application of both compounds offset each other at N170C.

Overall, the changes in cysteine accessibility in the transition zone caused by ACh

and PNU-120596 were similar but not identical.
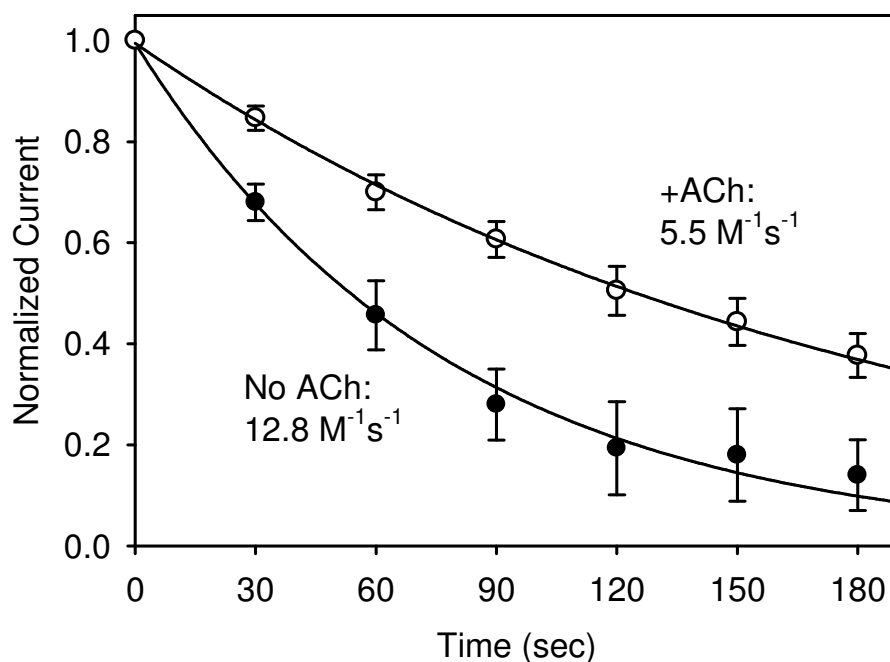
Figure 3.10: MTSCE modifies E44C at a slower rate than MTSEA, and ACh slows the rate of modification. n=3 for both data sets. The rate of modification by MTSCE in the absence of ACh (12.8 $M^{-1}s^{-1}$) was 2,500-fold slower than by MTSEA (33,700 $M^{-1}s^{-1}$; Table 2). After adjusting for the faster intrinsic modification rate of MTSEA (**Figure 3.9**), the modification of E44C by MTSCE was 180-fold slower than by MTSEA, indicating a strongly negative electrostatic environment surrounding E44C. ACh slowed the modification of E44C by MTSCE 2.3-fold, whereas ACh slowed the modification by MTSEA 23-fold (Table 2). This difference suggests there are electrostatic differences in the unliganded and agonist-bound conformations.

Interestingly, positive modulation of ACh-evoked currents by PNU-120596

was lost in the E172C mutant (**Table 3.1**), but PNU-120596 still caused a decrease

in thiol accessibility at this position (**Figure 3.5**). One explanation is that the PNU-120596 binding site includes E172, and the introduced cysteine (E172C) eliminates allosteric modulation but not binding. In this scenario, the observed reduction in the rate of MTSEA modification at E172C is due to physical occlusion by PNU-120596 of the substituted cysteine at the putative binding site. An alternative explanation is that PNU-120596 binds to a site outside of the transition zone, away from E172, and the observed reduction in the rate of E172C modification is due to conformational changes induced there. In this scenario, the binding of PNU-120596 is unaffected and can still induce conformational changes, but the electrostatic coupling within the transition zone [Xiu et al. 2005] is sufficiently disrupted by the cysteine mutation that the induced conformational changes no longer enhance receptor gating.

Lastly, we examined the effect of ACh and PNU-120596 on the rate of MTSEA modification at two residues in the orthosteric site (W54 and W148) (**Figure 3.6**). Structurally, these residues occupy two distinct locations within the agonist binding site. W148 is part of the principal subunit (**Figure 3.1, yellow subunit**). It lines the back wall of the agonist binding site and makes contact with agonists and competitive antagonists [Celie et al. 2004; Hansen et al. 2005]. W54 is part of the complimentary subunit and sits on the edge of the agonist binding site (**Figure 3.1, cyan subunit**) [Brejc et al. 2001]. ACh reduced the rate of MTSEA modification at these positions. In our interpretation, ACh reduces covalent modification at W148C by physically blocking access to the introduced cysteine. On the other hand, since carbamylcholine does not contact W54 [Celie et al. 2004], we hypothesize that ACh induces a short-range conformational change that makes W54C less accessible to

covalent modification. The ACh-dependent effect at W54C agrees with previously published work on wildtype α7 receptors [Gay et al. 2008]. PNU-120596 does not significantly affect the rate of MTSEA modification at W54C, but reduced the rate of MTSEA modification at W148C, suggesting that PNU-120596 induces allosteric conformational changes in the center of the agonist binding pocket, but not on the periphery.
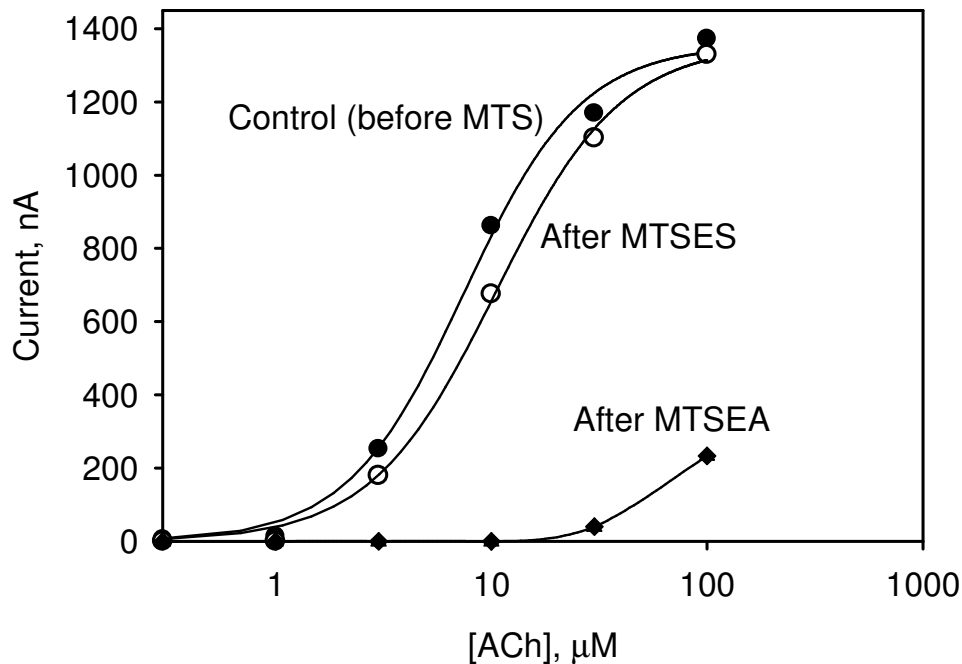
Figure 3.11: MTSES modification of M40C is very slow. Responses following an exposure to MTSES (1 mM, 3 min) were not significantly different from the control responses (n=4). After MTSES exposure, subsequent exposure to MTSEA (1 mM, 3 min) caused a maximal inhibition as observed previously (McLaughlin et al., 2007), indicating that the cysteine thiol was not modified by the previous exposure to MTSES. Modification by MTSCE of M40C was also too slow to measure (not shown). Thus, the modification of M40C by anionic modifiers is dramatically slower than by the cationic MTSEA, indicating a strongly negative electrostatic environment around M40.

Unexpectedly, we found that PNU-120596 was a full agonist of W148C receptor in C115A/L247T-containing α7 receptors (**Figure 3.7A**). One explanation is that the introduced cysteine allowed partial closure of the C-loop and lowered the

activation energy sufficiently to allow PNU-120596 to activate the receptor, while at the same time increased energetic barriers to ACh binding. The C-loop is a dynamic and flexible region that acts as a hinge of the orthosteric site [Hansen et al. 2005; Venkatachalan and Czajkowski 2008]. The EC_{50} for ACh-dependent activation of the W148C mutant receptor was increased ~100-fold (**Table 3.1**), as expected for a receptor with a mutation of an important aromatic residue of the agonist-binding pocket [Brejc et al. 2001]. We took advantage of this phenotype to test if PNU-120596's ability to alter cysteine accessibility was due to allostery or steric occlusion. Because ACh-evoked currents are more sensitive to covalent modification by different MTS reagents than PNU-evoked currents (**Figure 3.7**), we conclude that PNU-120596 induces conformational changes at this position through an allosteric mechanism. Consistant with this, a chemically-related PAM (NS-1738) does not affect equilibrium binding of [125I]α-bungarotoxin, also suggesting that it does not interact with the agonist binding site [Timmermann *et al.* 2007]. Recent work with chimeric α7 nAChR/5-HT$_3$ receptors and mutagenic studies suggests a binding site in the transmembrane domain for PNU-120596 and LY-2087101 [Bertrand et al. 2008; Young et al. 2008]. These data suggest that PNU-120596 and other modulators of α7 receptors bind at a conserved site within the transmembrane domain and cause conformational changes in the LBD to enhance gating of the receptor.

Table 3.3 - Comparison of α7 nAChR expression with and without RIC-3

Mutant	Without RIC-3			With RIC-3		
	EC_{50} (μM)	I_{max} (μA)	n	EC_{50} (μM)	I_{max} (μA)	n
M37C	4.5 ± 1.3	0.4 ± 0.12	10	5.2 ± 0.33	0.84 ± 0.06	3
W148C	N.R[‡]	-	4	205 ± 28	3.5 ± 0.52	11
N170C	12 ± 1.0	0.11 ± 0.03	5	12 ± 1.4	1.3 ± 0.24	15
E172C	39 ± 3.4	0.11 ± 0.02	5	30 ± 2.0	0.7 ± 0.11	16

[‡] = No measurable response (up to 10 mM ACh)

In the MWC model of allostery, positive allosteric modulators of ligand-gated ion channels enhance activation by stabilizing the protein in the open state. [Bertrand and Gopalakrishnan 2007]. Our results provide the first evidence that that PNU-120596 promotes activation of α7 receptors by causing some (but not all) of the same conformational changes in the LBD associated with agonists. We have previously shown that permeable divalent cations, which do not alter desensitization, also induce conformational changes in the LBD that are similar to those induced by agonists [McLaughlin *et al.* 2009]. Our work adds to a growing body of literature of both convergent and divergent conformational changes during gating of Cys-loop receptors [Chang and Weiss 2002; Pless et al. 2007; Sharkey and Czajkowski 2008].

Recent work suggests that the mechanisms of closed-to-open conformational changes induced by different agonists and of unliganded receptors are completely conserved regardless of the agonist applied; only the kinetics of the C-O transitions are affected [Purohit and Auerbach 2009]. While most of our data with PNU-120596 agrees with this idea, modulation and rate measurements for the N170C mutant

seem to be an exception. For this mutant, PNU-120596 slows the rate of

modification while ACh increases it (**Figure 3.5**). Thus, each ligand stabilizes a

population of conformational intermediates that are distinct from each other and from

the resting unliganded state(s). A model in which C-O transitions occur via a single

pathway, where agonists and PAMs can only change the forward or reverse rates

(**Figure 1.5**), would predict that PNU-120596 and ACh would cause similar changes

in accessibility at all residues. Our results conclusively show that PNU-120596 can

alter the α7 receptor in the absence of the C-O gating transition (**Figure 3.4-3.6**). If

there is a single path, then the observation that PNU-120596 causes a change in

accessibility of N170C opposite to that caused by ACh suggests that the receptor

would be stabilized in closed intermediate states further away from the open state,

and PNU-120596 would be unable to enhance the conserved C-O transition. But

PNU-120596 still acts as a positive allosteric modulator of N170C receptors,

suggesting that PNU-120596 induces conformational changes along alternative

pathways that lower energetic barriers to activation and lead to positive modulation.

The differences between the conformational intermediates induced by PNU-120596

and those induced by ACh are likely to be subtle, as they are not as apparent at

other cysteine mutants.

In conclusion, we have shown that PNU-120596 and ACh induce a set of

overlapping structural transitions in the extracellular ligand-binding domain. Our

results indicate that PAMs such as PNU-120596 enhance gating of ligand-gated ion

channels by inducing some of the same structural transitions caused by agonists. In

addition, we have identified mutations in the transition zone that eliminate

modulation of α7 nicotinic receptors by PNU-120596 via decoupling between the LBD and TMD. We have provided evidence that PNU-120596 does not bind to unoccupied agonist-binding site(s). The PAM-induced changes in receptor kinetics, while not usually sufficient to activate receptors, would lower the energy barriers to agonist-induced activation by both enhancing the agonist-evoked C-O transitions and unique transitions. This process would "prime" the receptors to undergo a gating transition, allowing more of the energy of agonist binding to drive changes in the conformational equilibrium towards activation [Jackson 1989].

CHAPTER 4

PERMEABLE DIVALENT CATIONS AND ACETYLCHOLINE CAUSE SIMILAR GATING TRANSITIONS IN THE EXTRACELLULAR LIGAND-BINDING DOMAIN OF THE α7 NICOTINIC RECEPTOR

Introduction

Allosteric modulation of membrane receptors is increasingly recognized as a common mechanism used to control cellular signal transduction [Lena and Changeux 1993; Gao and Jacobson 2006]. In general, allosteric modulator binding causes changes in the response of the receptor to the "native ligand", presumably by altering the energetic barrier between resting and activated conformations. In most cases the modulator does not activate the target receptor in the absence of agonist. While there has been substantial progress in identifying the binding sites for many allosteric modulators (for example, [Sigel 2002]), the mechanisms by which modulators induce their effects remain poorly defined.

Some of the best examples of allosteric modulation involve members of the Cys-loop family of ligand-gated ion channels that includes nAChRs as well as the $GABA_A$, glycine, and 5-hydroxytryptamine-3 receptors [Changeux and Taly 2008]. Cys-loop receptors transduce the energy of agonist binding into conformational changes that lead to channel opening [Sine 2002]. All family members share a similar structure: they are transmembrane proteins assembled from five homologous or identical subunits. Each of these subunits is comprised of a large amino terminal extracellular domain (LBD), a large intracellular loop, and a four α-helix bundle forming a transmembrane domain (TMD). Recent studies aimed at identifying the structural basis for ligand gating have focused on the "transition zone" [Gay and Yakel 2007] a region of the receptor at the boundary between the LBD the TMD. The transition zone includes structural elements thought to link the TMD and the ligand binding site [Lee and Sine 2005; Lummis et al. 2005; Mukhtasimova et al.

2005]. While the evidence for this linkage is preliminary, a number of experimental

approaches have unequivocally mapped the site for ligand binding to the interface of

adjacent subunit LBDs [Sine 2002]. More recently, the crystal structures of ACh-

binding proteins (AChBPs) from *Lymnea*, *Aplysia,* and *Bulinus* [Brejc et al. 2001;

Celie et al. 2004; Celie et al. 2005] have provided a structural context for these

biochemical and functional studies. The AChBPs are soluble proteins that act as

ACh buffers in invertebrates [Smit et al. 2001]; they share both sequence and

functional homology to the LBD of Cys-loop receptors. Recently, two structures of

homologous bacterial ligand-gated ion channels were added to the structural

database of Cys-loop receptors [Hilf and Dutzler 2008; Bocquet et al. 2009; Hilf and

Dutzler 2009]. These crystal structures have been used to develop and refine

homology models of Cys-loop receptors [Le Novere et al. 2002; Unwin 2005]. Our

goal is to use these refined models to test specific mechanistic hypotheses that

attempt to explain the dynamics of both ligand-induced receptor activation and

allosteric modulation [Kash *et al.* 2003; Lee and Sine 2005; Lummis *et al.* 2005;

Mukhtasimova *et al.* 2005].

Many neuronal nAChRs exhibit positive allosteric modulation by physiological

concentrations of Ca^{2+} [Mulle et al. 1992; Vernino et al. 1992]. In α7 nAChRs (but

not other nAChRs) Ba^{2+} or Sr^{2+} can elicit effects similar to Ca^{2+} [Vernino et al. 1992;

Galzi et al. 1996; Eddins et al. 2002a; Eddins et al. 2002b]. This modulation

consists of an increase in both the efficacy and the potency of ACh. The functional

effects of divalents are similar to those caused by an emerging class of nicotinic

modulating drugs collectively referred to as PAMs (positive allosteric modulators;

[Dani and Bertrand 2007]). Thus one rationale for a mechanistic characterization of divalent modulation of α7 nAChRs is to serve as a model for studies of drugs such as PAMs developed to elicit a similar effect.

Previous studies demonstrated that the modulation of α7 nAChRs by divalent cations is independent of divalent cation permeation, suggesting that the binding site for modulation is extracellular [Eddins et al. 2002b]. In addition, several studies have demonstrated the importance of conserved LBD glutamate residues (E44 and E172 in chick α7) in divalent cation modulation, and it has been suggested that these may form the allosteric modulation-binding site [Galzi et al. 1996; Le Novere et al. 2002; Lyford et al. 2003]. In this paper, we tested the hypothesis that conformational changes evoked by divalent cation modulators of the α7 receptor are similar to those evoked by ACh. In addition, we examined whether E44 and E172 are required for divalent cation-evoked conformational changes. We found some similarities between Ba^{2+} evoked conformational changes and those caused by ACh. Surprisingly, we also found that the effects Ba^{2+} on modification rates did not require E44 or E172, suggesting that these residues do not form the divalent cation binding site.

Results

The substituted cysteine accessibility method (SCAM) is an established experimental approach to examine protein conformational dynamics [Karlin and Akabas 1998]. We previously used this approach to scan regions of the chick α7 receptor and identified residues where the rates of thiol-specific modification by MTSEA were altered by ACh [Lyford et al. 2003; McLaughlin et al. 2007]. We consider two alternative mechanisms for ACh-dependent effects on modification rates. If the substituted cysteine is at a position that is part of the agonist binding site [Sine 2002], than the effect of ACh could be due to steric occlusion. Alternatively, if the substituted cysteine is not near the binding site, than we infer that a change in modification rates is a result of conformational or electrostatic change induced by agonist-dependent activation. In this way, these residues serve as reporters of intramolecular changes during receptor activation.

SCAM can be used in the same way to identify conformational changes caused by allosteric modulators. **Figure 4.1** shows a representation of the region of the α7 receptor LBD targeted in this study. A discrete region of the inner β sheet, including M37, M40, and N52 was initially chosen to examine the effects of the divalent cation Ba^{2+} on MTSEA modification rates. We also examined the effects of Ba^{2+} at transition zone residues previously implicated in modulation by divalent cations, including E44, E172, as well as an adjacent position N170. All of the cysteine replacements at these residues have previously been shown to exhibit agonist-sensitive MTSEA modification rates, allowing us a basis for comparison for the effects of Ba^{2+}.

81

For these studies we began by confirming the modulatory effects of Ba^{2+} on

ACh-dependent activation of our parental phenotype, containing the C115A/L247T

mutations. Wild-type α7 nAChRs exhibit a complex positive modulation by divalent

cations such as Ca^{2+} or Ba^{2+} that includes increases in both efficacy and potency

[Galzi et al. 1996]. In contrast, receptors with the L247T phenotype typically exhibit

a simplified modulatory response consisting only of a 5- to 10-fold left shift in the

ACh dose-response. The C115 position is the only accessible cysteine in the LBD,

and mutation to C115A simplifies our interpretation of MTSEA modification at

introduced cysteines.

Figure 4.2A shows the effect of 10 mM Ba^{2+} on the α7 C115A/L247T receptor.

There was a leftward shift in the dose-response curve corresponding to a ~ 10-fold

decrease in EC_{50} (increase in potency). Of note, we do not see an effect of Ba^{2+} on

efficacy in the parental background. We suspect this is due to the higher gating

constant of receptors with the L247T mutation. **Figure 4.2B** shows that modulation

by Ba^{2+} was eliminated in the E44C mutant, confirming that this conserved

glutamate is required for Ba^{2+} binding or allosteric coupling of Ba^{2+} binding to ACh-

dependent activation. This result is similar to the effect of an E44Q mutant

described in wild type and $L^{247}T$ α7 nAChRs [Galzi et al. 1996; Eddins et al. 2002b].

Table 4.1 provides a compilation of EC_{50}'s, modulatory effects of 10 mM Ba^{2+}, and

the maximal responses of the mutants described in this report. Neither of the

transition zone glutamate mutants (E44C and E172C) exhibited a positive

modulation, while the N52C mutant displayed a high partial agonism by Ba^{2+} in the

absence of ACh.
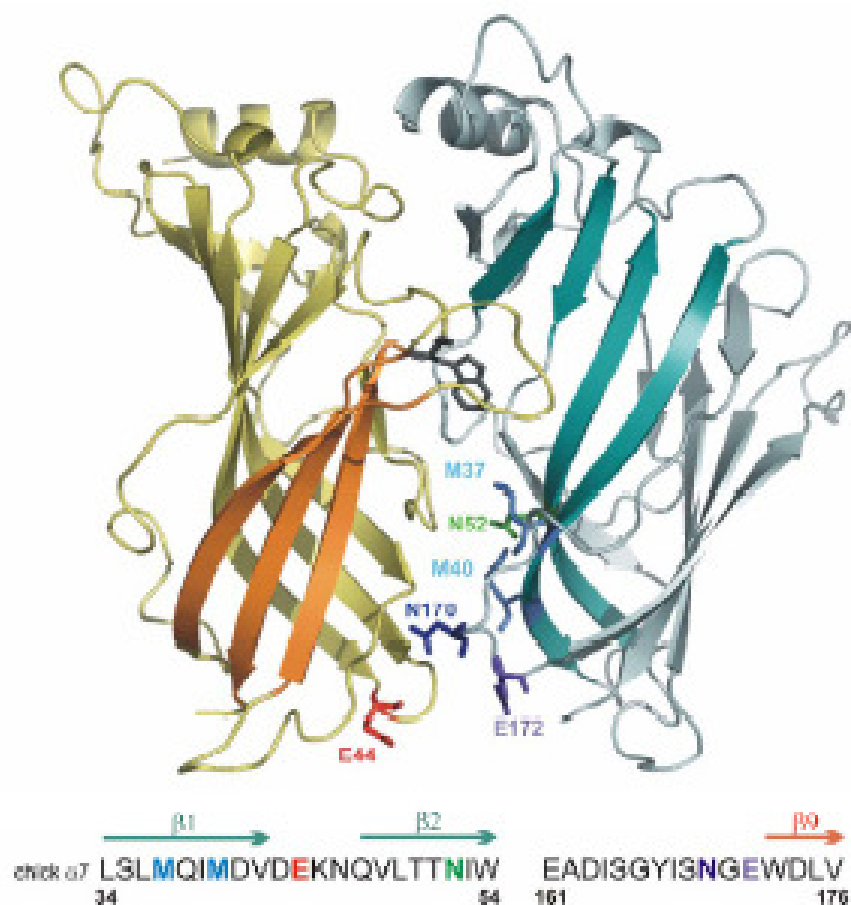
Figure 4.1: A model of the α7 AChR extracellular domain. Ribbon cartoon showing two of the five subunits viewed from the outside. In the subunit to the left of the central interface (yellow), the outer β sheet in is highlighted in orange, the transition zone E^{44} residue is orange, and the W^{148} residue is shown in gray to identify the ACh binding pocket [Zhong et al. 1998]. The subunit to the right shows a view of the inner sheet (teal), and other residues targeted in this study. The sequence surround mutants characterized in this study is shown beneath the cartoon: M37, M40 cyan; N52 green; N170 blue; E172 purple.

Previously, we measured the effects of ACh on reactivity of cysteine mutants in the inner β sheet of the chick α7 nAChR [McLaughlin et al. 2006]. Several residues (M37C, M40C, and N52C) exhibited a change MTSEA reaction rates in the presence of ACh. We interpret differences in modification rates in the absence or

presence of ACh to reflect differences in the apparent accessibility of the introduced cysteine between the unliganded and liganded states. To test if these sites could also be used as reporters of allosteric modulator-induced conformational change we examined the effects of Ba^{2+} on rates of MTSEA modification.

Figure 4.3 shows an example of the protocol used to measure the thiol modification rate of the receptors with the M37C mutation. ACh-evoked current amplitudes decreased following brief, repeated exposure to a limiting concentration of MTSEA (5 µM, 15 seconds). To ensure that the modification reactions were complete, all rate measurements included a final prolonged application of ~100-fold higher concentrations of MTSEA (**Fig. 4.3A and 4.3B**, right). Currents measured following this application represent the endpoint of the reaction between MTSEA and receptors. When the same protocol included Ba^{2+} pretreatment and co-application with MTSEA (see Methods), the decreases in current amplitudes were slowed but the same endpoint was obtained (**Fig. 4.3B**). Normalized current amplitudes were plotted as a function of the cumulative time of exposure to MTSEA, and pseudo first-order rates were extracted from the single-exponential fits (**Fig. 4.3C**). We observe a significant decrease in the MTSEA modification rate for M37C (**Fig. 4.4**) in the presence of 10 mM Ba^{2+}, demonstrating that this modulator caused changes in the conformation or electrostatic environment around the M37C side chain.

Table 4.1 - Effects of Ba^{2+} on ACh evoked currents.

mutant	ACh EC_{50}, µM		(n)	ACh I_{max} µA	Ba^{2+} efficacy[a]
	control	*+ 10 mM Ba^{2+}*			
C115A/L247T	1.8 ± 0.4	0.17 ± 0.02	4	6.9	0.1
M37C	2.0 ± 0.5	0.35 ± 0.12	4	0.92	0.2
M40C	7.7 ± 1.1	1.1 ± 0.1	5	3.0	0.1
N52C	2.6 ± 1.3	nd[b]	5	0.34	0.6
E44C	7.8 ± 0.4	10.1 ± 0.4	4	5.4	0.01
N170C[c]	13 ± 1.7	2.1 ± 0.4	6	1.7	0.03
E172C[c]	30 ± 2.7	50 ± 9.2	4	1.3	0.02
M40C/E172Q[c]	85 ± 6.2	134 ± 11	5	0.7	0.02

ACh dose-response measurements in the absence or presence of Ba^{2+}. EC_{50} estimates are mean values ± S.E.M. (*a*) Ba^{2+} efficacy is the fraction of maximal ACh-evoked current that is evoked by 10 mM Ba^{2+} in the absence of ACh. (*b*) nd: not determined because Ba^{2+} was a strong partial agonist. (*c*) Mutants studied using co-expression with human RIC-3 (Halevi et al., 2002).

Using the protocol described in **Figure 4.3**, we determined second-order rate constants for modification of the three reporter residues in the inner β sheet (M37C, M40C, and N52C). **Figure 4.4A** shows mean values of the rate constants measured in the presence of MTSEA alone, MTSEA plus ACh, and MTSEA plus Ba^{2+}. We observed significant decreases in reaction rates of both $M^{37}C$ and $M^{40}C$ in the presence of 10 mM Ba^{2+}. The effects are quantitatively similar to those measured in the presence of ACh [McLaughlin et al. 2006], consistent with the idea that Ba^{2+} causes conformational changes similar to those induced by agonist in this

region of the α7 nAChR. To more directly compare the effects of ACh and Ba^{2+} on reaction rates, we plot rate constants as ratios in **Figure 4.4B**. This figure highlights the differences in MTSEA rates under different conditions at these three positions. In contrast to M37C and M40C, we observed no significant effect of Ba^{2+} on MTSEA modification rate of N52C. This result parallels our previous study in which we found the effect of ACh on MTSEA modification rate of N52C was also different from that of neighboring residues M37C and M40C. Collectively, these results suggest that divalent cations such as Ba^{2+} act to promote some, but not all, of the conformational or electrostatic changes elicited by ACh. While ACh acts to stabilize the open state, Ba^{2+} acts to stabilize a state (or states) that are energetic intermediates between closed and open channels.
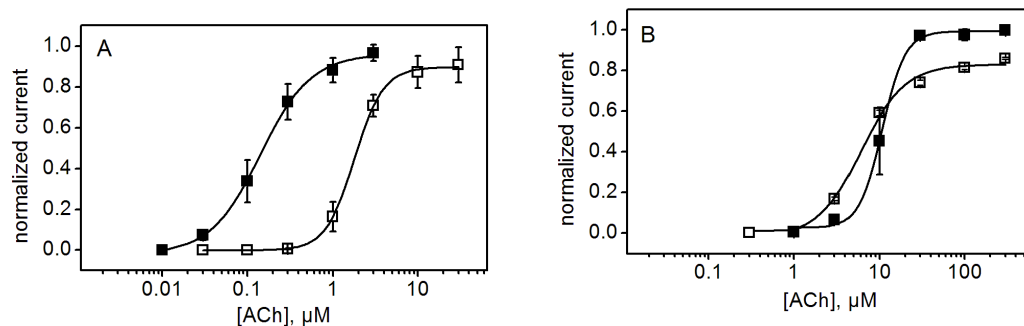
Figure 4.2: Positive allosteric modulation by divalent cations requires E44. ACh dose-response curves for the parental C115A/L247T (A) and the E44C mutant (B) in the absence (open squares) and presence (filled squares) of 10 mM $BaCl_2$. Data are fitted to the Hill equation (solid lines). The positive allosteric modulation (leftward shift in the dose response curve) typically exhibited by α7 nAChRs (A) is lost in the E44C mutant (B). Data are mean values (± S.E.M.) from three determinations, normalized to the maximal value of the Hill equation fit of each data set. Hill coefficients for C115A/L247T (A): 2.5±0.2 (open squares, -Ba^{2+}), 1.9±0.4 (filled squares, +Ba^{2+}); and for the E44C mutant (B) 1.7±0.2 (open squares, -Ba^{2+}), 2.9±0.7 (filled squares, +Ba^{2+}).
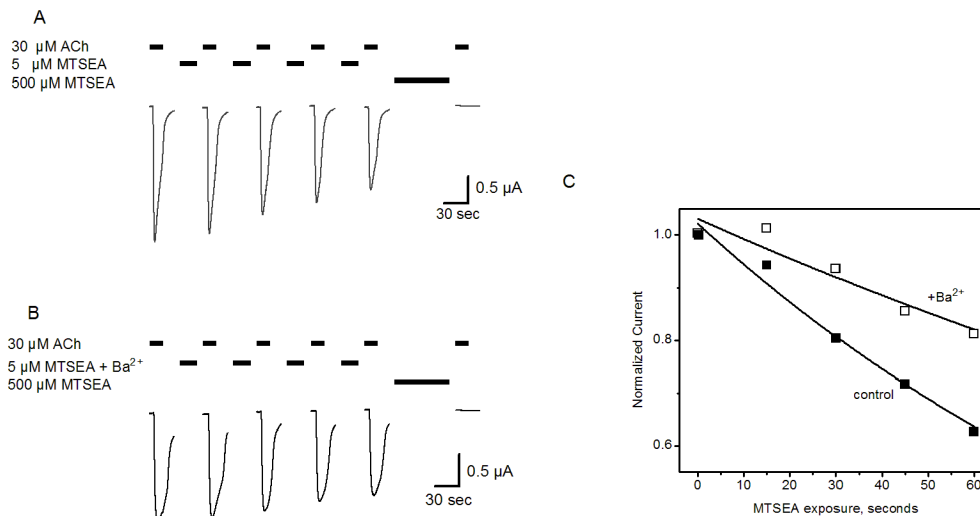
Figure 4.3: Barium slows the rate of MTSEA modification at M37C. Example of experimental paradigm used to assess Ba^{2+} effects on modification rates. (A) Successive ACh-evoked current traces recorded before and after repeated exposures to MTSEA (5 μM, 15 seconds), showing a decrement in responses to 30 μM ACh. Endpoints of MTSEA modification are determined by prolonged application of 500 μM MTSEA (right). (B) The same protocol, including Ba^{2+} pretreatment and co-application with MTSEA. Current traces are truncated in both (A) and (B) between consecutive MTSEA applications; in all cases the currents were allowed to return to baseline prior to the next application of MTSEA ± ACh. (C) Peak current amplitudes from (A) and (B) are normalized and plotted versus total MTSEA exposure time. Data from this single experiment (no error bars) are fitted to a single-exponential decay (solid line) to extract an apparent pseudo first-order rate constant. The pseudo first-order rate constants calculated in this experiment were 0.011 s^{-1} and 0.0019 s^{-1} for control (A) and $+Ba^{2+}$ (B) measurements, respectively. Second-order rate constants are calculated from these values (**Figures 4-6**; **Table 4.2**).

Modulation by divalent cations is known to require the conserved acidic residues at E44 and E172 [Karlin and Akabas 1998; Lyford et al. 2003]. We next tested whether Ba^{2+} could cause changes in the rates of MTSEA modification at E44C, N170C, and E172C. Similar to residues in the inner β sheet, each of these mutants has been shown to be a reporter of conformational or electrostatic changes induced by ACh [Lyford et al. 2003; McLaughlin et al. 2007]. **Figure 4.5A** shows mean values of second order rate constants measured in the presence of MTSEA alone, MTSEA plus ACh, and MTSEA plus Ba^{2+}. At N170C, a mutant that showed allosteric modulation (**Table 4.1**), the rate of MTSEA modification in the presence of

Ba^{2+} was the same as that measured in MTSEA alone, but was different from that measured in the presence of ACh. This observation suggests that conformational or electrostatic changes induced by modulators at this residue are distinct from those induced by ACh. Differences between the effects of ACh and Ba^{2+} were most pronounced at E44C; at this residue, the modification rate was ~10 fold higher in the presence of Ba^{2+} compared to that measured in the presence of ACh (**Figure 4.5B**). Surprisingly, despite the fact that both E44C and E172C show no positive allosteric modulation of ACh currents by Ba^{2+} (**Fig. 4.2, Table 4.1**), both exhibited significant Ba^{2+}-dependent decreases in MTSEA modification rate.

The hypothesized requirement for E44 and E172 in divalent cation modulation was based upon studies of charge neutralization mutants (E44Q, E172Q) in which modulation was lost. From these and other studies, both residues were proposed to be participants in a binding site which mediates the divalent cation allosterism [Galzi et al. 1996; Eddins et al. 2002b]. The loss of Ba^{2+} dependent modulation in E44C or E172C mutations (also charge neutralization mutations) is consistent with this proposal, but the effects of Ba^{2+} on MTSEA modification rates are not. One possible explanation for these observations is that Cys replacements at E44 and E172 do not prevent Ba^{2+} binding, but cause an uncoupling of binding and allosteric modulation. If Ba^{2+} binds near E44C and E172C, the slowed modification rate at E44C or E172C would be explained by physical occlusion of the thiol side-chain by bound Ba^{2+}.
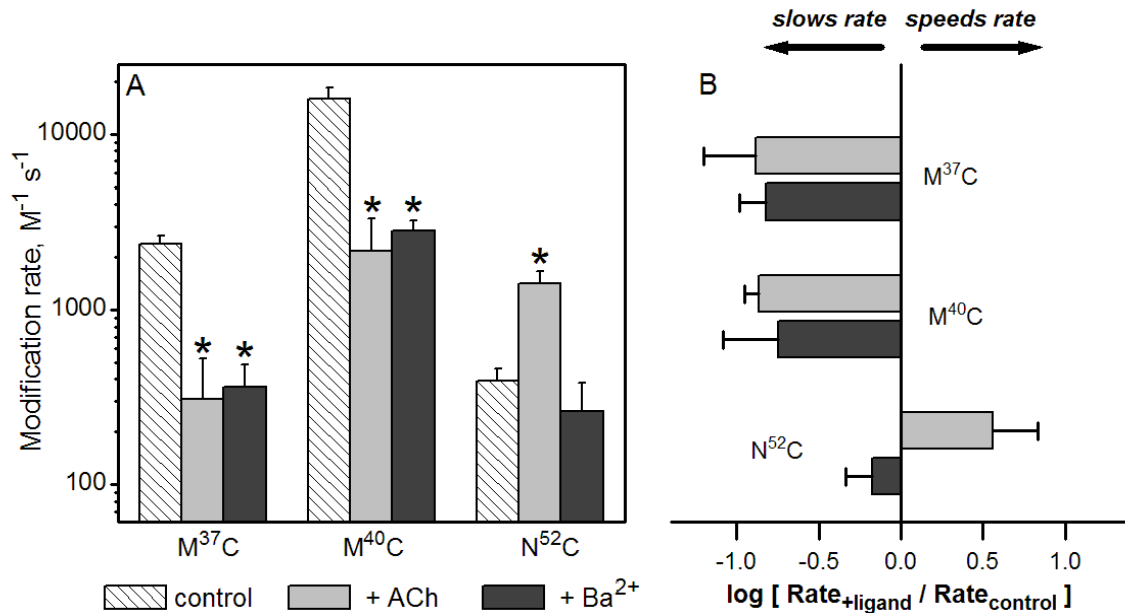
Figure 4.4: Barium alters the rate of MTSEA modification at inner β sheet residues. (A) Using the protocol described in Figure 3, we determined second-order rate constants for three reporter residues in the α7 nAChR inner β sheet (M37C, M40C, and N52C). Mean values for second-order rate constants for modification by MTSEA alone (control), MTSEA + ACh, and MTSEA + Ba^{2+} are shown. * Rate was significantly different from control ($P<0.05$). (B) A plot of the ratios of second-order rate constants. Ba^{2+} and ACh both slowed the rates of modification of M37C and M40C. At N52C, however, the rate of modification in the presence of Ba^{2+} was not significantly different from control, while ACh accelerated the modification rate. See **Table 4.2** for summary including (n) for each condition.

Alternatively, the glutamates could be a required component in the transduction pathway between Ba^{2+} binding and receptor modulation, but are not direct participants in the binding site. In this case divalent cations bind at a different site and elicit conformational or electrostatic changes (detected as changes in E44C and E172C modification rates), but binding does not lead to modulation. To test this possibility we examined MTSEA modification rates at M40C α7 nAChRs in which a second, charge-neutralizing mutation (E172Q) was introduced. We reasoned that if E172 is required for binding of divalent cations, than the modification rate of M40C should be insensitive to Ba^{2+}. If, however, Ba^{2+} binds to the receptor and causes

conformational changes, despite the mutation at E172, this would be reflected by changes in the rate of modification of M40C.
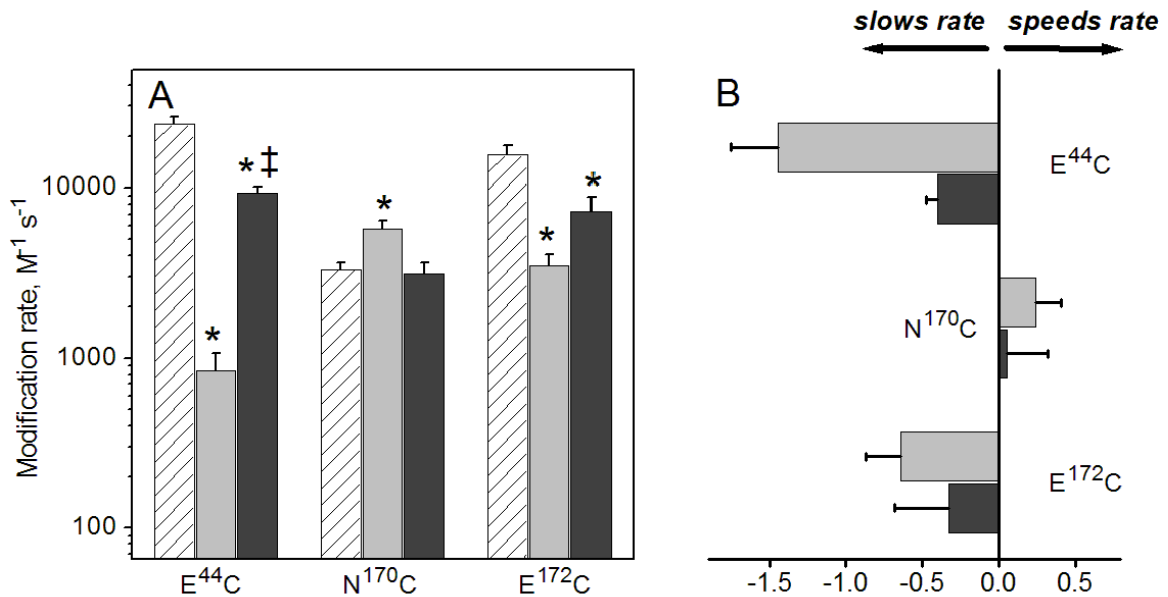
Figure 4.5: Barium alters the rate of MTSEA modification at residues required for modulation by divalent cations. Second-order rate constants were measured for three residues in the "transition zone" of the α7 nAChR (E44C, N170C, and E172C). (A) Mean values for second-order rate constants for modification by MTSEA alone, MTSEA + ACh, and MTSEA + Ba^{2+}. Ba^{2+} caused a significant decrease in MTSEA modification rates of both $E^{44}C$ and E172C, despite the loss of divalent cation-dependent modulation. Ba^{2+} did not have a significant effect on the modification rate of N170C, although ACh significantly increased the rate of modification of this residue. *Rate was significantly different from control ($P<0.05$). ‡Rate was significantly different from that obtained in presence of ACh ($P<0.05$). The plot of rate constant ratios (B) shows that the effect of Ba^{2+} on the rate of modification of $E^{44}C$ was significantly less than the effect of ACh. See **Table 4.2** for summary including (n) for each condition.

We measured dose-response relationships for the M40C/E172Q double mutant in the absence and presence of 10 mM Ba^{2+} and confirmed that it was not positively modulated by Ba^{2+} (**Table 4.1**). When the rates of MTSEA modification of the M40C in this background were measured, we found that Ba^{2+} caused a significant slowing of MTSEA modification rate (**Figure 4.6**). The modification rates of M40C were independent of the E^{172} mutation. This result suggests that the binding site for Ba^{2+}

modulation is somewhere other than a site which includes E^{44} and E^{172} in the α7

nAChR transition zone [Le Novere et al. 2002].
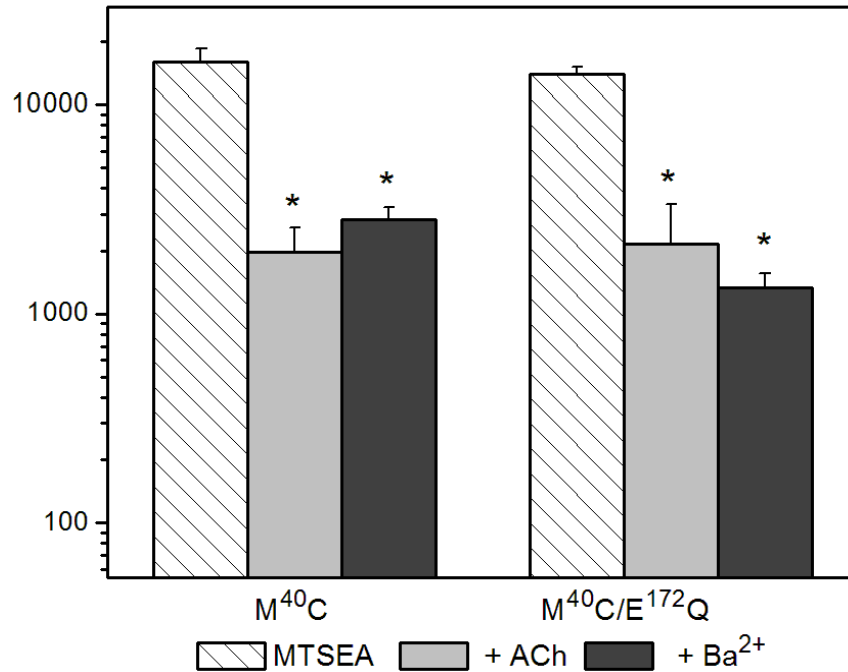
Figure 4.6: Charge neutralization at E172 does not alter the rate of modification M40C by MTSEA. Mean values for second-order modification rate constants for M40C (left, data from Fig. 3) compared to those obtained in receptors containing the E172Q mutation (M40C/E172Q). *Rates were significantly different from control (P<0.05). See Table 2 for summary, including (n) for each condition.

Discussion

The mechanisms of protein allosterism have been the subject of exhaustive modeling and model refinement since studies of Monod, Wyman and Changeux [Monod et al. 1965] and those of Koshland and colleagues [Koshland et al. 1966]. In the nicotinic receptors, several different types of allosteric behavior have been described. The concerted, or MWC model, for example, refers to the allosteric effect of ligand binding on channel opening; this model suggested that binding of multiple agonists acted in concert to yield their "at a distance" effect. Experimental tests of the MWC model with combinations of agonists and antagonists suggest that a stepwise process more accurately describes the activation process [Prince and Sine 1999; Krauss et al. 2000].

Another type of allosterism seen in some nicotinic receptors is the positive allosteric modulation by divalents such as Ca^{2+} or Ba^{2+} [Vernino et al. 1992; Galzi et al. 1996]. For this type of allosterism, a fundamental question is whether the modulation alters the conformational "pathway" from closed to open states or simply modifies the kinetics of an agonist-dependent closed to open transition. Few studies have attempted to address this question, but a recent report does examine the conformational effects of positive allosteric modulators (benzodiazepines) in $GABA_A$ receptors [Sharkey and Czajkowski 2008]. This study used SCAM to show that a prominent effect of benzodiazepines is to increase the access of GABA to its binding site, reducing the energetic barrier to the initial step in receptor activation, GABA association. Divalent cation effects on α7 nAChRs provide a similar paradigm in which to examine the conformational changes evoked by allosteric modulators.

In an earlier report we described an α7 nAChR mutant with a pair of cysteine substitutions positioned to introduce a disulfide bond in the outer β sheet [McLaughlin et al. 2006]. In our parental background this mutant was fully activated by divalent cations in the absence of ACh, but when expressed in an α7 nAChR without the L247T mutation it required both ACh and divalent cations for channel activation. If we assume that activation of this mutant occurs because of Ba^{2+} interaction with the divalent cation allosteric site, then it suggests that Ba^{2+} and ACh promote two overlapping but distinct sets conformational changes. The experiments presented in this report provide further evidence that conformational effects of divalent cations are similar to those elicited by ACh. Thus the simplest interpretation of our data is that divalent cations act by enhancing transitions in an ACh-dependent activation pathway without substantial effect on the final closed to open transition.

Le Novere and colleagues [Le Novere et al. 2002] proposed a model for a divalent cation binding site that was based on earlier experiments, homology between the α7 nAChR LBD and the *Lymnea* AChBP, and the known database of divalent cation binding proteins [Galzi et al. 1996; Brejc et al. 2001]. The focus of this model was a cluster of 4 negatively charged residues in the transition zone: D41, D43, E44, and E172. Mutational analysis suggested that the glutamate residues were critical, since charge neutralization at either of the aspartate residues had only modest effects on divalent modulation. While the geometry of these residues in models of the LBD is consistent with their proposed model, our results with Ba^{2+}-induced conformational changes are not. A mutation of either E44 or E172 to cysteine eliminates the modulation, but not the conformational changes

93

associated with Ba^{2+} modulation. This strongly suggests that the allosteric effects of Ba^{2+} are "transmitted" in a conformational pathway that requires these glutamates for some role other than divalent cation binding. It is unlikely that the Cys substitution is able to act as a functional substitute for Glu in a divalent cation site: a survey of all known Ca^{2+} binding sites found that Cys was never a contributor to a Ca^{2+} co-ordination site, while it often plays this role in Zn^{2+} binding sites [Harding 2004]. Other possible candidates for a divalent cation modulation site in the α7 LBD include acidic residues in β6 and β8, which may combine with neighboring carbonyl groups to form a site for divalent cation binding. Alternatively, the recent work of Horn and colleagues [Santarelli et al. 2007] has demonstrated that aromatic residues may provide the negative electrostatic environment required for formation of a physiologically relevant divalent cation binding site through the π-cation-type interactions. This is the same structural motif that has been shown to provide the negative electrostatic environment in the cholinergic agonist binding site [Zhong et al. 1998].

In summary, we have shown that the permeable divalent cation Ba^{2+} induces similar conformational changes as the agonist ACh in the extracellular-ligand binding domain of the α7 nAChR. The next section of this dissertation will introduce new methodologies to determine what those specific mechanisms are.

Table 4.2 - Summary of MTSEA modification data.

MUTANT	MTSEA modification rate x 10^3, M^{-1} S^{-1} (n)		
	control	*+ ACh*	*+ Ba^{2+}*
M37C	2.4 ± .03 (10)	0.30 ± 0.05 (4)	0.40 ± 0.02 (5)
M40C	16 ± 0.2 (13)	2.2 ± 0.4 (3)	2.8 ± 0.05 (7)
N52C	0.40 ± .08 (9)	1.4 ± 0.04 (7)	0.26 ± 0.02 (7)
E44C	23 ± 0.7 (4)	0.90 ± 0.05 (4)	9.3 ± 0.1(8)
N170C[a]	3.3 ± .05 (7)	5.7 ± 0.1 (7)	3.7 ± 0.06 (9)
E172C[a]	15 ± 0.4 (5)	3.5 ± 0.1 (5)	7.3 ± 0.3 (6)
M40C/E172Q[a]	14 ± 0.5 (5)	1.3 ± 0.1 (5)	2.0 ± 0.3 (6)

Second-order rate constants ± S.E.M. for various conditions at each Cys mutant. (n), number of determinations. (*a*) Mutants studied using co-expression with human RIC-3 (Halevi et al., 2002).

CHAPTER 5

HOMOLOGY MODELS OF THE α7 RECEPTOR DERIVED FROM BACTERIAL CYS-LOOP RECEPTORS

Introduction

Nicotinic acetylcholine receptors (nAChRs) are the prototypical member of the Cys-loop family of ligand-gated ion channels that also includes $GABA_A$, serotonin type 3, and glycine receptors. This family of receptors assembles as heteromeric or homomeric pentamers around a central pore. Each subunit contains an extracellular ligand-binding domain, an α-helical transmembrane domain, and an intracellular domain.

The crystallization of the *Lymnaea* Acetylcholine Binding Protein (AChBP) provided a wealth of information regarding the ligand-binding site of Cys-loop ionotropic receptors [Brejc et al. 2001]. Subsequently, the *Aplysia* AChBP was discovered and structures have been solved for proteins in the presence of various agonists, antagonists, and allosteric modulators [Hansen et al. 2002; Celie et al. 2004; Celie et al. 2005; Hansen et al. 2005; Hansen and Taylor 2007]. Information from these structures as well as a combination of functional and computer modeling have shown that movement of the C-loop towards bound agonist is one of the first conformational changes associated with gating of Cys-loop receptors [Szarecka et al. 2007; Venkatachalan and Czajkowski 2008]. This rearrangement at the agonist-binding site is followed by additional conformational changes that converge on the channel gate in the pore-lining M2 helices [Gay and Yakel 2007]. However, the AChBP lacks the ion-conducting transmembrane domain and cannot provide a complete picture of the structure and conformational changes of this family of ionotropic receptors.

One approach to this problem has been to develop hybrid homology models, consisting of a fusion of the AChBP structures to cryo-EM images of the transmembrane domain of *Torpedo* nAChR [Miyazawa et al. 1999; Taly et al. 2005; Unwin 2005]. However the 4Å resolution of the ion-conducting domain was refined computationally and is not a *de novo* structure, which limits a detailed analysis of receptor gating at the atomic level. Another limitation of the *Torpedo* nAChR model is that electrophysiological data does not support the rigid-body rotation model of gating for this receptor [Miyazawa *et al.* 2003; Cymes *et al.* 2005; Cymes and Grosman 2008]. Accordingly, the validation of computational (*in silico)* studies with electrophysiological data is crucial for eludicating the gating mechanisms of the Cys-loop family of receptors.

To address these limitations, we have developed homology models of the α7 nicotinic receptor in the closed and open states, based on the full-length, high-resolution structures of bacterial Cys-loop receptors [Hilf and Dutzler 2008; Bocquet et al. 2009; Hilf and Dutzler 2009]. We have validated these models using computational and electrophysiological data, and address the utility and limitations of these models to study receptor gating. We find that changes in electrostatics are a better predictor of MTSEA accessibility in the LBD than solvent accessibility. Our long-term goal is to use these homology models for molecular dynamics simulations to identify mechanisms of gating of the α7 nicotinic receptor.

Results

Homology models of the α7 nicotinic receptor generated from the closed state structure (ELIC) [Hilf and Dutzler 2008] and open state structure (GLIC) [Bocquet *et al.* 2009] are shown in **Figure 5.1-5.2.** Qualitatively, both models retain the secondary structure of the Cys-loop receptor family, including a perpendicular beta sheet array in the extracellular domain, and a bundle of four transmembrane helices. Both models show a tilting of the pore-lining M2 helix from the closed to the open state, which is thought to be an important for channel gating (**Figure 5.3**) [Hilf and Dutzler 2009]. An important difference between our models and the existing AChBP structures is that ELIC and GLIC lack the aromatic residues that are required for binding of cholinergic ligands [Hilf and Dutzler 2008; Bocquet et al. 2009]. As a result, the ligand-binding residues of the α7 homology models are oriented such that the agonist-binding site cannot accommodate cholinergic ligands (**Figure 5.4**). Another limitation is that GLIC receptor, does not desensitize even when maximally activated by acidic pH [Bocquet et al. 2007], whereas α7 nAChR is inhibited by acidic pH and quickly desensitizes[10].

The strength of these new homology models is not in providing additional details about the agonist-binding site. There is a wealth of structural and pharmacological data on the agonist-binding site from the AChBPs [Brejc et al. 2001; Celie et al. 2004; Hansen et al. 2004]. Rather, these new homology models are useful because they provide a higher resolution picture of the transmembrane domain, with the extracellular and transmembrane domains coupled in a full-length

---

[10] Barron SC and McLaughlin JT, unpublished observations that α7 receptors are inhibited by protons. There is precedent for acidic pH enhancing and inhibiting β2* , β4* nAChRs and GABA$_A$Rs [Abdrakhmanova *et al.* 2004; Wilkins *et al.* 2005].

receptor. The loops that connect the extracellular and transmembrane domains are critical for the function of Cys-loop receptors [Xiu et al. 2005; Hanek et al. 2008]. Additionally, loop 2, loop 9, and the Cys-loop from the AChBP cannot form functional chimeric channel when fused with the 5-HT$_{3A}$ receptor; replacement of the AChBP sequence with that of the 5-HT$_{3A}$ for these three loops is required [Bouzat et al. 2004]. These models can be used to study to conformational changes that occur downstream of the agonist-binding site, which lead to gating and an increase in ion conduction.
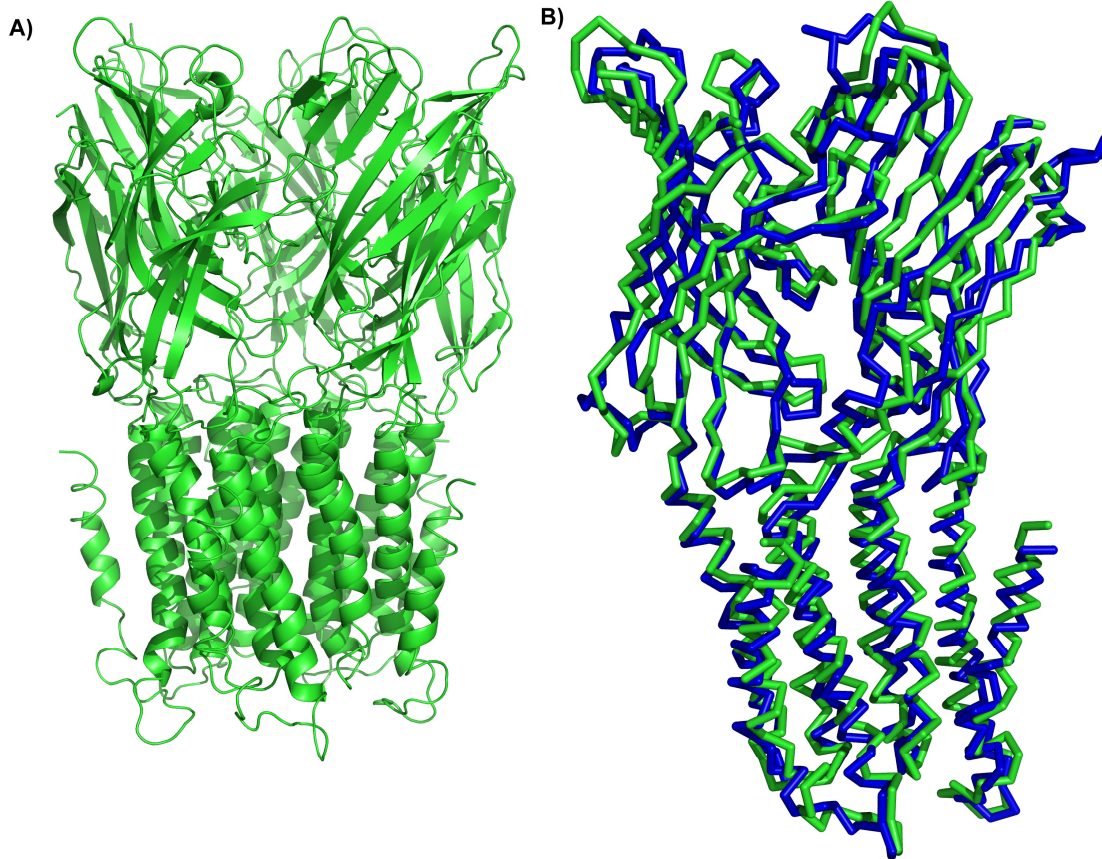
Figure 5.1: α7 homology model in the closed (non-conducting) state. The entire pentameric model is shown in (A). An overlay of the α7 model (green) with the ELIC starting structure (blue) is shown in (B).

Three independent techniques were used to evaluate the quality of the homology models. For the closed and open state model, the template structure (ELIC and GLIC, respectively) was overlaid with the corresponding homology model, as shown in **Figure 5.1B and 5.2B**. The RMSD was calculated between the respective template structure and homology model, to determine the average atomic distances [Maiorov and Crippen 1994]. The RMSD for backbone carbons in the closed state model was 1.2 Å, and 1.1 Å for the open state model, suggesting the structural sequence alignment and locations of inserted and deleted sequence retained the secondary structure of the bacterial Cys-loop receptors in the homology models.

Secondly, a Profiles 3D self-compatibility score based on the compatibility of each amino acid with its surrounding environment was generated [Luthy et al. 1992]. The Profiles 3D algorithms reduces the three-dimensional structure of a protein into a one dimensional score; this score is calculated based on eighteen environmental classes that account for the fraction of the side chain that is solvent exposed, side chain polarity, and the local secondary structure [Bowie *et al.* 1991]. The one-dimensional score is then aligned with the amino acid sequence of the protein based on a 3D-1D scoring matrix, creating a Profiles 3D score[11]. For the closed state model, the Profiles 3D score was 493 with an acceptable range of 312-691. For the open state model, the Profiles 3D score was 605 with an acceptable range of 329-729. The Profiles 3D score was further analyzed by plotting the individual scores for each residue (**Figure 5.5)** for the homology models and their respective starting

---

[11] The 3D-1D scoring matrix measures the compatibility of the twenty amino acids with the eighteen possible environmental classes. A higher score represents a higher compatibility between the amino acid and the local environment [Bowie *et al.* 1991; Luthy *et al.* 1991].

structures. The M4 helix has the lowest Profiles 3D score among ELIC and GLIC

structures, meaning that the fit of the original x-ray diffraction data to the three-

dimensional model was poor. Not surprisingly, the M4 helix also has the lowest

Profiles 3D score in the corresponding closed state and open state homology

models. The closed state model has a poorer fit in the first 100 residues for four of

the five subunits relative to the ELIC structure. This region corresponds to the β1,

β2, β6, Loop 2, and the A Loop of the ligand-binding domain, suggesting that the fit

of the closed state homology model to these regions of the α7 nAChR is not as good

as the starting structure. The Profiles 3D scores of the open state model very closely

match those of the GLIC structure, which may be the result of the higher resolution

of GLIC compared to ELIC (2.8 Å vs. 3.3 Å, respectively). The numerical and plotted

Profiles 3D score show that the internal residue compatibility of the closed and open

state models closely match their respective bacterial Cys-loop receptor template.
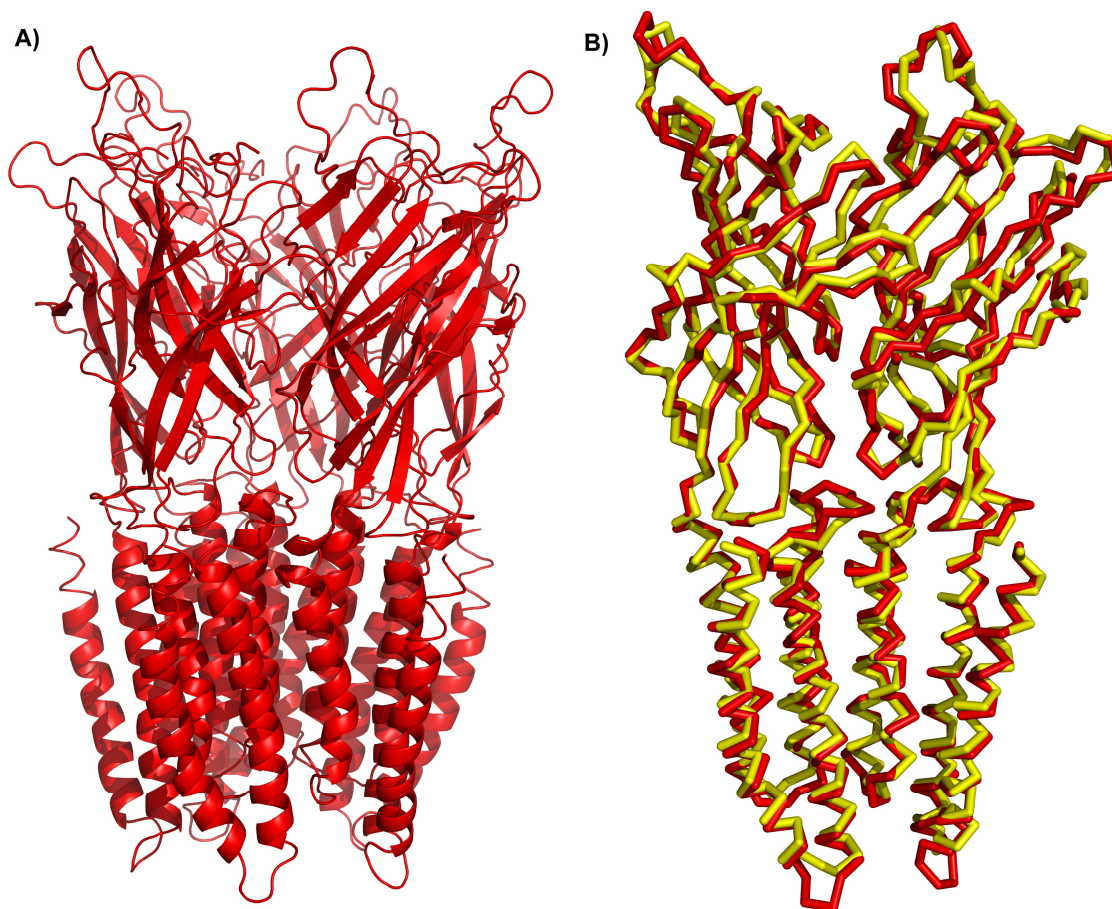
Figure 5.2: α7 homology model in the open (ion conducting) state. The entire pentameric model is shown in (A). An overlay of the α7 model (red) with the GLIC starting structure (yellow) is shown in (B).

Figure 5.6 and 5.7 shows stereochemical validation experiments, carried out with Procheck [Laskowski et al. 1993]. Specific parameters for bond length, bond angles, and energetics are conserved within a narrow range for all protein structures found in the PDB databank [Morris et al. 1992]. Homology models and *de novo* structures can be analyzed against the existing data set to look for gross distortions in amino acid stereochemistry. A limitation of this analysis is that good stereochemistry does not necessarily indicate a well-fit homology model, as these

parameters can be tightly constrained during energy minimization. To circumvent this limitation, the closed and open state models were energy minimized in a simple two-step process.
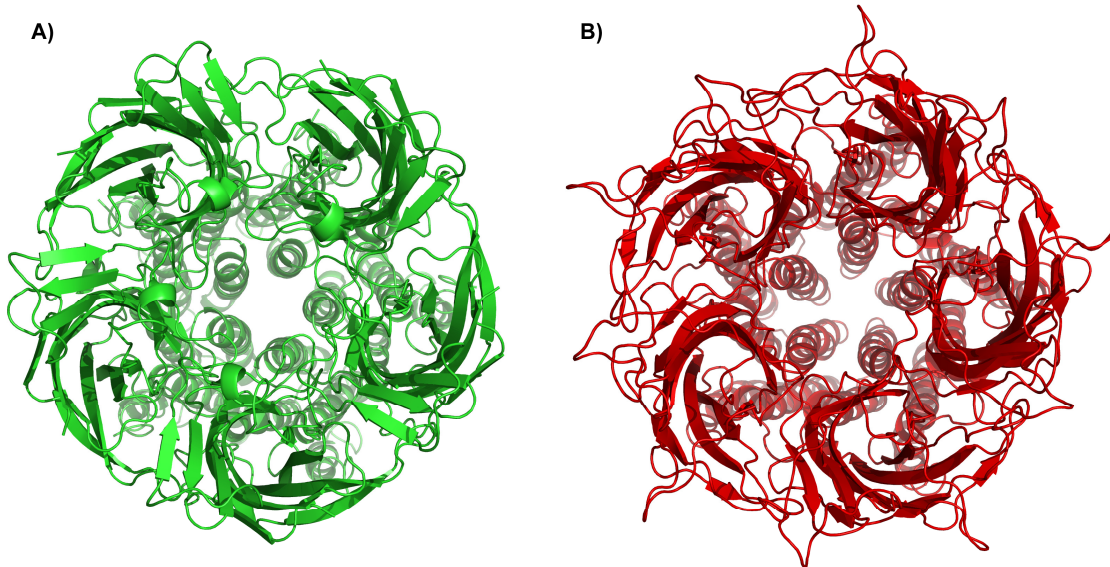
Figure 5.3: Top down view of the α7 homology models. The closed model is shown in (A), and the open model is shown in (B). Both views are from the extracellular side looking down the ion conduction pathway.

Procheck was used to analyze five parameters of the peptide bond for each model (**Figure 5.6**): φ-ψ angles (Ramachadran Plot), peptide bond planarity (ω angle), bad contacts (non-bonded atoms that violate van der Waals radii), C^α tetrahedral distortion (ζ angle), and hydrogen bond energies (deviations from -2.0 kcal/mol) [Kabsch and Sander 1983; Morris et al. 1992]. The analysis of these five parameters is dependent on the resolution of the starting structure, with less deviation expected/accepted for higher resolution structures. The omega torsion angle showed significant deviation compared to protein structures with the same resolution for both models. In order to address this, a stepwise energy minimization

was carried out. The heavy atoms, backbone, and side chain atoms were successively constrained and energy minimized as described in the Methods. However, improvement in the omega torsion angle was offset by distortion in the other parameters and these modifications and models were ultimately discarded (data not shown). The ELIC and GLIC structures were also analyzed using Procheck, and omega angle distortion was not observed (data not shown). Nevertheless, all other parameters were either better than expected or acceptable, compared to structural models of other proteins with the same resolution.

Five parameters of the side chain angles were also evaluated using Procheck (**Figure 5.7**), focusing on the C^{α}-C^{β} ($\chi 1$) and C^{β}-C^{γ} ($\chi 2$) angles. For both models, all parameters were better than expected for protein structures with the same resolution. The results of these experiments show that the closed and open state models maintain favorable amino acid stereochemistry.

A) CCh-bound AChBP (side) B) CCH-bound AChBP (bottom)
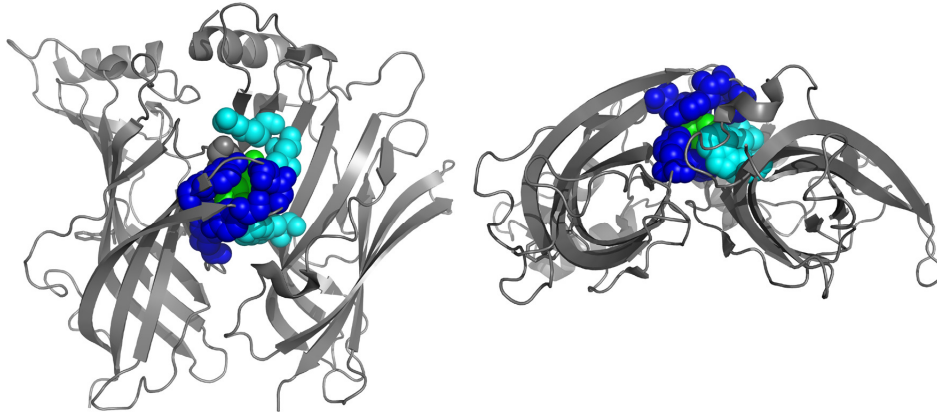
C) a7 model - closed (side)   D) a7 model - closed (bottom)
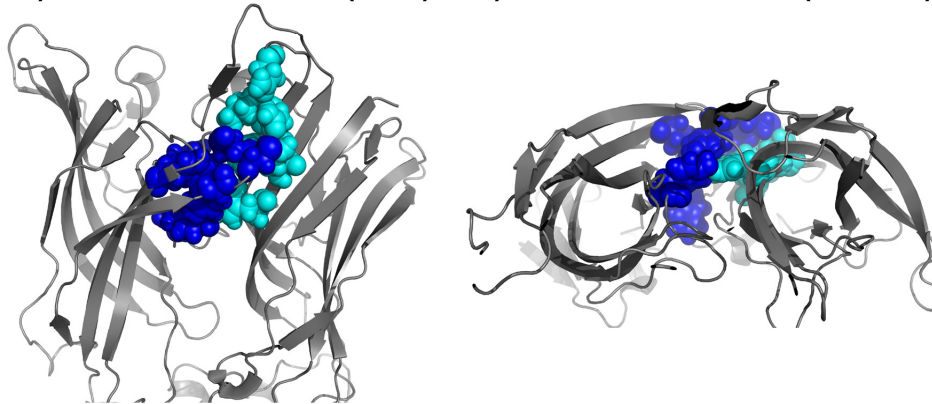
E) a7 model - open (side)   F) a7 model - open (bottom)
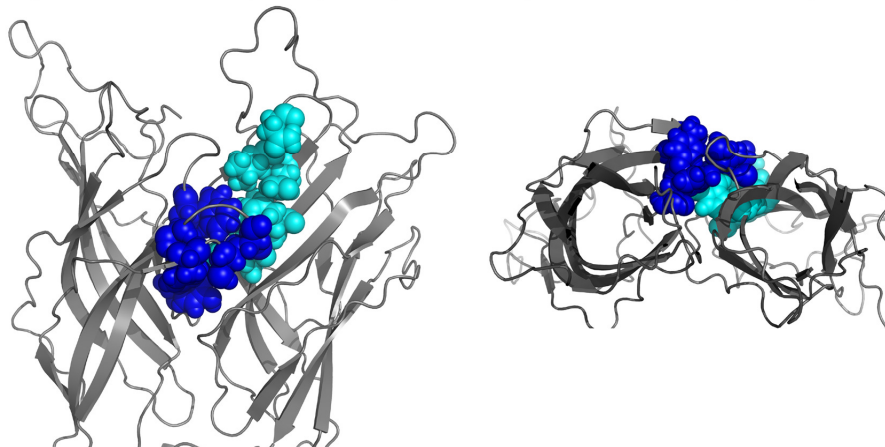
Figure 5.4:- Collapsed agonist-binding site of homology models. (A) and (B) show the *Lymnaea* AChBP bound to carbamylcholine (PDB code: 1uv6) in green [Celie et al. 2004]. Agonist-binding residues from the Primary subunit are shown in blue, and those from the Complimentary subunit are shown in cyan. In the homology models, the agonist-binding residues point in towards the pocket that would be occupied by agonists and antagonists.

The software program MOLE was used to visualize the ion conducting pore of the homology models to verify that each model accurately represented the closed and open state [Petrek et al. 2007]. As a control, MOLE was also used to visualize the ion-conducting pore of the ELIC and GLIC structures. As expected, the closed state model is in a non-conducting state, as a permeant ion cannot travel past a blockage in the region of Loop2 and the top of the pore-lining M2 helix (**Figure 5.8**). A unique observation is the presence of a constriction in the inner vestibule of the ligand-binding domain, at position R98 (**Figure 5.8B**). This constriction is not seen in the *Lymnaea* and *Aplysia* AChBPs, the cryo-EM images from the *Torpedo* nicotinic receptor, and subsequent homology models derived from these structures [Brejc et al. 2001; Hansen et al. 2004; Taly et al. 2005; Unwin 2005]. The open state model is in a conducting state, as a conduction pathway is evident over the entire length of the M2 helix (**Figure 5.8D**).

Because of the importance of the inner vestibule in ion selectivity [Hansen et al. 2008], we tested the hypothesis that a constriction at R98 in the closed state relaxes in the open state upon gating of the receptor. We hypothesized that if a constriction is present in the closed state, than chemical modification of introduced cysteines "below" the constriction would not be accessible to cysteine reagents with a diameter larger than that of the constriction at R98. In the open state model, the diameter of the vestibule is ≈ 20 Å and would no longer hinder accessibility to introduced cysteines located "below" position R98. Cysteine-modifying reagents with a diameter smaller than the constriction should be equally accessible in both the closed and open states (**Figure 5.9**).
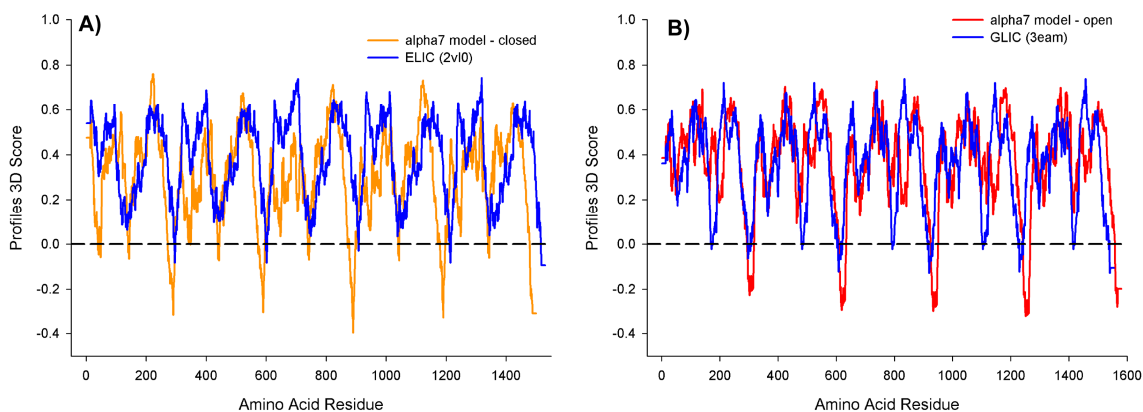
Figure 5.5: Profiles 3D scores. The Profiles 3D score is plotted against the residue position for closed state (A) and the open state (B) models. Scores approaching zero (dashed line) and negative scores are interpreted as a poor fit in that region of the model. Note that the homology models generally follow the trendline of their respective starting structure, including regions of poor fit.

We chose three neutral cysteine-modifying reagents to work with; MTSBn, MTSEA-biotin, and DTNB. After examining the constriction in PyMOL (**Figure 5.9**), we hypothesize that Benzyl MTS should be able to pass through the approximately 7Å x 5Å constriction, and should be equally accessible in both the closed and open states at residues "below" the constriction. MTSEA-biotin and DTNB are larger than the constriction in at least two dimensions and should not be able to pass through it. Therefore, we hypothesize that MTSEA-biotin and DTNB should have less access to introduced cysteines "below" the constriction in the closed state, and more access to the same position in the open state in which there is no constriction. The use of MTS reagents to probe the diameter and structural features of ion channels is a well described and validated method [del Camino and Yellen 2001].
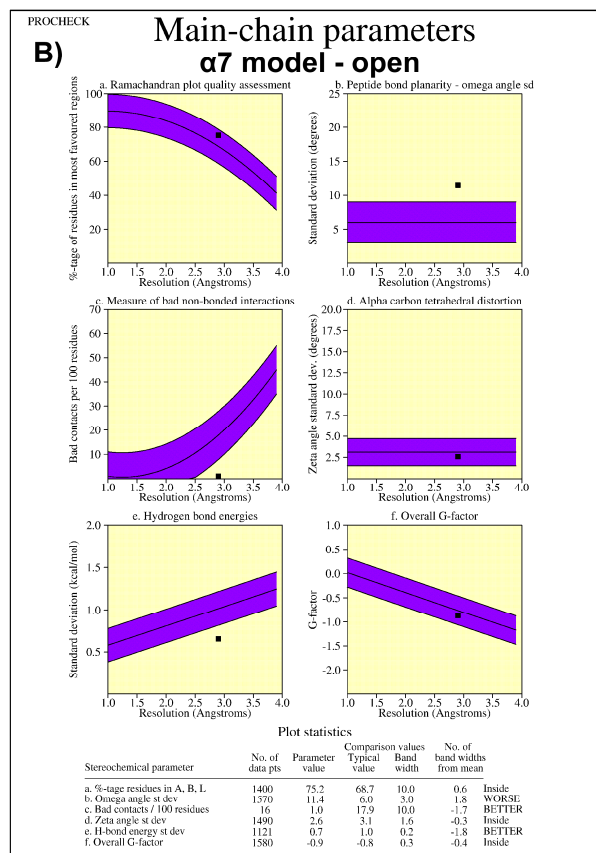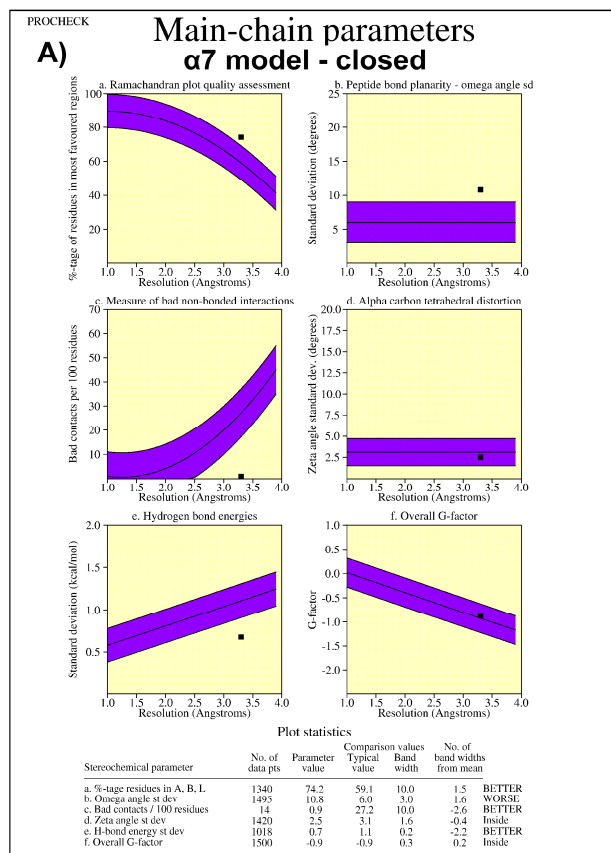
Figure 5.6: Model evaluation – Main chain. Procheck was used to evaluate the backbone stereochemistry of the α7 models in the closed (18A), and open states (18B). The evaluation depends on the resolution of the starting structures, which is 3.3Å for ELIC and 2.7Å for GLIC. A written summary of each plot is below each figure. Except for the omega torsion angle, all other parameters are either acceptable or better than expected for structures/models with the same resolution.
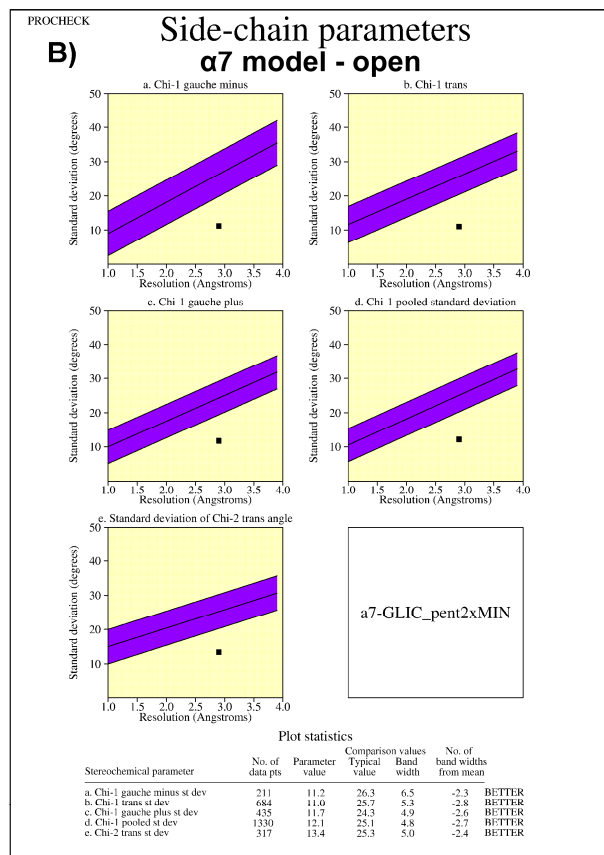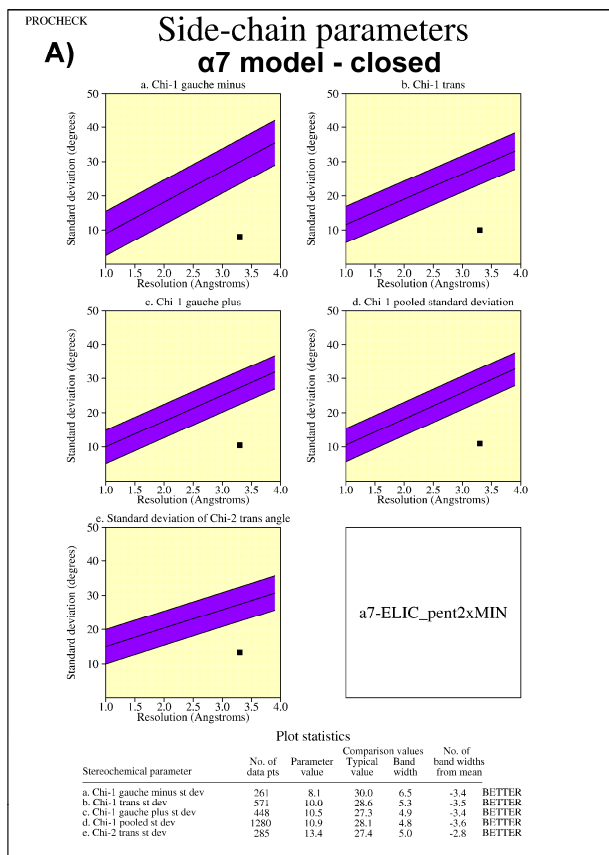
Figure 5.7: Model evaluation – Side chains. Procheck was used to evaluate the side chain stereochemistry of the α7 models in the closed (19A), and open states (19B). A written summary of each plot is below each figure. All parameters were better than expected for structures/models with the same resolution.
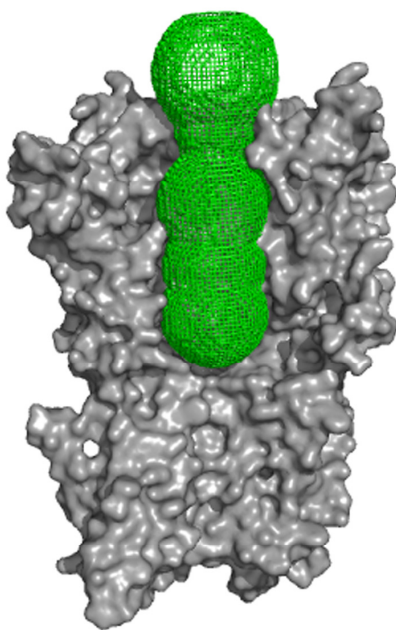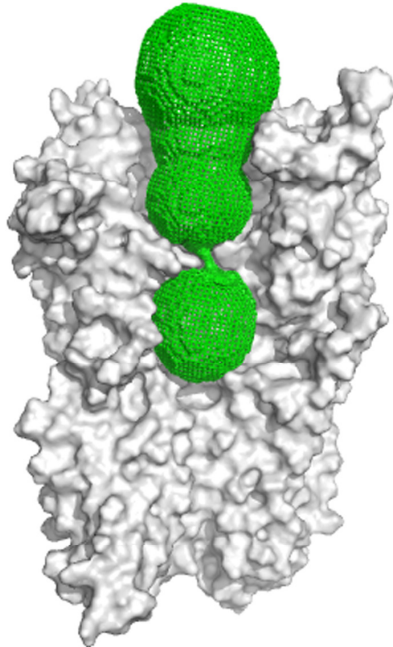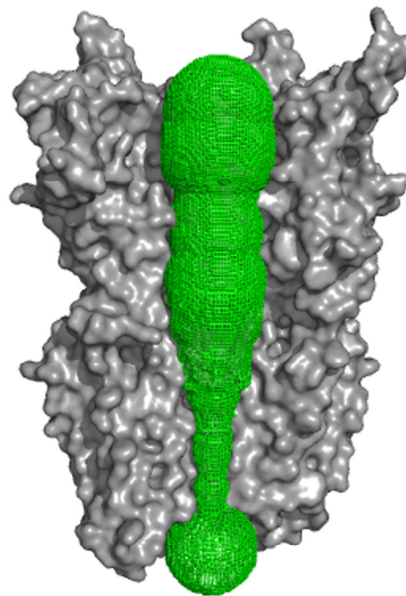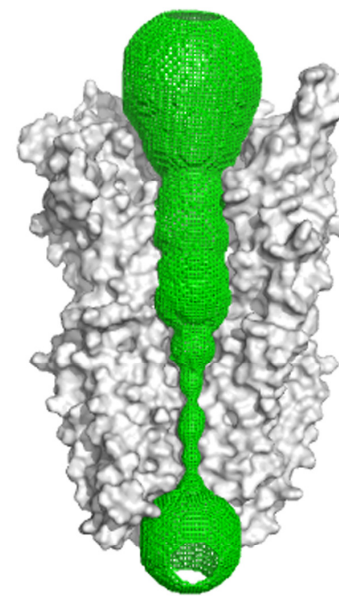
Figure 5.8: Outline of ion-conducting surfaces. The inner vestibule and channel pore for each structure was outlined with Voronoi mesh diagrams and displayed as green mesh using MOLE (Petrek 2007). Starting structures are shown in grey and α7 homology models are shown in white, with only three of five subunits displayed. Note that both homology models are similar to their respective starting structure.

An ACh-response curve was generated before and after application of the cysteine-modifying reagent. To measure accessibility in the closed state, the Cys-modifying reagents were applied individually (2mM for 60 seconds). To measure accessibility in the open state, the Cys-modifying reagent was applied with the maximal-effective dose of ACh (EC_{100}). Accessibility of the Cys-modifying reagent was measured as either a right-shift or left-shift in ACh-dose response curve (ACh EC_{50}), a change in the normalized peak-evoked current (I_{max}), and/or a change in the Hill coefficient .

Two residues were chosen as sites to introduce cysteines and validate the presence of a vestibular constriction. Glutamate 44 is more distal from the site of constriction, and is part of the transition zone that couples agonist binding to receptor gating. Glutamate 44 undergoes agonist and modulator-dependent changes in MTSEA accessibility, most likely due to changes in local electrostatic potential [Barron *et al.* 2009; McLaughlin *et al.* 2009]. Threonine 50 is more proximal to the site of constriction and has not been previously characterized. The results of cysteine accessibility at residue E44C and T50C on ACh-evoked currents are shown in **Table 5.2** and **Figure 5.10-5.11**. MTSBn and MTSEA-biotin had a significant functional effect on the peak current at E44C, but there was no significant difference between modifications in the closed state versus open state. There was no significant effect of exposure to DTNB (data not shown). The same pattern was evident at T50C. There was a significant effect of modification with MTSBn and MTSEA-biotin on the ACh EC_{50}, but there was no significant difference between modifications in the closed state versus the open state. MTSEA-biotin significantly

112

reduced the peak current amplitude, but again there was no significant different between modification in the closed versus the open state. At T50C there was no significant effect of exposure to DTNB (data not shown). This suggests that E44C and T50C are not modified by DTNB, or that there is no functional effect of modification. Because DTNB is the largest cysteine-modifiying reagent that was tested, this compound was predicted to have the greatest functional effect and was expected to reveal a significant change in cysteine accessibility from the closed to open state if a vestibular constriction was present, contrary to the observations. Overall these results suggest that there is no difference in closed state and open state modification with MTSBn and MTSEA-biotin, arguing against the presence of a vestibular constriction.

To further explore the predictive power of the homology models, *in silico* calculations of solvent accessibility and continuum electrostatics were compared against the rate of MTSEA modification of introduced cysteines in the ligand-binding domain of the α7 receptor. These physical parameters determine the reaction rate of a charged MTS reagent with an introduced cysteine in a protein [Karlin and Akabas 1998]. Reaction of an MTS reagent with a thiol with deprotonated thiols (-S⁻) is upwards of 5×10^9 faster than with protonated thiols (-SH) [Bezanilla and Stefani 1998]. Because ionization of thiol groups is suppressed in environments with a low dielectric constant, such as the lipid membrane in protein interior, MTS reagents react almost exclusively with thiols exposed to an aqueous environment [Karlin and Akabas 1998]. For small, charged MTS reagents, the rate of reaction also depends

on the local electrostatic potential. Localized areas of charge would attract or repel

the charged MTS reagent, depending on the sign of the charge .
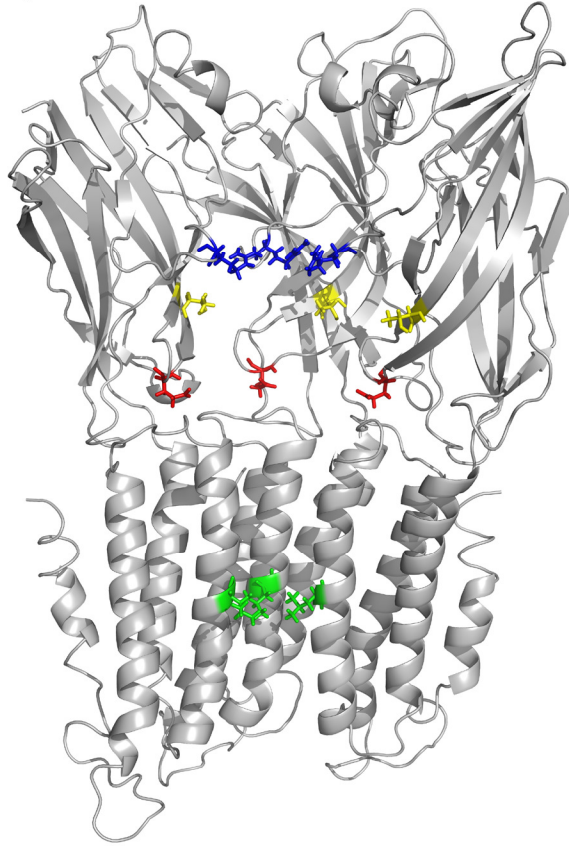
A) - Closed state   **B) Open state**
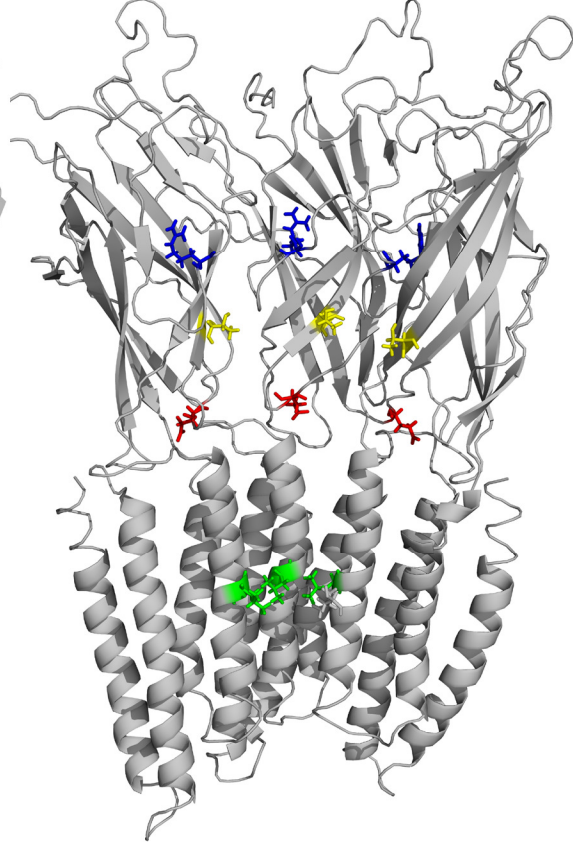
Figure 5.9: Vestibular constriction as a gating mechanism. A constriction in the LBD at position

R98 (blue) in the closed state model (A) of approximately 7 x 5 Å that expands to approximately 20 x

20 Å in the open state (B). Positions distal to the constriction, towards the plasma membrane, are

predicted to be more solvent accessible in the open state as the vestibular constriction releases.

Accessibility at positions T50C (yellow) and E44C (red) were tested using cysteine modifiers in the

closed and open states of the α7 receptor to verify the presence of this constriction as a gating

mechanism. Only three subunits are shown in order to visualize the ion conduction pore. For

reference, L247 (green) is shown as well.

Solvent accessible surface area was calculated using nAccess, as described in Chapter 2. Two different methods exist for calculating the solvent accessible surface area; the relative accessible area (RSA) measures the percentage of accessibility compared to a tri-amino acid peptide, and the atomic accessible area (ASA) measures the absolute accessibility in square angstroms [Hubbard et al. 1991]. Both methodologies utilize the "rolling ball" model where the solvent is reduced to a sphere of equal radius to the starting three dimensional structure (1.4Å for water) and rolled along the surface of the protein (Hubbard and Thornton 1993, [Lee and Richards 1971; Shrake and Rupley 1973]. We compared the RSA of the endogenous residue to the ASA of the introduced cysteine at the same position (**Figure 5.10**). The high correlation coefficient (R^2) values confirm a significant linear relationship between both methodologies in the closed and open state homology models. Either relative accessible area or atomic accessible area can be used to determine the solvent accessible surface area of the amino acid side chain, and subsequent experiments used RSA method.

Figure 5.14 shows the comparison of relative surface accessibility to the rate of reaction of MTSEA at introduced cysteines **(Figure 5.12)**[12]. Calculations of solvent accessibility from the closed state model were compared against MTSEA rates determined in the closed state (no additional ligands). Solvent accessibilities from the open state model were compared to MTSEA rates when an EC_{100} dose of ACh was coapplied with MTSEA. This maximally effective dose of agonist ensured

---

[12] Previously published data was used for these calculations [McLaughlin *et al.* 2007], except for the new data in **Figure 5.12.**

that the maximum number of nicotinic receptors were in the open state when exposed to MTSEA. There is no quantitative correlation between the solvent accessibility and rate of MTSEA modification in either the closed or the open state (**Figure 5.14A**). However, grouping solvent accessibility versus MTSEA modification by amino acid position showed a qualitative trend (**Figure 5.14B**). Of the 14 residues where MTSEA modification data was available, solvent accessibility qualitatively predicts the change in MTSEA rate of modification at nine residues: M37, V42, D43, E44, W54, W148, E172, A262, and T263. This suggests that the rate of MTSEA modification in the ligand-binding domain does not strictly represent a conformational change of the α7 nicotinic receptor.
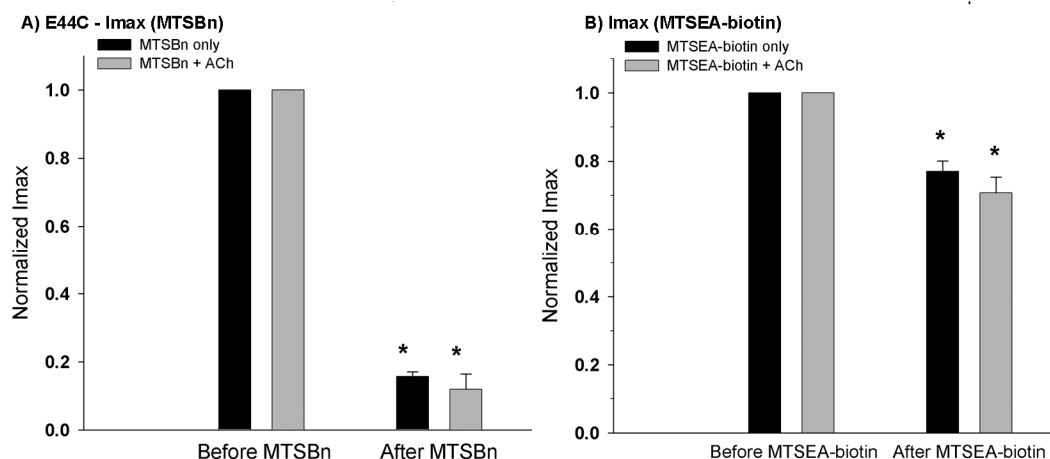
Figure 5.10: Neutral modification of E44C is not altered in the closed vs. open states. ACh-response parameters were analyzed for differences between cysteine modification in the closed state (Cys-modifier alone) or the open state (Cys-modifier plus EC_{100} ACh). While a significant effect of modification was observed with MTSBn (A) and MTSEA-biotin (B) on peak current amplitude, there was no significant effect of modification in the open state (+ ACh). * = P < 0.01, Tukey's posthoc test, compared before and after MTS modification.

Next, we examined the contribution of continuum electrostatics to the rate of MTSEA modification of the α7 receptor. Continuum electrostatics calculations were performed using APBS as described in the Methods [Baker et al. 2001]. This software utilizes the Poisson-Boltzmann (PB) equation, a differential equation that

describes the energetic interactions of molecules in ionic solutions. An excellent review on the theory, derivation, and application of the Poisson-Boltzmann equation to structural biology is available elsewhere [Fogolari et al. 2002]. Due to limits of computational resources, calculations were carried out using a linearized form of the PB equation. Briefly, atomic coordinates are converted to units of charge and radii in PDB2PQR using the PARSE forcefield, as this forcefield is optimized for Poisson-Boltzmann applications [Sitkoff et al. 1994]. The linearized PB equation overlays a coordinate grid over the protein structure, and the electrostatic energy at any given grid point depends on the ionic strength and composition, dielectric constant of surrounding environment, temperature, and the distance and charge of nearby atoms.

Figure 5.15 shows the results of continuum electrostatics calculations along the surface of the ion conduction pathway of the closed and open state α7 receptor homology models. For the vestibule of the ligand-binding domain, no change in electrostatic potential was observed between the closed and open state. The vestibule is composed of a portion of the A-loop, starting just past a critical agonist-binding residue (Y92). There is no available MTS modification data from the nicotinic receptor family, so a comparison is not possible at this time. For the pore-lining M2 helix, the large electronegative field in the closed state also becomes less negative in the open state. In the inner beta sheet and transition zone (midway along the vertical pore axis,) the large electronegative field in the closed state becomes less negative in the open state. This result is in agreement with our existing MTSEA rate

data, where nearly every residue tested shows a reduction in the rate of MTSEA

modification in the open state compared to the closed state (**Figure 5.15B**).
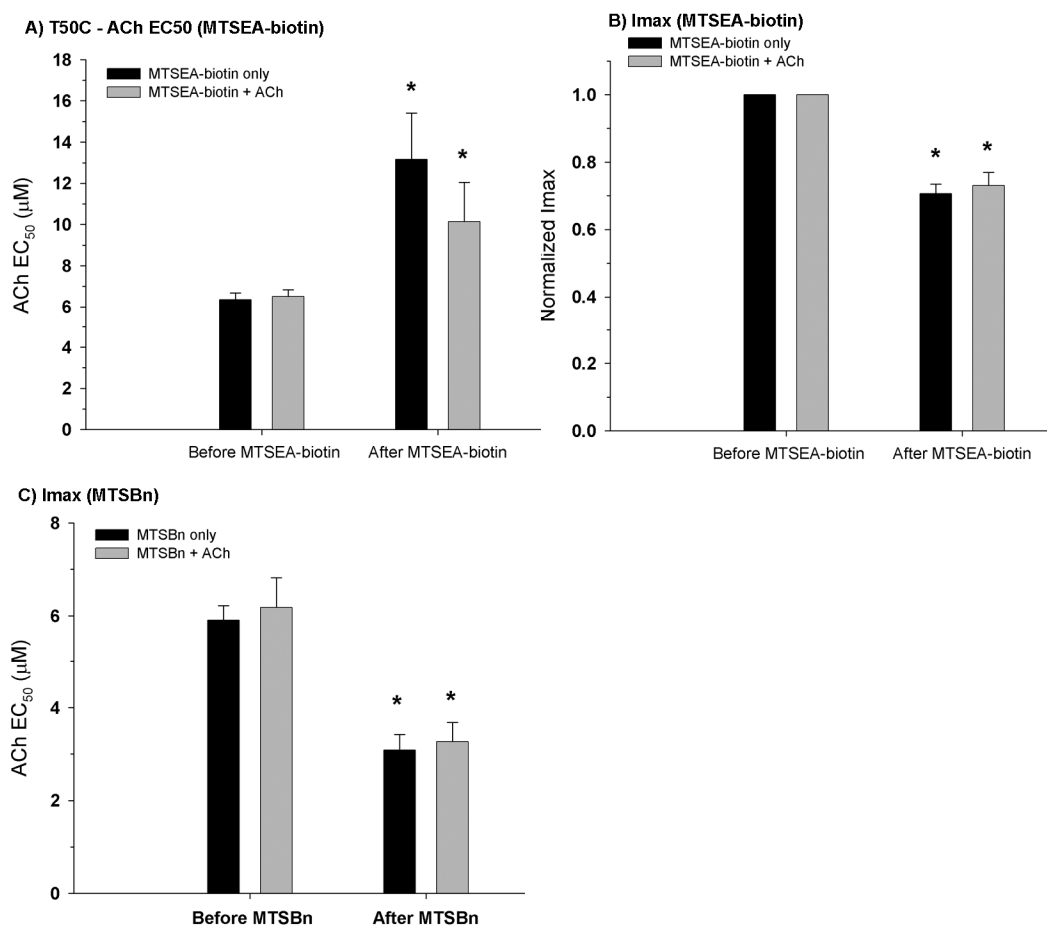
Figure 5.11: Neutral modification of T50C is not altered in the closed vs. open states. ACh-response parameters were analyzed for differences between cysteine modification in the closed state (Cys-modifier alone) or the open state (Cys-modifier plus EC_{100} ACh). A significant effect of modification was observed with MTSEA-biotin on ACh EC_{50} peak current amplitude (A) and peak current amplitude (B), but was no significant effect of modification in the open state (+ ACh). MTSBn significantly lowered the ACh EC_{50} (C), but there was no difference ± ACh. * = P < 0.01, Tukey's posthoc test, compared before and after MTS modification.

Discussion

In this study, we provide the first evidence that homology models of the α7

receptor derived from bacterial Cys-loop homologs can partially predict structural

transitions from the closed to open state. The α7 receptor homology models were

118

validated using a combination self-validation, stereochemical, visual methods

(**Figure 5.1-5.8**). Electrophysiological measurements of conformational change, as

measured using SCAM [Akabas et al. 1992], were compared against *in silico*

measurements of solvent accessible surface area and local electrostatic potential for

the closed and open state of the α7 receptor (**Figure 5.9-5.15**). The strengths and

limitations of this approach are detailed.
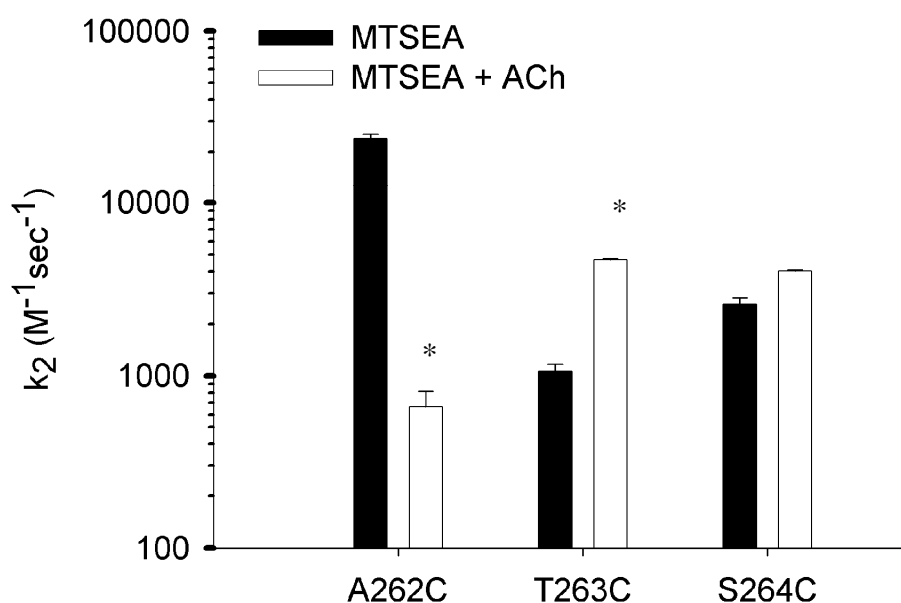
Figure 5.12: MTSEA modification in the M2-M3 linker in the closed and open states.
acetylcholine significantly reduces the rate of MTSEA modification at A262C, and increases the rate
of modification at T263C (P < =0.05, n = 3).

When compared against MTSEA modification at introduced cysteines in the

inner beta sheet and the transition zone, *in silico* solvent accessible surface

qualitatively predicted the changes in accessibility with an accuracy of ≈ 66%

(**Figure 5.14B**). Because electrostatic potential also influences the rate of

modification of charged MTS reagents, it is not surprising that there is not a

quantitative relationship between solvent accessible surface area and rates of

119

MTSEA modification (**Figure 5.14A**). Small, charged MTS reagents have been used

extensively to study conformational changes and residue accessibility in the Cys-

loop family of ligand-gated ion channels [Reeves et al. 2001; Wilson and Karlin

2001; Hanson and Czajkowski 2008; Barron et al. 2009]. Our results suggest that

changes in the accessibility of introduced cysteines to charged chemical modifiers

cannot be strictly interpreted as a structural transition or the presence of a unique

conformation of the receptor. In the context of our previous studies of MTSEA

accessibility in the extracellular-ligand binding domain [Barron *et al.* 2009;

McLaughlin *et al.* 2009], the term "conformational change" should be broadened to

include changes in electrostatic potential energy. This interpretation is supported by

structural and single-channel data from other Cys-loop receptors where relatively

small structural changes away from the agonist-binding site can lead to a large

changes in ion conductivity [Cymes et al. 2005; Cymes and Grosman 2008; Hilf and

Dutzler 2009]
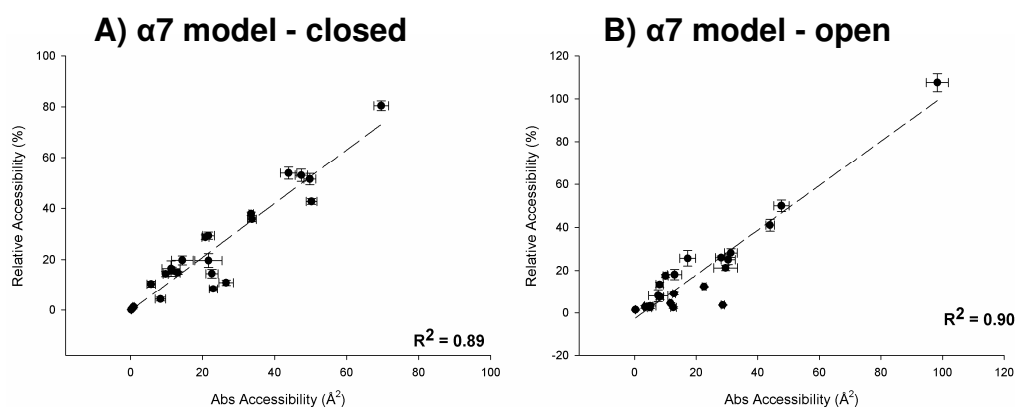
Figure 5.13: Relative vs. Absolute Surface Accessibility. Surface accessibility was calculated as described in the Chapter 2. The Relative Surface Accessibility of endogenous residues is linearly related to the Absolute Surface Accessibility of introduced cysteines for both the closed and open homology models.

For charged cysteine-modifying reagents, such as cationic MTSEA, the local electrostatic field potential determines the accessibility of the introduced cysteine. The inner beta sheet and transition zone become less electronegative in the open state model of the α7 receptor, in agreement with our accessibility measurements with MTSEA (**Figure 5.15A and 5.15B**). There is no change in electrostatic potential in the inner vestibule, corresponding to the A-loop that is directly behind the agonist-binding site.

Interestingly, no change in electrostatic potential was observed between the closed and open state homology models in the pore-lining M2 helix (Figure **5.15**). While there is no comparable MTS rate data from the α7 nicotinic receptor, work on the muscle nicotinic receptor shows faster rates of MTSEA modification in the open state compared to the closed state and an increase in electronegativity [Pascual and Karlin 1998; Wilson and Karlin 2001]. One explanation is that the PB equation exaggerates the effects of ionic shielding and underestimates the force in systems with a radii smaller than the Debye length due to the continuous distribution of mobile ions [Moy et al. 2000]. The Debye length for our working ionic strength of 129 mM is 8.8 Å (see **Methods** for calculations). For our models of the α7 receptor, the vestibule of the extracellular ligand-binding domain has a diameter of ≈ 20 Å and application of the PB equation should not suffer from shielding effects. However, the diameter of the transmembrane pore narrows down to ≈ 2Å at the position of the channel gate (-3' to 2'). The transmembrane pores of α7 receptor and most other ion channels have a radii that are smaller than the Debye length calculated at physiological ionic strength [Hille 2001], which calls into question using the PB

equation and other continuum methodologies in these restricted environments. Non-continuum methods, such as Brownian Dynamics, may be better suited because this approach better predicts forces in artificial and pore-like environments compared to the PB equation [Moy et al. 2000].
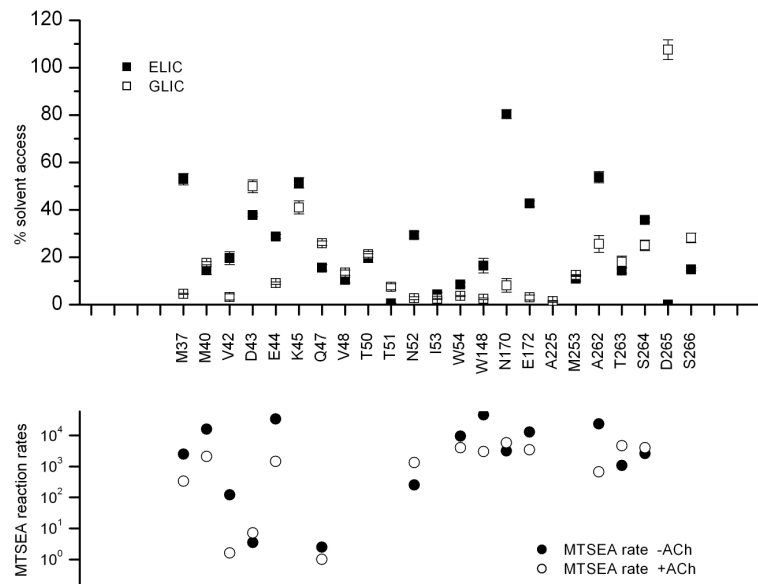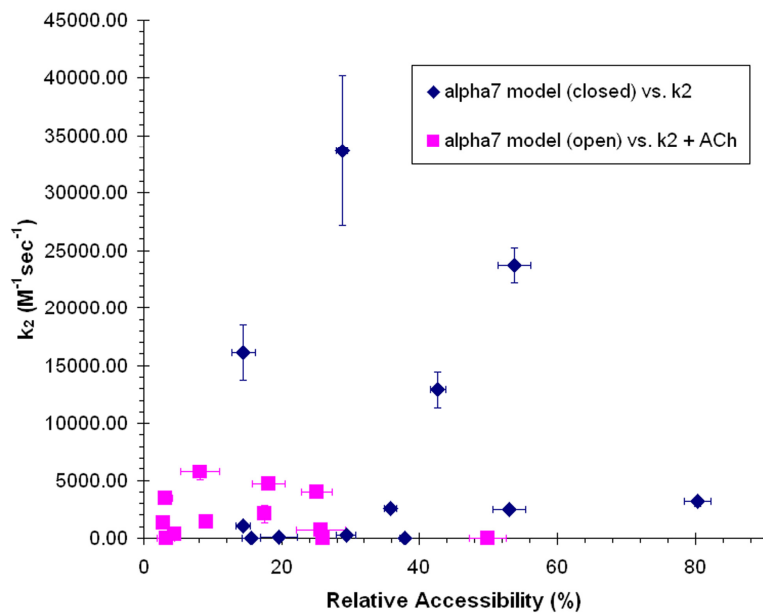
Figure 5.14: MTSEA rate of modification vs. Relative Accessibility. The MTSEA rate of modification at introduced cysteines (k_2, $M^{-1}sec^{-1}$) in the inner beta sheet, transition zone ([McLaughlin et al. 2007], **Figure 5.12**) plotted against the Relative Surface Accessibility (%) of the endogenous residue for the closed and open α7 homology models. The data is plotted independent (A) and dependent (B) on the amino acid residue. "ELIC" stands for the α7 model in the closed state, and "GLIC" stands for the α7 model in the open state.

Finally, we used cysteine accessibility experiments to test the hypothesis that the predicted constriction in the vestibule was a part of the gating mechanism. While both E44C and T50C were modified by MTSBn and MTSEA-biotin, there was no significant change in modification in the open state (+ ACh) versus the closed state (- ACh), arguing against our hypothesis (**Figure 5.10-5.11**). One possibility for this result is that the change in vestibular diameter from the closed to open state is smaller in magnitude than predicted by our homology models. In this case, the rates of cysteine modification would be more sensitive to subtle changes in the closed and open states of the α7 receptor, rather than large effects on ACh-evoked currents before and after maximal cysteine modification.

It should be noted that our *in silico* studies are limited to static models of the α7 receptor in closed and open state. Computational simulations such as molecular dynamics and elastic network models have provided insight into the initial and long timescale conformational changes associated with gating of nicotinic receptors, respectively. Both approaches have revealed a combination of twisting of the ligand-binding domain and tilting of the M2 helices that allosterically converge on the channel gate [Hurst et al. 2005; Taly et al. 2005; Szarecka et al. 2007; Cheng et al. 2009]. The gate is located between the -3' and 2' positions on the M2 helix [Wilson and Karlin 2001], and is preceded by a hydrophobic girdle between the 9'-17' positions. Over the length of the entire M2 helix, cations are excluded but water is present [Beckstein and Sansom 2006; Ivanov et al. 2007]. Finally, The L9'T mutation is another factor to consider but our previous studies have shown that the rate of MTSEA modification at introduced cysteines in wildtype receptors is not significantly

124

different at receptors carrying the L9'T mutation [Barron et al. 2009]. This work demonstrates the limitations and pitfalls of homology models as predictors of receptor structure, and illustrates the importance of validation using non-computational methods before proceeding with additional *in silico* studies.

However, several important questions about gating remain unanswered. Functional studies of slow onset desensitization have suggested the presence of a separate desensitization gate that extends from the -3' to 9' positions [Karlin 2002; Paas et al. 2005]. As all of the previously described computational simulations were on closed state receptor models, the conformational changes associated from the open state to the desensitized state are unknown. Since desensitization of nicotinic receptors increases proportionally to the number of binding sites [Rayes et al. 2009], homology models based on the heteromeric *Torpedo* nAChR may not accurately capture conformational changes associated with desensitization of the homomeric α7 receptor. Our validated open state model will be an excellent tool to study open to desensitized conformational and electrostatic changes.

The long-term goal of this research is to understand the conformational changes that underlie gating of the α7 receptor. We have presented evidence that closed and open state homology models of the α7 receptor are valid, and partially predict structural transitions associated with changes in solvent accessible surface area and local electrostatic potential. However, a vestibular constriction in the closed state could not be verified using cysteine modification, and illustrating the pitfalls of using only computational methodology to study gating mechanisms of ion channel receptors.

A)
α7 model - closed
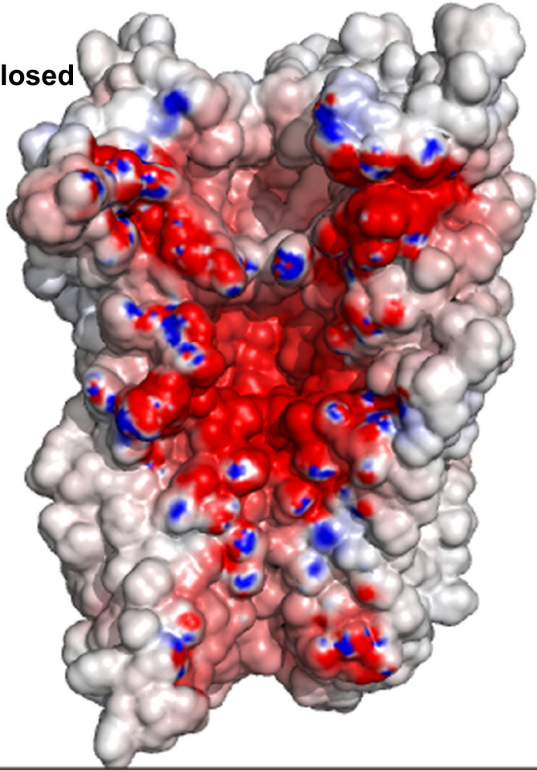
B) α7 model - open
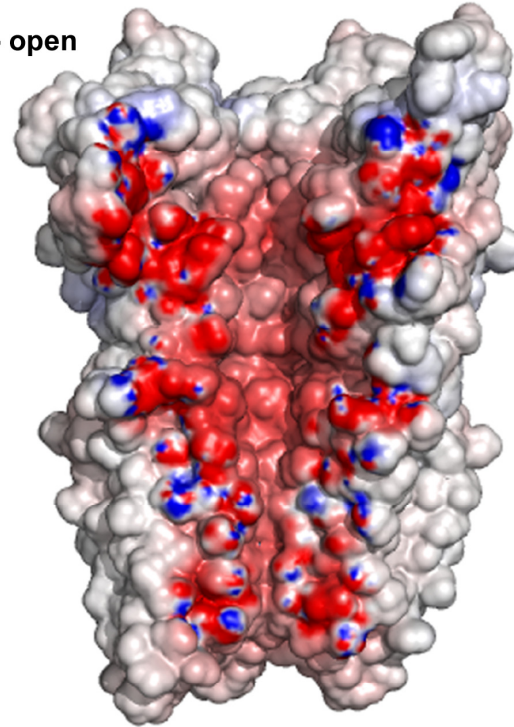
Figure 5.15: Reduction of electronegativity better predicts conformational changes in the LBD. Calculations were carried out using APBS, as described in the Chapter 2. Units are in kT/e [(Boltzmann's Constant * Temperature)/Elementary Charge], with the scale bars shown below the protein model. Only three of the five subunits for each receptor is shown, in order to visualize the ion-conducting surface. The change to a more positive electrostatic potential from the closed to open state in the inner beta sheet region agrees with previously published data from our lab (McLaughlin 2007, Barron 2009).

Table 5.1 - Summary of ACh responses before cysteine modification

Mutant	cysteine Modifier	ACh EC_{50} (µM)			Hill Coefficient			Imax (µA)			n
E44C	MTSBn	7.74	±	1.46	2.33	±	0.22	5.66	±	0.94	3
	MTSBn + ACh	8.57	±	0.69	2.15	±	0.22	5.37	±	2.21	3
	MTSEA-biotin	9.13	±	1.51	2.74	±	0.35	7.10	±	1.92	3
	MTSEA-biotin + ACh	8.63	±	1.41	3.15	±	0.79	6.79	±	1.15	4
	DTNB	6.70	±	0.92	2.97	±	0.26	5.89	±	2.11	3
	DTNB + ACh	7.71	±	0.34	2.46	±	0.18	8.45	±	2.13	3
E44C	Average	9.29	±	1.13	2.51	±	0.21	6.59	±	0.65	19
T50C[†]	MTSBn	5.90	±	0.32	3.03	±	0.21	2.08	±	1.34	3
	MTSBn + ACh	6.18	±	0.64	2.99	±	0.53	2.95	±	2.05	3
	MTSEA-biotin	6.35	±	0.33	3.17	±	0.31	1.47	±	1.19	3
	MTSEA-biotin + ACh	6.51	±	0.32	3.55	±	0.52	1.76	±	1.45	3
	DTNB	5.98	±	0.53	3.14	±	0.85	3.61	±	0.75	3
	DTNB + ACh	6.56	±	0.40	2.86	±	0.45	1.73	±	1.46	3
T50C[†]	Average	2.27	±	0.52	3.12	±	0.19	2.27	±	0.52	18

† = denotes co-expression with human RIC-3 (see Chapter 2).

Table 5.2 - Summary of ACh responses after cysteine modification

Mutant	cysteine Modifier	ACh EC$_{50}$ (µM)	Hill Coefficient	Change in Peak Current[+]	n
E44C	MTSBn	18.60 ± 7.83	1.74 ± 0.22	0.16 ± 0.01 *	3
	MTSBn + ACh	7.96 ± 1.16	2.68 ± 0.84	0.12 ± 0.04 *	3
	MTSEA-biotin	5.84 ± 0.91	2.33 ± 0.38	0.80 ± 0.02 *	3
	MTSEA-biotin + ACh	5.94 ± 0.79	2.31 ± 0.12	0.71 ± 0.06 *	4
	DTNB	6.91 ± 0.65	2.81 ± 0.09	0.97 ± 0.03	3
	DTNB + ACh	7.22 ± 0.35	2.65 ± 0.19	1.02 ± 0.05	3
T50C[†]	MTSBn	3.09 ± 0.34 *	3.02 ± 0.89	1.03 ± 0.15	3
	MTSBn + ACh	3.27 ± 0.41 *	3.10 ± 0.96	0.99 ± 0.10	3
	MTSEA-biotin	13.17 ± 2.24 *	3.08 ± 0.51	0.71 ± 0.03 *	3
	MTSEA-biotin + ACh	10.14 ± 1.90 *	3.03 ± 0.18	0.73 ± 0.04 *	3
	DTNB	7.45 ± 1.47	2.40 ± 0.48	1.10 ± 0.11	3
	DTNB + ACh	6.64 ± 0.71	3.10 ± 0.60	0.93 ± 0.05	3

+ = The Change in Peak current was calculated as the Imax after cysteine modification divided by the Imax before cysteine modification

* = P < 0.01, before cysteine modification within the same treatment group.

† = denotes co-expression with human RIC-3 (see Chapter 2).

CHAPTER 6

CONCLUSIONS AND FUTURE DIRECTIONS

The goal of this work was to define the molecular mechanisms of positive allosteric modulation of the α7 nicotinic acetylcholine receptor. The development of new agonists and PAMs targeting the α7 and other nAChRs is an area of active of research because of their unique neurophysiology and connection to a wide variety of neurological disorders [Gotti and Clementi 2004]. In particular, PAMs may have a unique therapeutic potential because of the requirement of agonists to enhance channel current. In the synaptic cleft, cholinergic neurotransmission is tightly controlled by the rapid degradation of ACh by acetylcholinesterase and the recovery of choline by the high-affinity choline transporter [Amenta and Tayebati 2008]. PAMs of the α7 nAChR (Type I or Type II) should preserve the tight temporal timing of cholinergic neurotransmission because these compounds (with the notable exception of galanthamine; [Samochocki *et al.* 2003]) do not alter the kinetics of ACh degradation or choline transport.

In order to elucidate the mechanisms of allostery, we used SCAM to probe to conformation transitions of the α7 receptor in the closed, open, and "modulated" states. We have demonstrated that two positive allosteric modulators (Ba^{2+} and PNU-120596) cause similar changes in the rate of cysteine accessibility as of the agonist acetylcholine in the agonist-binding domain, in spite of large differences in chemical structure and effects on macroscopic desensitization. As a complimentary technique, we also developed homology models of the α7 receptor from the structures of bacterial Cys-loop receptors to study receptor gating. We found that electrostatics are a better predictor of cysteine accessibility in the LBD than physical rearrangements. The significance of these findings, future studies and additional

methods to elucidate the mechanisms of positive allosteric modulation and receptor gating will be discussed below.

Agonists and PAMS cause similar conformational changes in the LBD

In order to investigate mechanisms of allostery of the nAChRs, we utilized the Substituted cysteine Accessibility Method (SCAM). This method has several advantages with respect to ion channels, such as using changes in peak current amplitude as an instant readout of cysteine modification, and is a well-established technique to study mechanisms of gating and surface accessibility in ion channels. Because of the infinite combinations of possible sites to mutate to a cysteine and cysteine-modifying reagents to test, our experiments were designed to test representative allosteric modulators and sites of interest with our most sensitive cysteine-modifying reagent, MTSEA. We chose two positive allosteric modulators, Ba^{2+} and PNU-120596, because of their different size and chemistry, and because of their different effects on macroscopic desensitization. Barium and other permeable divalent cations to do not alter macroscopic desensitization (making them Type I modulators) [Eddins et al. 2002a], whereas PNU-120596 eliminates receptor desensitization (Type II) [Gronlien et al. 2007]. We chose 2-3 residues each from different regions of the LBD; the agonist-binding site, the inner beta sheet, and the transition zone (**Figure 1.1, 3.1**). Other possible and published experimental designs include complete sampling of a sub region with a single cysteine-modifying reagent [Kloda and Czajkowski 2007], studying fewer residues with a larger number of pharmacological compounds and cysteine-modifying reagents [Chang and Weiss

2002], or studying the desensitized state in addition to the closed and open states of the receptor [Wilson and Karlin 2001]. Our experimental design is a useful template for the initial characterization of a new or untested compound and understanding the broader mechanisms of allostery for the entire protein.

Using SCAM, we determined that Ba^{2+} and PNU-120596 cause similar but non-identical changes in the rate of cysteine modification with MTSEA in the extracellular agonist-binding domain of the α7 receptor, compared to acetylcholine. Whether the change in cysteine accessibility is reflective of a structural transition or a change in the local electrostatic potential, it appears that PAMs induce some of the critical rearrangements associated with activation as agonists. Determining if these conformational changes are associated with an increase in the binding affinity for agonists, or an increase in channel gating is an important area for future studies. Radioligand binding experiments with labeled competitive antagonist in the presence of positive allosteric modulators could be used to assay changes in binding affinity at the agonist-binding site. A decrease in the dissociation constant (K_i) for a competitive antagonist or agonist in the presence of a positive allosteric modulator would provide evidence of a direct interaction between the agonist-binding site and putative binding sites for permeable divalent cations and PNU-120596 [Galzi et al. 1996; Bertrand et al. 2008; Young et al. 2008]. Work on the GABA$_A$ receptors suggests that benzodiazepines and agonists cause a reciprocal increase the binding affinity at their respective binding sites, [Olsen and Snowman 1982; Rogers et al. 1994], but pentobarbital does not induce conformational changes at the benzodiazepine binding site [Sharkey and Czajkowski 2008]. This suggests that

coupling between different allosteric sites to the orthosteric site(s) may not be conserved.

In addition, single channel recordings could be used to study the role of both increased channel gating and increased agonist binding affinity as a mechanism for positive allosteric modulators. The limited single-channel data from PNU-120596 on α7 receptors suggests that this compound increases the mean open time [Hurst et al. 2005]. However, because PNU-120596 does not evoke currents on wildtype α7 receptors in the absence of agonists, it is unknown if this compound simply enhances the kinetic reaction scheme employed by agonists (**Figure 1.2**), or utilizes an alternative conformational pathway. This body of work identified a pair of mutations that convert PNU-120596 to a full agonist (W148C-L247T; **Figure 3.7A**), which could be used to directly study the effect of PNU-120596 on single channels. Another approach would be to study PNU-evoked currents on a mutant receptor that has a high spontaneous open probability. In both experiments, PNU-evoked currents would be studied as a surrogate for allosteric modulation, but would need to be well controlled to ensure that introduction of these mutations preserves the pharmacological profile of this compound. The equivalent mutations in the muscle nAChR that increase spontaneous opening have not yet been studied in the α7 receptor [Purohit and Auerbach 2009]. However, we have studied the W148C-L247T mutant and found that the PNU EC_{50} value and Type II modulation profile were not affected (**Figure 3.2, 3.7A**), which would make this mutant receptor a suitable model for single-channel recordings.

Evidence against the putative Ca^{2+} binding site

One particular challenge in studying allosteric modulators of ion channels is the complex relationship between macroscopic half-maximal excitatory dose (EC_{50}), binding affinity, and channel gating. In short, the EC_{50} value for an agonist or a positive allosteric modulator is an aggregate of the binding affinity of the compound, and the ability of that binding energy to induce and/or enhance the conformational changes from the closed to open states [Jackson 1989; Colquhoun 1998]. For the α7 nicotinic receptor, the EC_{50} values of several allosteric modulators (including PNU-120596) are in the low micromolar to low millimolar range [Gronlien et al. 2007; Timmermann et al. 2007], which likely translates into binding affinities that are too low to be directly measured using radioligand binding assays. Our results support this, as direct binding of [^{3}H]PNU-120596 to α7 receptor-enriched membranes did not yield any specific binding (data not shown). Therefore, the study of allosteric modulators has been limited to site-directed mutagenesis to discover important residues.

The putative permeable divalent cation binding site was initially characterized using site-directed mutagenesis of glutamates in the LBD and luminescent resonance energy transfer of Tb^{3+} binding to α7 receptor peptides [Galzi et al. 1996]. While E44 and E172 play an important role in allosteric modulation by divalent cations, there are several caveats concluding these residues constitute a binding site. First, a short α7 receptor peptide is not likely to have the same three-dimensional structure as the full length, membrane-embedded receptor. Secondly, the distances between the conserved glutamates in α7 receptor homology models

are too great to coordinate a calcium ion [Le Novere et al. 2002; Harding 2004; Taly et al. 2005]. To test the existing hypothesis of a Ca^{2+} binding site at E44 and E172, we combined a cysteine mutation that is sensitive to allosteric transitions by Ba^{2+} (M40C, **Figure 4.4**) and a charge neutralization mutation in the putative binding site (E172Q) that eliminates allosteric modulation by Ca^{2+} [Galzi et al. 1996]. If E172 is part of a Ca^{2+} binding site, then the charge neutralization mutation should also eliminate structural transitions measured at a reporter residue. Because Ba^{2+} induced conformational changes at M40C with the addition of the E172Q mutation (**Figure 4.6**), we conclude that E172 is not part of a divalent cation binding site.

Given our results, the location of the divalent cation-binding site remains an open question. Previous work from our lab suggests that the permeable divalent cation binding site is in the LBD of the α7 receptor [Eddins et al. 2002a; Eddins et al. 2002b], and one likely candidate would be the agonist-binding site. Cations can interact at the agonist-binding site, as monovalent cations act as low affinity, competitive antagonists in muscle-type nAChRs [Akk and Auerbach 1996]. In α7 receptors, divalent cations could act as PAMs at unoccupied agonist-binding sites, similar to benzodiazepines and $GABA_A$ receptors. Other possible divalent cation sites were identified in the structure of the AChBP [Brejc et al. 2001], but have not yet been tested.

Methodologies to study low-affinity sites

While mutagenesis studies are limited in their ability to conclusively identify a binding site, several alternative techniques exist to study low-affinity binding sites on

membrane receptors. One alternative method to determine the divalent cation site would be the $^{45}Ca^{2+}$ overlay [Bian et al. 2001]. Briefly, overexpressed α7 receptor would be separated by SDS-PAGE, transferred to polyvinyl fluoride membranes, exposed to $^{45}CaCl_2$ and visualized with autoradiography. The relative amount of $^{45}Ca^{2+}$ binding could be compared between wildtype and receptors mutated at putative binding sites. While this technique cannot be used to calculate a binding affinity, changes in $^{45}Ca^{2+}$ binding would provide evidence for or against the importance of those locations[13]. Another technique that could be used to calculate a binding affinity for Ba^{2+}, PNU-120596, and other low-affinity compounds would be isothermal titration calorimetry [Turnbull and Daranas 2003]. In brief, changes in the enthalpy of detergent-solubilized receptor caused by the binding of compounds can be used to calculate association and dissociation constants. Photoaffinity labeling studies can be used to independently determine compound binding sites without the requirement for site-directed mutagenesis [Nirthanan et al. 2008]. Finally, techniques such as diffusion-enhanced luminescent energy transfer from Tb^{3+} to α7 receptor agonists and PAMs could be used to directly calculate changes electrostatic potential as well as the amount of energy transferred to the receptor from the modulating compound [Meltzer et al. 2006a; Meltzer et al. 2006b; Meltzer et al. 2006c].

The common thread in the above-mentioned techniques is that they all require large amounts of highly purified protein. Historically, the *Torpedo marmorata*

---

[13] This technique has been successfully used to identify high-affinity calcium binding sites, such as the EF-hand motif found in calmodulin [Bian *et al.* 2001]. This approach could not identify a calcium-binding site at the interface between receptor subunits, because the protein samples are denatured prior to running on an SDS-PAGE gel.

nAChR has been the receptor of choice because large amounts of receptor can be purified from the electric organ [Nirthanan et al. 2005]. In contrast, the ability to overexpress and purify large quantities of full-length α7 receptor has long been a technical challenge due in part to the low surface expression of this receptor from *in vitro* systems [Fischer et al. 2001]. However, two technical advances in the last seven years may facilitate overexpression of large quantities of the α7 receptor. First, the chaperone protein RIC-3 is required for proper cycling of the α7 receptor to the plasma membrane in eukaryotes. [Halevi et al. 2002; Lansdell et al. 2005; Castelan et al. 2008]. Increasing the cell surface expression of the α7 nAChR would allow more protein to be purified in subsequent experiments. Second, the standardization of vectors and methodology for overexpression and purification of membrane receptors from *Saccharomyces cerevisiae* (Baker's Yeast) has been outlined in thorough detail, and is an attractive model system to ensure proper receptor folding and retention of post-translational modifications [Newstead et al. 2007; Drew et al. 2008]. Coexpression of RIC-3 and the α7 nicotinic receptor in *S. cerevisiae* and subsequent purification by GFP and Ni^{2+} affinity columns would be an active area of future work as a prerequisite to additional biophysical and biochemical studies of allosteric modulation.

Electrostatic compensation as a unifying model for receptor gating

        A broader goal of this work is to elucidate the gating mechanism of the Cys-loop receptor family, and the isomerization from an ion-impermeable to an ion-permeable conformational state. Since the initial cryo-EM characterization of the

Torpedo nAChR by Unwin and colleagues [Toyoshima and Unwin 1988; Unwin 1993; Unwin 1995], multiple and sometimes conflicting mechanisms for receptor gating have been proposed. The initial hypothesis of a rigid-body rotation of individual subunits [Miyazawa *et al.* 2003] has evolved into the quaternary twist hypothesis, which incorporates both rotational and tilting motions [Taly *et al.* 2005; Taly *et al.* 2006]. Subtle tilting of the transmembrane α-helices is supported by higher-resolution x-ray crystallography of bacterial Cys-loop receptors [Hilf and Dutzler 2008; Bocquet *et al.* 2009; Hilf and Dutzler 2009]. Importantly, relatively small conformational changes in the TMD as a gating mechanism (such as helix tilting) are also supported by protonization of titratable residues [Cymes *et al.* 2005; Cymes and Grosman 2008]. Experimental confirmation of these proposed mechanisms is crucial to determining the true gating mechanisms of the Cys-loop receptor family.

In order to explore the role of the LBD in gating of the α7 receptor, we developed homology models in the closed and open states of the bacterial Cys-loop receptor structures and compared our existing MTSEA accessibility data [McLaughlin *et al.* 2007]. In particular, we assayed changes in structure (solvent accessibility) and electrostatics in closed vs. the open state models. While individual residues are predicted to undergo large structural transitions (**Figure 5.14)**, changes in electrostatics in the LBD are a better predictor of the closed to open isomerization (**Figure 5.15)**. This conclusion is also supported by structural observations from the closed and open state models, where the large diameter of the extracellular vestibule remains the same [Taly *et al.* 2009].

In particular, we observed **decrease** in the electronegative surface area in the inner beta sheet and transition zone. This result seems counterintuitive, as an **increase** in electronegative surface area would likely attract a greater number of cations and increase cation flux through the ion-permeation pathway of the receptor. So how can we reconcile this observation? First, we will assume that a large macromolecule such as the α7 nAChR maintains a constant net charge under physiological pH and ionic strength. Because only a small transference of charge is necessary to alter cellular membrane potential, this is a reasonable assumption [Hille 2001]. Second, we will assume that structural transitions precede changes in electrostatics. With these assumptions in mind, we hypothesize that any change in local electrostatic potential during the closed-open gating transition would be **compensated by an opposite change in potential** in other regions of the receptor. In other words, if the electrostatic potential decreases in one region it would have to increase in a different region of the receptor in order to maintain a constant net charge. For an ion channel, the most likely candidate site for electrostatic compensation would be the TMD, where the energy barrier to ion permeation is the highest. This hypothesis is attractive as it reconciles our observations using MTSEA modification and electrostatic modeling with the existing theories on ion permeation through the Cys-loop receptor, including electric focusing by charged rings along the ion permeation path and the hydrophobic girdle in the M2 helix. A decrease in the electrostatic potential (less negative) in the LBD could be compensated by an increase in electrostatic potential (more negative) in the TMD, which would further lower the energy barrier to ion translocation in the open state.

MTS analysis of electrostatics in the M2 helix of muscle nAChRs supports our "electrostatic compensation" hypothesis, as the electrostatic potential dramatically increases by -75 to -125 mV from the closed to open states. [Pascual and Karlin 1998]. To further test our hypothesis, we will want to be able to directly compare and quantify changes in electrostatic potential. Cysteine modification with either a neutral or a positively charged compound, in addition to our existing MTSEA data, can be used to calculate changes in electrostatic potential. While we have found the LBD to be insensitive to cationic cysteine modifiers (**Figure 3.11**), small hydrophobic modifiers such as MTSBn or MMTS would likely work, and our results of E44C modification with MTSBn are encouraging (**Figure 5.10).** Therefore, one important future direction would be to measure rates of MTSBn modification at our existing cysteine mutants in the agonist-binding site, inner beta sheet, transition zone, and M1-M2 linker (**Table 3.2, Figure 5.12**) and calculate changes in electrostatic potential in the open and modulated states. An added advantage to adding a small, hydrophobic MTS reagent to our repertoire is that these reagents will allow us to better distinguish between conformational changes and changes in electrostatics.

Another line of future experiments to test our "electrostatic compensation" model would be to investigate agonist- and PAM-induced structural transitions in the M2 helix using SCAM. While some might argue that pursuing these experiments in the α7 receptor is too similar to the work done in the muscle nAChR [Pascual and Karlin 1998; Wilson and Karlin 2001], there are several compelling reasons to pursue these experiments. Alpha7 nAChRs are different from muscle nAChRs with respect to Ca^{2+} permeability and rate of desensitization, so there is no *a priori*

reason to assume that agonist-induced structural transitions of α7 receptor will be identical to those of the muscle nAChR. Secondly, the real novelty of these experiments would be to explore PAM-induced structural transitions, and comparing these results to parallel experiments examining agonist-induced changes. Because PAMs do not directly gate the α7 receptor, we would predict a divergence in structural transitions between PAMs and agonists somewhere in the M2 helix.

The findings presented in this dissertation indicate that positive allosteric modulators and agonists share a conserved gating mechanism in the extracellular ligand-binding domain of the α7 nicotinic receptor. Further analysis using high-resolution homology models showed that a change in electrostatics between the closed and open states is primary mechanism associated with receptor gating. These findings advance our understanding of allostery and receptor gating, and could enhance the drug discovery process. Future studies will focus on the molecular mechanisms associated from the open to desensitized transition using the open state model and cysteine accessibility, and modulation of these processes by positive allosteric modulators.

REFERENCES

Abdrakhmanova G, Cleemann L, Lindstrom J and Morad M. (2004). Differential modulation of beta2 and beta4 subunits of human neuronal nicotinic acetylcholine receptors by acidification. *Mol Pharmacol* **66**: 347-55.

Adelsberger H, Lepier A and Dudel J. (2000). Activation of rat recombinant alpha(1)beta(2)gamma(2S) GABA(A) receptor by the insecticide ivermectin. *Eur J Pharmacol* **394**: 163-70.

Akabas MH, Kaufmann C, Archdeacon P and Karlin A. (1994). Identification of acetylcholine receptor channel-lining residues in the entire M2 segment of the α subunit. *Neuron* **13**: 919-27.

Akabas MH, Stauffer DA, Xu M and Karlin A. (1992). Acetylcholine receptor channel structure probed in cysteine-substitution mutants. *Science* **258**: 307-10.

Akk G and Auerbach A. (1996). Inorganic, monovalent cations compete with agonists for the transmitter binding site of nicotinic acetylcholine receptors. *Biophys J* **70**: 2652-8.

Allwright JC. (1976). CONJUGATE GRADIENT VERSUS STEEPEST DESCENT. *Journal of Optimization Theory and Applications* **20**: 129-134.

Amenta F and Tayebati SK. (2008). Pathways of acetylcholine synthesis, transport and release as targets for treatment of adult-onset cognitive dysfunction. *Curr Med Chem* **15**: 488-98.

Amin J, Brooks-Kayal A and Weiss DS. (1997). Two tyrosine residues on the α subunit are crucial for benzodiazepine binding and allosteric modulation of gamma-aminobutyric acidA receptors. *Mol Pharmacol* **51**: 833-41.

Arias HR. (1998). Binding sites for exogenous and endogenous non-competitive inhibitors of the nicotinic acetylcholine receptor. *Biochim Biophys Acta* **1376**: 173-220.

Atack JR. (2003). Anxioselective compounds acting at the GABA(A) receptor benzodiazepine binding site. *Curr Drug Targets CNS Neurol Disord* **2**: 213-32.

Auerbach A. (2007). How to turn the reaction coordinate into time. *J Gen Physiol* **130**: 543-6.

Auerbach A and Akk G. (1998). Desensitization of mouse nicotinic acetylcholine receptor channels. A two-gate mechanism. *J Gen Physiol* **112**: 181-97.

Auerbach A and Sachs F. (1983). Flickering of a nicotinic ion channel to a subconductance state. *Biophys J* **42**: 1-10.

Azam L and McIntosh JM. (2006). Characterization of nicotinic acetylcholine receptors that modulate nicotine-evoked [3H]norepinephrine release from mouse hippocampal synaptosomes. *Mol Pharmacol* **70**: 967-76.

Baker NA, Sept D, Joseph S, Holst MJ and McCammon JA. (2001). Electrostatics of nanosystems: application to microtubules and the ribosome. *Proc Natl Acad Sci U S A* **98**: 10037-41.

Barrantes FJ. (2002). Lipid matters: nicotinic acetylcholine receptor-lipid interactions (Review). *Mol Membr Biol* **19**: 277-84.

Barron SC, McLaughlin JT, See JA, Richards VL and Rosenberg RL. (2009). An allosteric modulator of alpha7 nicotinic receptors, N-(5-Chloro-2,4-dimethoxyphenyl)-N'-(5-methyl-3-isoxazolyl)-urea (PNU-120596), causes conformational changes in the extracellular ligand binding domain similar to those caused by acetylcholine. *Mol Pharmacol* **76**: 253-63.

Beckstein O and Sansom MS. (2006). A hydrophobic gate in an ion channel: the closed state of the nicotinic acetylcholine receptor. *Phys Biol* **3**: 147-59.

Bera AK, Chatav M and Akabas MH. (2002). GABA(A) receptor M2-M3 loop secondary structure and changes in accessibility during channel gating. *J Biol Chem* **277**: 43002-10.

Bertrand D, Bertrand S, Cassar S, Gubbins E, Li J and Gopalakrishnan M. (2008). Positive allosteric modulation of the α7 nicotinic acetylcholine receptor: ligand interactions with distinct binding sites and evidence for a prominent role of the M2-M3 segment. *Mol Pharmacol* **74**: 1407-16.

Bertrand D, Galzi JL, Devillers-Thiery A, Bertrand S and Changeux JP. (1993). Mutations at two distinct sites within the channel domain M2 alter calcium permeability of neuronal alpha 7 nicotinic receptor. *Proc Natl Acad Sci U S A* **90**: 6971-5.

Bertrand D and Gopalakrishnan M. (2007). Allosteric modulation of nicotinic acetylcholine receptors. *Biochem Pharmacol* **74**: 1155-63.

Bezanilla F and Stefani E. (1998). Gating currents. *Methods Enzymol* **293**: 331-52.

Bian S, Favre I and Moczydlowski E. (2001). Ca2+-binding activity of a COOH-terminal fragment of the Drosophila BK channel involved in Ca2+-dependent activation. *Proc Natl Acad Sci U S A* **98**: 4776-81.

Bianchi MT and Macdonald RL. (2001). Mutation of the 9' leucine in the GABA(A) receptor gamma2L subunit produces an apparent decrease in desensitization by stabilizing open states without altering desensitized states. *Neuropharmacology* **41**: 737-44.

Bocquet N, Nury H, Baaden M, Le Poupon C, Changeux JP, Delarue M and Corringer PJ. (2009). X-ray structure of a pentameric ligand-gated ion channel in an apparently open conformation. *Nature* **457**: 111-4.

Bocquet N, Prado de Carvalho L, Cartaud J, Neyton J, Le Poupon C, Taly A, Grutter T, Changeux JP and Corringer PJ. (2007). A prokaryotic proton-gated ion channel from the nicotinic acetylcholine receptor family. *Nature* **445**: 116-9.

Bormann J, Hamill OP and Sakmann B. (1987). Mechanism of anion permeation through channels gated by glycine and gamma-aminobutyric acid in mouse cultured spinal neurones. *J Physiol* **385**: 243-86.

Bouzat C, Gumilar F, Spitzmaul G, Wang HL, Rayes D, Hansen SB, Taylor P and Sine SM. (2004). Coupling of agonist binding to channel gating in an ACh-binding protein linked to an ion channel. *Nature* **430**: 896-900.

Bowie JU, Luthy R and Eisenberg D. (1991). A method to identify protein sequences that fold into a known three-dimensional structure. *Science* **253**: 164-70.

Boyd ND and Cohen JB. (1980). Kinetics of binding of [3H]acetylcholine to Torpedo postsynaptic membranes: association and dissociation rate constants by rapid mixing and ultrafiltration. *Biochemistry* **19**: 5353-8.

Braff DL, Grillon C and Geyer MA. (1992). Gating and habituation of the startle reflex in schizophrenic patients. *Arch Gen Psychiatry* **49**: 206-15.

Brejc K, van Dijk WJ, Klaassen RV, Schuurmans M, van Der Oost J, Smit AB and Sixma TK. (2001). Crystal structure of an ACh-binding protein reveals the ligand-binding domain of nicotinic receptors. *Nature* **411**: 269-76.

Briggs CA, Anderson DJ, Brioni JD, Buccafusco JJ, Buckley MJ, Campbell JE, Decker MW, Donnelly-Roberts D, Elliott RL, Gopalakrishnan M, Holladay MW, Hui YH, Jackson WJ, Kim DJ, Marsh KC, O'Neill A, Prendergast MA, Ryther KB, Sullivan JP and Arneric SP. (1997). Functional characterization of the novel neuronal nicotinic acetylcholine receptor ligand GTS-21 in vitro and in vivo. *Pharmacol Biochem Behav* **57**: 231-41.

Briggs CA, McKenna DG and Piattoni-Kaplan M. (1995). Human alpha 7 nicotinic acetylcholine receptor responses to novel ligands. *Neuropharmacology* **34**: 583-90.

Broad LM, Zwart R, Pearson KH, Lee M, Wallace L, McPhie GI, Emkey R, Hollinshead SP, Dell CP, Baker SR and Sher E. (2006). Identification and pharmacological profile of a new class of selective nicotinic acetylcholine receptor potentiators. *J Pharmacol Exp Ther* **318**: 1108-17.

Buonomano DV and Maass W. (2009). State-dependent computations: spatiotemporal processing in cortical networks. *Nat Rev Neurosci* **10**: 113-25.

Castelan F, Castillo M, Mulet J, Sala S, Sala F, Dominguez Del Toro E and Criado M. (2008). Molecular characterization and localization of the RIC-3 protein, an effector of nicotinic acetylcholine receptor expression. *J Neurochem* **105**: 617-27.

Celie PH, Kasheverov IE, Mordvintsev DY, Hogg RC, van Nierop P, van Elk R, van Rossum-Fikkert SE, Zhmak MN, Bertrand D, Tsetlin V, Sixma TK and Smit AB. (2005). Crystal structure of nicotinic acetylcholine receptor homolog AChBP in complex with an α-conotoxin PnIA variant. *Nat Struct Mol Biol* **12**: 582-8.

Celie PH, van Rossum-Fikkert SE, van Dijk WJ, Brejc K, Smit AB and Sixma TK. (2004). Nicotine and carbamylcholine binding to nicotinic acetylcholine receptors as studied in AChBP crystal structures. *Neuron* **41**: 907-14.

Chakrapani S and Auerbach A. (2005). A speed limit for conformational change of an allosteric membrane protein. *Proc Natl Acad Sci U S A* **102**: 87-92.

Chakrapani S, Bailey TD and Auerbach A. (2004). Gating dynamics of the acetylcholine receptor extracellular domain. *J Gen Physiol* **123**: 341-56.

Chang Y and Weiss DS. (2002). Site-specific fluorescence reveals distinct structural changes with GABA receptor activation and antagonism. *Nat Neurosci* **5**: 1163-8.

Changeux JP and Edelstein SJ. (2005). Allosteric mechanisms of signal transduction. *Science* **308**: 1424-8.

Changeux JP and Taly A. (2008). Nicotinic receptors, allosteric proteins and medicine. *Trends Mol Med* **14**: 93-102.

Chen L. (2009). In pursuit of high-resolution structure of nicotinic acetylcholine receptors. *J Physiol*.

Cheng X, Ivanov I, Wang H, Sine SM and McCammon JA. (2007). Nanosecond-timescale conformational dynamics of the human α7 nicotinic acetylcholine receptor. *Biophys J* **93**: 2622-34.

Cheng X, Ivanov I, Wang H, Sine SM and McCammon JA. (2009). Molecular-dynamics simulations of ELIC-a prokaryotic homologue of the nicotinic acetylcholine receptor. *Biophys J* **96**: 4502-13.

Chu NS. (2005). Contribution of a snake venom toxin to myasthenia gravis: the discovery of alpha-bungarotoxin in Taiwan. *J Hist Neurosci* **14**: 138-48.

Cohen JE and Fields RD. (2004). Extracellular calcium depletion in synaptic transmission. *Neuroscientist* **10**: 12-7.

Colquhoun D. (1998). Binding, gating, affinity and efficacy: the interpretation of structure-activity relationships for agonists and of the effects of mutating receptors. *Br J Pharmacol* **125**: 924-47.

Colquhoun D and Hawkes AG. (1981). On the stochastic properties of single ion channels. *Proc R Soc Lond B Biol Sci* **211**: 205-35.

Colquhoun D and Sakmann B. (1981). Fluctuations in the microsecond time range of the current through single acetylcholine receptor ion channels. *Nature* **294**: 464-6.

Conn PJ, Christopoulos A and Lindsley CW. (2009). Allosteric modulators of GPCRs: a novel approach for the treatment of CNS disorders. *Nat Rev Drug Discov* **8**: 41-54.

Corringer PJ, Bertrand S, Galzi JL, Devillers-Thiery A, Changeux JP and Bertrand D. (1999). Mutational analysis of the charge selectivity filter of the alpha7 nicotinic acetylcholine receptor. *Neuron* **22**: 831-43.

Couturier S, Bertrand D, Matter JM, Hernandez MC, Bertrand S, Millar N, Valera S, Barkas T and Ballivet M. (1990). A neuronal nicotinic acetylcholine receptor subunit (α 7) is developmentally regulated and forms a homo-oligomeric channel blocked by α-BTX. *Neuron* **5**: 847-56.

Cymes GD and Grosman C. (2008). Pore-opening mechanism of the nicotinic acetylcholine receptor evinced by proton transfer. *Nat Struct Mol Biol* **15**: 389-96.

Cymes GD, Ni Y and Grosman C. (2005). Probing ion-channel pores one proton at a time. *Nature* **438**: 975-80.

Dale H. (1914). The action of certain esters and ethers of choline, and their relation to muscarine. *The Journal of Pharmacology and Experimental Therapeutics* **6**: 147-190.

Dale HH. (1954). The beginnings and the prospects of neurohumoral transmission. *Pharmacol Rev* **6**: 7-13.

Daly JW. (1995). The chemistry of poisons in amphibian skin. *Proc Natl Acad Sci U S A* **92**: 9-13.

Daly JW. (2005). Nicotinic agonists, antagonists, and modulators from natural sources. *Cell Mol Neurobiol* **25**: 513-52.

Dani JA. (2001). Overview of nicotinic receptors and their roles in the central nervous system. *Biol Psychiatry* **49**: 166-74.

Dani JA and Bertrand D. (2007). Nicotinic acetylcholine receptors and nicotinic cholinergic mechanisms of the central nervous system. *Annu Rev Pharmacol Toxicol* **47**: 699-729.

Dawson GR, Wafford KA, Smith A, Marshall GR, Bayley PJ, Schaeffer JM, Meinke PT and McKernan RM. (2000). Anticonvulsant and adverse effects of avermectin

analogs in mice are mediated through the gamma-aminobutyric acid(A) receptor. *J Pharmacol Exp Ther* **295**: 1051-60.

de Fiebre CM, Meyer EM, Henry JC, Muraskin SI, Kem WR and Papke RL. (1995). Characterization of a series of anabaseine-derived compounds reveals that the 3-(4)-dimethylaminocinnamylidine derivative is a selective agonist at neuronal nicotinic alpha 7/125I-alpha-bungarotoxin receptor subtypes. *Mol Pharmacol* **47**: 164-71.

del Camino D and Yellen G. (2001). Tight steric closure at the intracellular activation gate of a voltage-gated K(+) channel. *Neuron* **32**: 649-56.

Del Castillo J and Katz B. (1954). Quantal components of the end-plate potential. *J Physiol* **124**: 560-73.

Dolinsky TJ, Nielsen JE, McCammon JA and Baker NA. (2004). PDB2PQR: an automated pipeline for the setup of Poisson-Boltzmann electrostatics calculations. *Nucleic Acids Res* **32**: W665-7.

Dopico AM and Lovinger DM. (2009). Acute alcohol action and desensitization of ligand-gated ion channels. *Pharmacol Rev* **61**: 98-114.

Drew D, Newstead S, Sonoda Y, Kim H, von Heijne G and Iwata S. (2008). GFP-based optimization scheme for the overexpression and purification of eukaryotic membrane proteins in Saccharomyces cerevisiae. *Nat Protoc* **3**: 784-98.

Dunlop J, Lock T, Jow B, Sitzia F, Grauer S, Jow F, Kramer A, Bowlby M, Randall A, Kowal D, Gilbert A, Comery T, Larocque J, Soloveva V, Brown J and Roncarati R. (2008). Old and New Pharmacology: Positive Allosteric Modulation of the {alpha}7 Nicotinic Acetylcholine Receptor by the 5-HT2B/C Receptor Antagonist SB-206553. *J Pharmacol Exp Ther*.

Eddins D, Lyford LK, Lee JW, Desai SA and Rosenberg RL. (2002a). Permeant but not impermeant divalent cations enhance activation of nondesensitizing α(7) nicotinic receptors. *Am J Physiol Cell Physiol* **282**: C796-804.

Eddins D, Sproul AD, Lyford LK, McLaughlin JT and Rosenberg RL. (2002b). Glutamate 172, essential for modulation of L247T α7 ACh receptors by Ca2+, lines the extracellular vestibule. *Am J Physiol Cell Physiol* **283**: C1454-60.

Elenes S and Auerbach A. (2002). Desensitization of diliganded mouse muscle nicotinic acetylcholine receptor channels. *J Physiol* **541**: 367-83.

Filatov GN and White MM. (1995). The role of conserved leucines in the M2 domain of the acetylcholine receptor in channel gating. *Mol Pharmacol* **48**: 379-84.

Fischer M, Corringer PJ, Schott K, Bacher A and Changeux JP. (2001). A method for soluble overexpression of the alpha7 nicotinic acetylcholine receptor extracellular domain. *Proc Natl Acad Sci U S A* **98**: 3567-70.

Fogolari F, Brigo A and Molinari H. (2002). The Poisson-Boltzmann equation for biomolecular electrostatics: a tool for structural biology. *J Mol Recognit* **15**: 377-92.

Freedman R, Hall M, Adler LE and Leonard S. (1995). Evidence in postmortem brain tissue for decreased numbers of hippocampal nicotinic receptors in schizophrenia. *Biol Psychiatry* **38**: 22-33.

Fryer JD and Lukas RJ. (1999a). Antidepressants noncompetitively inhibit nicotinic acetylcholine receptor function. *J Neurochem* **72**: 1117-24.

Fryer JD and Lukas RJ. (1999b). Noncompetitive functional inhibition at diverse, human nicotinic acetylcholine receptor subtypes by bupropion, phencyclidine, and ibogaine. *J Pharmacol Exp Ther* **288**: 88-92.

Fucile S. (2004). Ca2+ permeability of nicotinic acetylcholine receptors. *Cell Calcium* **35**: 1-8.

Galzi JL, Bertrand S, Corringer PJ, Changeux JP and Bertrand D. (1996). Identification of calcium binding sites that regulate potentiation of a neuronal nicotinic acetylcholine receptor. *EMBO J* **15**: 5824-32.

Galzi JL, Devillers-Thiery A, Hussy N, Bertrand S, Changeux JP and Bertrand D. (1992). Mutations in the channel domain of a neuronal nicotinic receptor convert ion selectivity from cationic to anionic. *Nature* **359**: 500-5.

Gao F, Bren N, Burghardt TP, Hansen S, Henchman RH, Taylor P, McCammon JA and Sine SM. (2005). Agonist-mediated conformational changes in acetylcholine-binding protein revealed by simulation and intrinsic tryptophan fluorescence. *J Biol Chem* **280**: 8443-51.

Gao ZG and Jacobson KA. (2006). Keynote review: allosterism in membrane receptors. *Drug Discov Today* **11**: 191-202.

Gay EA, Giniatullin R, Skorinkin A and Yakel JL. (2008). Aromatic residues at position 55 of rat α7 nicotinic acetylcholine receptors are critical for maintaining rapid desensitization. *J Physiol* **586**: 1105-15.

Gay EA and Yakel JL. (2007). Gating of nicotinic ACh receptors; new insights into structural transitions triggered by agonist binding that induce channel opening. *J Physiol* **584**: 727-33.

Gilbert CD and Sigman M. (2007). Brain states: top-down influences in sensory processing. *Neuron* **54**: 677-96.

Girod R and Role LW. (2001). Long-lasting enhancement of glutamatergic synaptic transmission by acetylcholine contrasts with response adaptation after exposure to low-level nicotine. *J Neurosci* **21**: 5182-90.

Glendinning JI and Gonzalez NA. (1995). GUSTATORY HABITUATION TO DETERRENT ALLELOCHEMICALS IN A HERBIVORE - CONCENTRATION AND COMPOUND SPECIFICITY. *Animal Behaviour* **50**: 915-927.

Gotti C and Clementi F. (2004). Neuronal nicotinic receptors: from structure to pathology. *Prog Neurobiol* **74**: 363-96.

Gotti C, Clementi F, Fornari A, Gaimarri A, Guiducci S, Manfredi I, Moretti M, Pedrazzi P, Pucci L and Zoli M. (2009). Structural and functional diversity of native brain neuronal nicotinic receptors. *Biochem Pharmacol* **78**: 703-11.

Gotti C, Moretti M, Gaimarri A, Zanardi A, Clementi F and Zoli M. (2007). Heterogeneity and complexity of native brain nicotinic receptors. *Biochem Pharmacol* **74**: 1102-11.

Greenblatt DJ, Shader RI, Divoll M and Harmatz JS. (1981). Benzodiazepines: a summary of pharmacokinetic properties. *Br J Clin Pharmacol* **11 Suppl 1**: 11S-16S.

Gronlien JH, Hakerud M, Ween H, Thorin-Hagene K, Briggs CA, Gopalakrishnan M and Malysz J. (2007). Distinct profiles of α7 nAChR positive allosteric modulation revealed by structurally diverse chemotypes. *Mol Pharmacol* **72**: 715-24.

Grosman C, Zhou M and Auerbach A. (2000). Mapping the conformational wave of acetylcholine receptor channel gating. *Nature* **403**: 773-6.

Guan ZZ, Zhang X, Blennow K and Nordberg A. (1999). Decreased protein level of nicotinic receptor alpha7 subunit in the frontal cortex from schizophrenic brain. *Neuroreport* **10**: 1779-82.

Gunther U, Benson J, Benke D, Fritschy JM, Reyes G, Knoflach F, Crestani F, Aguzzi A, Arigoni M, Lang Y and et al. (1995). Benzodiazepine-insensitive mice generated by targeted disruption of the gamma 2 subunit gene of gamma-aminobutyric acid type A receptors. *Proc Natl Acad Sci U S A* **92**: 7749-53.

Gunthorpe MJ and Lummis SC. (2001). Conversion of the ion selectivity of the 5-HT(3a) receptor from cationic to anionic reveals a conserved feature of the ligand-gated ion channel superfamily. *J Biol Chem* **276**: 10977-83.

Gusev AG and Uteshev VV. (2009). Physiological concentrations of choline activate native {alpha}7-containing nicotinic acetylcholine receptors in the presence of PNU-120596. *J Pharmacol Exp Ther*.

Hajos M, Hurst RS, Hoffmann WE, Krause M, Wall TM, Higdon NR and Groppi VE. (2005). The selective α7 nicotinic acetylcholine receptor agonist PNU-282987 [N-[(3R)-1-Azabicyclo[2.2.2]oct-3-yl]-4-chlorobenzamide hydrochloride] enhances GABAergic synaptic activity in brain slices and restores auditory gating deficits in anesthetized rats. *J Pharmacol Exp Ther* **312**: 1213-22.

Halevi S, McKay J, Palfreyman M, Yassin L, Eshel M, Jorgensen E and Treinin M. (2002). The C. elegans ric-3 gene is required for maturation of nicotinic acetylcholine receptors. *EMBO J* **21**: 1012-20.

Hanek AP, Lester HA and Dougherty DA. (2008). A stereochemical test of a proposed structural feature of the nicotinic acetylcholine receptor. *J Am Chem Soc* **130**: 13216-8.

Hansen SB, Radic Z, Talley TT, Molles BE, Deerinck T, Tsigelny I and Taylor P. (2002). Tryptophan fluorescence reveals conformational changes in the acetylcholine binding protein. *J Biol Chem* **277**: 41299-302.

Hansen SB, Sulzenbacher G, Huxford T, Marchot P, Taylor P and Bourne Y. (2005). Structures of Aplysia AChBP complexes with nicotinic agonists and antagonists reveal distinctive binding interfaces and conformations. *EMBO J* **24**: 3635-46.

Hansen SB, Talley TT, Radic Z and Taylor P. (2004). Structural and ligand recognition characteristics of an acetylcholine-binding protein from Aplysia californica. *J Biol Chem* **279**: 24197-202.

Hansen SB and Taylor P. (2007). Galanthamine and non-competitive inhibitor binding to ACh-binding protein: evidence for a binding site on non-α-subunit interfaces of heteromeric neuronal nicotinic receptors. *J Mol Biol* **369**: 895-901.

Hansen SB, Wang HL, Taylor P and Sine SM. (2008). An ion selectivity filter in the extracellular domain of Cys-loop receptors reveals determinants for ion conductance. *J Biol Chem* **283**: 36066-70.

Hanson SM and Czajkowski C. (2008). Structural mechanisms underlying benzodiazepine modulation of the GABA(A) receptor. *J Neurosci* **28**: 3490-9.

Harding MM. (2004). The architecture of metal coordination groups in proteins. *Acta Crystallogr D Biol Crystallogr* **60**: 849-59.

Hilf RJ and Dutzler R. (2008). X-ray structure of a prokaryotic pentameric ligand-gated ion channel. *Nature* **452**: 375-9.

Hilf RJ and Dutzler R. (2009). Structure of a potentially open state of a proton-activated pentameric ligand-gated ion channel. *Nature* **457**: 115-8.

Hille B (2001). Ion Channels of Excitable Membranes, Sinauer Associates.

Hodgkin AL and Huxley AF. (1952a). The components of membrane conductance in the giant axon of Loligo. *J Physiol* **116**: 473-96.

Hodgkin AL and Huxley AF. (1952b). Currents carried by sodium and potassium ions through the membrane of the giant axon of Loligo. *J Physiol* **116**: 449-72.

Hodgkin AL and Huxley AF. (1952c). The dual effect of membrane potential on sodium conductance in the giant axon of Loligo. *J Physiol* **116**: 497-506.

Hodgkin AL and Huxley AF. (1952d). A quantitative description of membrane current and its application to conduction and excitation in nerve. *J Physiol* **117**: 500-44.

Hodgkin AL, Huxley AF and Katz B. (1952). Measurement of current-voltage relations in the membrane of the giant axon of Loligo. *J Physiol* **116**: 424-48.

Horenstein J, Wagner DA, Czajkowski C and Akabas MH. (2001). Protein mobility and GABA-induced conformational changes in GABA(A) receptor pore-lining M2 segment. *Nat Neurosci* **4**: 477-85.

Hu M, Gopalakrishnan M and Li J. (2009). Positive allosteric modulation of alpha7 neuronal nicotinic acetylcholine receptors: lack of cytotoxicity in PC12 cells and rat primary cortical neurons. *Br J Pharmacol* **158**: 1857-64.

Hubbard SJ, Campbell SF and Thornton JM. (1991). Molecular recognition. Conformational analysis of limited proteolytic sites and serine proteinase protein inhibitors. *J Mol Biol* **220**: 507-30.

Hughes JR, Hatsukami DK, Mitchell JE and Dahlgren LA. (1986). Prevalence of smoking among psychiatric outpatients. *Am J Psychiatry* **143**: 993-7.

Hurst RS, Hajos M, Raggenbass M, Wall TM, Higdon NR, Lawson JA, Rutherford-Root KL, Berkenpas MB, Hoffmann WE, Piotrowski DW, Groppi VE, Allaman G, Ogier R, Bertrand S, Bertrand D and Arneric SP. (2005). A novel positive allosteric modulator of the α7 neuronal nicotinic acetylcholine receptor: in vitro and in vivo characterization. *J Neurosci* **25**: 4396-405.

Ifune CK and Steinbach JH. (1990). Rectification of acetylcholine-elicited currents in PC12 pheochromocytoma cells. *Proc Natl Acad Sci U S A* **87**: 4794-8.

Ifune CK and Steinbach JH. (1991). Voltage-dependent block by magnesium of neuronal nicotinic acetylcholine receptor channels in rat phaeochromocytoma cells. *J Physiol* **443**: 683-701.

Imoto K, Busch C, Sakmann B, Mishina M, Konno T, Nakai J, Bujo H, Mori Y, Fukuda K and Numa S. (1988). Rings of negatively charged amino acids determine the acetylcholine receptor channel conductance. *Nature* **335**: 645-8.

Ivanov I, Cheng X, Sine SM and McCammon JA. (2007). Barriers to ion translocation in cationic and anionic receptors from the Cys-loop family. *J Am Chem Soc* **129**: 8217-24.

Jackson MB. (1989). Perfection of a synaptic receptor: kinetics and energetics of the acetylcholine receptor. *Proc Natl Acad Sci U S A* **86**: 2199-203.

Jha A, Cadugan DJ, Purohit P and Auerbach A. (2007). Acetylcholine receptor gating at extracellular transmembrane domain interface: the cys-loop and M2-M3 linker. *J Gen Physiol* **130**: 547-58.

Jones HC and Keep RF. (1988). Brain fluid calcium concentration and response to acute hypercalcaemia during development in the rat. *J Physiol* **402**: 579-93.

Kabsch W and Sander C. (1983). Dictionary of protein secondary structure: pattern recognition of hydrogen-bonded and geometrical features. *Biopolymers* **22**: 2577-637.

Karlin A. (2002). Emerging structure of the nicotinic acetylcholine receptors. *Nat Rev Neurosci* **3**: 102-14.

Karlin A and Akabas MH. (1998). Substituted-cysteine accessibility method. *Methods Enzymol* **293**: 123-45.

Kash TL, Jenkins A, Kelley JC, Trudell JR and Harrison NL. (2003). Coupling of agonist binding to channel gating in the GABA(A) receptor. *Nature* **421**: 272-5.

Kelley SP, Dunlop JI, Kirkness EF, Lambert JJ and Peters JA. (2003). A cytoplasmic region determines single-channel conductance in 5-HT3 receptors. *Nature* **424**: 321-4.

Keramidas A, Moorhouse AJ, French CR, Schofield PR and Barry PH. (2000). M2 pore mutations convert the glycine receptor channel from being anion- to cation-selective. *Biophys J* **79**: 247-59.

Keramidas A, Moorhouse AJ, Schofield PR and Barry PH. (2004). Ligand-gated ion channels: mechanisms underlying ion selectivity. *Prog Biophys Mol Biol* **86**: 161-204.

Khakh BS, Proctor WR, Dunwiddie TV, Labarca C and Lester HA. (1999). Allosteric control of gating and kinetics at P2X(4) receptor channels. *J Neurosci* **19**: 7289-99.

Kienker P, Tomaselli G, Jurman M and Yellen G. (1994). Conductance mutations of the nicotinic acetylcholine receptor do not act by a simple electrostatic mechanism. *Biophys J* **66**: 325-34.

Kim JS, Padnya A, Weltzin M, Edmonds BW, Schulte MK and Glennon RA. (2007). Synthesis of desformylflustrabromine and its evaluation as an alpha4beta2 and alpha7 nACh receptor modulator. *Bioorg Med Chem Lett* **17**: 4855-60.

Kleywegt GJ. (1996). Use of non-crystallographic symmetry in protein structure refinement. *Acta Crystallogr D Biol Crystallogr* **52**: 842-57.

Kloda JH and Czajkowski C. (2007). Agonist-, antagonist-, and benzodiazepine-induced structural changes in the α1 Met113-Leu132 region of the GABAA receptor. *Mol Pharmacol* **71**: 483-93.

Koshland DE, Jr., Nemethy G and Filmer D. (1966). Comparison of experimental binding data and theoretical models in proteins containing subunits. *Biochemistry* **5**: 365-85.

Krause RM, Buisson B, Bertrand S, Corringer PJ, Galzi JL, Changeux JP and Bertrand D. (1998). Ivermectin: a positive allosteric effector of the alpha7 neuronal nicotinic acetylcholine receptor. *Mol Pharmacol* **53**: 283-94.

Krauss M, Korr D, Herrmann A and Hucho F. (2000). Binding properties of agonists and antagonists to distinct allosteric states of the nicotinic acetylcholine receptor are incompatible with a concerted model. *J Biol Chem* **275**: 30196-201.

Kucken AM, Wagner DA, Ward PR, Teissere JA, Boileau AJ and Czajkowski C. (2000). Identification of benzodiazepine binding site residues in the gamma2 subunit of the gamma-aminobutyric acid(A) receptor. *Mol Pharmacol* **57**: 932-9.

Lansdell SJ, Gee VJ, Harkness PC, Doward AI, Baker ER, Gibb AJ and Millar NS. (2005). RIC-3 enhances functional expression of multiple nicotinic acetylcholine receptor subtypes in mammalian cells. *Mol Pharmacol* **68**: 1431-8.

Laskowski RA, Macarthur MW, Moss DS and Thornton JM. (1993). PROCHECK - A PROGRAM TO CHECK THE STEREOCHEMICAL QUALITY OF PROTEIN STRUCTURES. *Journal of Applied Crystallography* **26**: 283-291.

Le Novere N, Grutter T and Changeux JP. (2002). Models of the extracellular domain of the nicotinic receptors and of agonist- and Ca2+-binding sites. *Proc Natl Acad Sci U S A* **99**: 3210-5.

Lee B and Richards FM. (1971). The interpretation of protein structures: estimation of static accessibility. *J Mol Biol* **55**: 379-400.

Lee WY and Sine SM. (2005). Principal pathway coupling agonist binding to channel gating in nicotinic receptors. *Nature* **438**: 243-7.

Lena C and Changeux JP. (1993). Allosteric modulations of the nicotinic acetylcholine receptor. *Trends Neurosci* **16**: 181-6.

Leprince P, Noble RL and Hess GP. (1981). Comparison of the interactions of a specific neurotoxin (alpha-bungarotoxin) with the acetylcholine receptor in Torpedo californica and Electrophorus electricus membrane preparations. *Biochemistry* **20**: 5565-70.

Lester HA. (1991). Strategies for studying permeation at voltage-gated ion channels. *Annu Rev Physiol* **53**: 477-96.

Lester HA. (1992). The permeation pathway of neurotransmitter-gated ion channels. *Annu Rev Biophys Biomol Struct* **21**: 267-92.

Lester HA and Dougherty DA. (1998). New Views of Multi-Ion Channels. *J. Gen. Physiol.* **111**: 181-183.

Lioudyno MI, Verbitsky M, Holt JC, Elgoyhen AB and Guth PS. (2000). Morphine inhibits an alpha9-acetylcholine nicotinic receptor-mediated response by a mechanism which does not involve opioid receptors. *Hear Res* **149**: 167-77.

Lopes C, Pereira EF, Wu HQ, Purushottamachar P, Njar V, Schwarcz R and Albuquerque EX. (2007). Competitive antagonism between the nicotinic allosteric potentiating ligand galantamine and kynurenic acid at alpha7* nicotinic receptors. *J Pharmacol Exp Ther* **322**: 48-58.

Lummis SC, Beene DL, Lee LW, Lester HA, Broadhurst RW and Dougherty DA. (2005). Cis-trans isomerization at a proline opens the pore of a neurotransmitter-gated ion channel. *Nature* **438**: 248-52.

Luthy R, Bowie JU and Eisenberg D. (1992). Assessment of protein models with three-dimensional profiles. *Nature* **356**: 83-5.

Luthy R, McLachlan AD and Eisenberg D. (1991). Secondary structure-based profiles: use of structure-conserving scoring tables in searching protein sequence databases for structural similarities. *Proteins* **10**: 229-39.

Lyford LK, Sproul AD, Eddins D, McLaughlin JT and Rosenberg RL. (2003). Agonist-induced conformational changes in the extracellular domain of α 7 nicotinic acetylcholine receptors. *Mol Pharmacol* **64**: 650-8.

Maiorov VN and Crippen GM. (1994). Significance of root-mean-square deviation in comparing three-dimensional structures of globular proteins. *J Mol Biol* **235**: 625-34.

McCavera S, Walsh TK and Wolstenholme AJ. (2007). Nematode ligand-gated chloride channels: an appraisal of their involvement in macrocyclic lactone resistance and prospects for developing molecular markers. *Parasitology* **134**: 1111-21.

McGhie A and Chapman J. (1961). Disorders of attention and perception in early schizophrenia. *Br J Med Psychol* **34**: 103-16.

McKernan RM, Rosahl TW, Reynolds DS, Sur C, Wafford KA, Atack JR, Farrar S, Myers J, Cook G, Ferris P, Garrett L, Bristow L, Marshall G, Macaulay A, Brown N, Howell O, Moore KW, Carling RW, Street LJ, Castro JL, Ragan CI, Dawson GR and Whiting PJ. (2000). Sedative but not anxiolytic properties of benzodiazepines are mediated by the GABA(A) receptor α1 subtype. *Nat Neurosci* **3**: 587-92.

McLaughlin JT, Barron SC, See JA and Rosenberg RL. (2009). Conformational changes in alpha 7 acetylcholine receptors underlying allosteric modulation by divalent cations. *BMC Pharmacol* **9**: 1.

McLaughlin JT, Fu J and Rosenberg RL. (2007). Agonist-driven conformational changes in the inner β-sheet of α7 nicotinic receptors. *Mol Pharmacol* **71**: 1312-8.

McLaughlin JT, Fu J, Sproul AD and Rosenberg RL. (2006). Role of the outer β-sheet in divalent cation modulation of α7 nicotinic receptors. *Mol Pharmacol* **70**: 16-22.

Meltzer RH, Lurtz MM, Wensel TG and Pedersen SE. (2006a). Nicotinic acetylcholine receptor channel electrostatics determined by diffusion-enhanced luminescence energy transfer. *Biophys J* **91**: 1315-24.

Meltzer RH, Thompson E, Soman KV, Song XZ, Ebalunode JO, Wensel TG, Briggs JM and Pedersen SE. (2006b). Electrostatic steering at acetylcholine binding sites. *Biophys J* **91**: 1302-14.

Meltzer RH, Vila-Carriles W, Ebalunode JO, Briggs JM and Pedersen SE. (2006c). Computed pore potentials of the nicotinic acetylcholine receptor. *Biophys J* **91**: 1325-35.

Metcalf RL, Metcalf, R. A. (1992). Destructive and Useful Insects. New York, McGraw-Hill Inc.

Meyer EA, Castellano RK and Diederich F. (2003). Interactions with aromatic rings in chemical and biological recognition. *Angew Chem Int Ed Engl* **42**: 1210-50.

Mihalak KB, Carroll FI and Luetje CW. (2006). Varenicline is a partial agonist at α4β2 and a full agonist at α7 neuronal nicotinic receptors. *Mol Pharmacol* **70**: 801-5.

Miller C. (1989). Genetic manipulation of ion channels: a new approach to structure and mechanism. *Neuron* **2**: 1195-205.

Mineur YS and Picciotto MR. (2008). Genetics of nicotinic acetylcholine receptors: Relevance to nicotine addiction. *Biochem Pharmacol* **75**: 323-33.

Miyazawa A, Fujiyoshi Y, Stowell M and Unwin N. (1999). Nicotinic acetylcholine receptor at 4.6 A resolution: transverse tunnels in the channel wall. *J Mol Biol* **288**: 765-86.

Miyazawa A, Fujiyoshi Y and Unwin N. (2003). Structure and gating mechanism of the acetylcholine receptor pore. *Nature* **423**: 949-55.

Mohr PJ, Taylor BN and Newell DB. (2008). CODATA recommended values of the fundamental physical constants: 2006. *Reviews of Modern Physics* **80**: 633-730.

Monod J, Wyman J and Changeux JP. (1965). On the Nature of Allosteric Transitions: A Plausible Model. *J Mol Biol* **12**: 88-118.

Moorhouse AJ, Keramidas A, Zaykin A, Schofield PR and Barry PH. (2002). Single channel analysis of conductance and rectification in cation-selective, mutant glycine receptor channels. *J Gen Physiol* **119**: 411-25.

Morris AL, MacArthur MW, Hutchinson EG and Thornton JM. (1992). Stereochemical quality of protein structure coordinates. *Proteins* **12**: 345-64.

Moy G, Corry B, Kuyucak S and Chung SH. (2000). Tests of continuum theories as models of ion channels. I. Poisson-Boltzmann theory versus Brownian dynamics. *Biophys J* **78**: 2349-63.

Mukhtasimova N, Free C and Sine SM. (2005). Initial coupling of binding to gating mediated by conserved residues in the muscle nicotinic receptor. *J Gen Physiol* **126**: 23-39.

Mulle C, Lena C and Changeux JP. (1992). Potentiation of nicotinic receptor response by external calcium in rat central neurons. *Neuron* **8**: 937-45.

Neher E and Sakmann B. (1976). Single-channel currents recorded from membrane of denervated frog muscle fibres. *Nature* **260**: 799-802.

Neher E, Sakmann B and Steinbach JH. (1978). The extracellular patch clamp: a method for resolving currents through individual open channels in biological membranes. *Pflugers Arch* **375**: 219-28.

Nelson ME, Kuryatov A, Choi CH, Zhou Y and Lindstrom J. (2003). Alternate stoichiometries of alpha4beta2 nicotinic acetylcholine receptors. *Mol Pharmacol* **63**: 332-41.

Newstead S, Kim H, von Heijne G, Iwata S and Drew D. (2007). High-throughput fluorescent-based optimization of eukaryotic membrane protein overexpression and purification in Saccharomyces cerevisiae. *Proc Natl Acad Sci U S A* **104**: 13936-41.

Ng HJ, Whittemore ER, Tran MB, Hogenkamp DJ, Broide RS, Johnstone TB, Zheng L, Stevens KE and Gee KW. (2007). Nootropic α7 nicotinic receptor allosteric modulator derived from GABAA receptor modulators. *Proc Natl Acad Sci U S A* **104**: 8059-64.

Nicke A, Wonnacott S and Lewis RJ. (2004). Alpha-conotoxins as tools for the elucidation of structure and function of neuronal nicotinic acetylcholine receptor subtypes. *Eur J Biochem* **271**: 2305-19.

Nirthanan S, Garcia G, 3rd, Chiara DC, Husain SS and Cohen JB. (2008). Identification of binding sites in the nicotinic acetylcholine receptor for TDBzl-etomidate, a photoreactive positive allosteric effector. *J Biol Chem* **283**: 22051-62.

Nirthanan S, Ziebell MR, Chiara DC, Hong F and Cohen JB. (2005). Photolabeling the Torpedo nicotinic acetylcholine receptor with 4-azido-2,3,5,6-tetrafluorobenzoylcholine, a partial agonist. *Biochemistry* **44**: 13447-56.

Oblatt-Montal M, Buhler LK, Iwamoto T, Tomich JM and Montal M. (1993). Synthetic peptides and four-helix bundle proteins as model systems for the pore-forming structure of channel proteins. I. Transmembrane segment M2 of the nicotinic cholinergic receptor channel is a key pore-lining structure. *J Biol Chem* **268**: 14601-7.

Olsen RW and Snowman AM. (1982). Chloride-dependent enhancement by barbiturates of gamma-aminobutyric acid receptor binding. *J Neurosci* **2**: 1812-23.

Orr-Urtreger A, Broide RS, Kasten MR, Dang H, Dani JA, Beaudet AL and Patrick JW. (2000). Mice homozygous for the L250T mutation in the α7 nicotinic acetylcholine receptor show increased neuronal apoptosis and die within 1 day of birth. *J Neurochem* **74**: 2154-66.

Orr-Urtreger A, Goldner FM, Saeki M, Lorenzo I, Goldberg L, De Biasi M, Dani JA, Patrick JW and Beaudet AL. (1997). Mice deficient in the α7 neuronal nicotinic acetylcholine receptor lack α-bungarotoxin binding sites and hippocampal fast nicotinic currents. *J Neurosci* **17**: 9165-71.

Paas Y, Gibor G, Grailhe R, Savatier-Duclert N, Dufresne V, Sunesen M, de Carvalho LP, Changeux JP and Attali B. (2005). Pore conformations and gating mechanism of a Cys-loop receptor. *Proc Natl Acad Sci U S A* **102**: 15877-82.

Pascual JM and Karlin A. (1998). State-dependent accessibility and electrostatic potential in the channel of the acetylcholine receptor. Inferences from rates of reaction of thiosulfonates with substituted cysteines in the M2 segment of the α subunit. *J Gen Physiol* **111**: 717-39.

Perry DC, Xiao Y, Nguyen HN, Musachio JL, Davila-Garcia MI and Kellar KJ. (2002). Measuring nicotinic receptors with characteristics of α4β2, α3β2 and α3β4 subtypes in rat tissues by autoradiography. *J Neurochem* **82**: 468-81.

Petrek M, Kosinova P, Koca J and Otyepka M. (2007). MOLE: a Voronoi diagram-based explorer of molecular channels, pores, and tunnels. *Structure* **15**: 1357-63.

Piotrowski DW RB, McWhorter WW, Walker DP, Corbett JW, Groppi VE, Rudmann DG. (2005). Positive Allosteric Modulators of the Nicotinic Acetylcholine Receptor. . 11/174,239, *US20050250816*

Pless SA, Dibas MI, Lester HA and Lynch JW. (2007). Conformational variability of the glycine receptor M2 domain in response to activation by different agonists. *J Biol Chem* **282**: 36057-67.

Ponder JW and Case DA. (2003). Force fields for protein simulations. *Adv Protein Chem* **66**: 27-85.

Price KL, Millen KS and Lummis SC. (2007). Transducing agonist binding to channel gating involves different interactions in 5-HT3 and GABAC receptors. *J Biol Chem* **282**: 25623-30.

Prince RJ and Sine SM. (1999). Acetylcholine and epibatidine binding to muscle acetylcholine receptors distinguish between concerted and uncoupled models. *J Biol Chem* **274**: 19623-9.

Purohit P and Auerbach A. (2007a). Acetylcholine receptor gating at extracellular transmembrane domain interface: the "pre-M1" linker. *J Gen Physiol* **130**: 559-68.

Purohit P and Auerbach A. (2007b). Acetylcholine receptor gating: movement in the α-subunit extracellular domain. *J Gen Physiol* **130**: 569-79.

Purohit P and Auerbach A. (2009). Unliganded gating of acetylcholine receptor channels. *Proc Natl Acad Sci U S A* **106**: 115-20.

Purohit P, Mitra A and Auerbach A. (2007). A stepwise mechanism for acetylcholine receptor channel gating. *Nature* **446**: 930-3.

Rabenstein RL, Caldarone BJ and Picciotto MR. (2006). The nicotinic antagonist mecamylamine has antidepressant-like effects in wild-type but not β2- or α7-nicotinic acetylcholine receptor subunit knockout mice. *Psychopharmacology (Berl)* **189**: 395-401.

Radcliffe KA, Fisher JL, Gray R and Dani JA. (1999). Nicotinic modulation of glutamate and GABA synaptic transmission of hippocampal neurons. *Ann N Y Acad Sci* **868**: 591-610.

Rayes D, De Rosa MJ, Sine SM and Bouzat C. (2009). Number and locations of agonist binding sites required to activate homomeric Cys-loop receptors. *J Neurosci* **29**: 6022-32.

Reeves DC, Goren EN, Akabas MH and Lummis SC. (2001). Structural and electrostatic properties of the 5-HT3 receptor pore revealed by substituted cysteine accessibility mutagenesis. *J Biol Chem* **276**: 42035-42.

Revah F, Bertrand D, Galzi JL, Devillers-Thiery A, Mulle C, Hussy N, Bertrand S, Ballivet M and Changeux JP. (1991). Mutations in the channel domain alter desensitization of a neuronal nicotinic receptor. *Nature* **353**: 846-9.

Rezvani AH and Levin ED. (2001). Cognitive effects of nicotine. *Biol Psychiatry* **49**: 258-67.

Rogers CJ, Twyman RE and Macdonald RL. (1994). Benzodiazepine and beta-carboline regulation of single GABAA receptor channels of mouse spinal neurones in culture. *J Physiol* **475**: 69-82.

Russel WBS, D. A.; Schowalter, William R. (1989). Colloidal Dispersions. New York, Cambridge University Press.

Sakmann B, Patlak J and Neher E. (1980). Single acetylcholine-activated channels show burst-kinetics in presence of desensitizing concentrations of agonist. *Nature* **286**: 71-3.

Samochocki M, Hoffle A, Fehrenbacher A, Jostock R, Ludwig J, Christner C, Radina M, Zerlin M, Ullmer C, Pereira EF, Lubbert H, Albuquerque EX and Maelicke A. (2003). Galantamine is an allosterically potentiating ligand of neuronal nicotinic but not of muscarinic acetylcholine receptors. *J Pharmacol Exp Ther* **305**: 1024-36.

Sands SB, Costa AC and Patrick JW. (1993). Barium permeability of neuronal nicotinic receptor alpha 7 expressed in Xenopus oocytes. *Biophys J* **65**: 2614-21.

Santarelli VP, Eastwood AL, Dougherty DA, Ahern CA and Horn R. (2007). Calcium block of single sodium channels: role of a pore-lining aromatic residue. *Biophys J* **93**: 2341-9.

Shannon RD. (1976). REVISED EFFECTIVE IONIC-RADII AND SYSTEMATIC STUDIES OF INTERATOMIC DISTANCES IN HALIDES AND CHALCOGENIDES. *Acta Crystallographica Section A* **32**: 751-767.

Sharkey LM and Czajkowski C. (2008). Individually monitoring ligand-induced changes in the structure of the GABAA receptor at benzodiazepine binding site and non-binding-site interfaces. *Mol Pharmacol* **74**: 203-12.

Shrake A and Rupley JA. (1973). Environment and exposure to solvent of protein atoms. Lysozyme and insulin. *J Mol Biol* **79**: 351-71.

Sigel E. (2002). Mapping of the benzodiazepine recognition site on GABA(A) receptors. *Curr Top Med Chem* **2**: 833-9.

Sine SM. (2002). The nicotinic receptor ligand binding domain. *J Neurobiol* **53**: 431-46.

Sine SM and Engel AG. (2006). Recent advances in Cys-loop receptor structure and function. *Nature* **440**: 448-55.

Sine SM and Steinbach JH. (1986). Activation of acetylcholine receptors on clonal mammalian BC3H-1 cells by low concentrations of agonist. *J Physiol* **373**: 129-62.

Sine SM and Steinbach JH. (1987). Activation of acetylcholine receptors on clonal mammalian BC3H-1 cells by high concentrations of agonist. *J Physiol* **385**: 325-59.

Sine SM and Taylor P. (1982). Local anesthetics and histrionicotoxin are allosteric inhibitors of the acetylcholine receptor. Studies of clonal muscle cells. *J Biol Chem* **257**: 8106-104.

Sine SM, Wang HL, Hansen S and Taylor P. (2009). On the Origin of Ion Selectivity in the Cys-Loop Receptor Family. *J Mol Neurosci*.

Sitkoff D, Sharp KA and Honig B. (1994). ACCURATE CALCULATION OF HYDRATION FREE-ENERGIES USING MACROSCOPIC SOLVENT MODELS. *Journal of Physical Chemistry* **98**: 1978-1988.

Smit AB, Syed NI, Schaap D, van Minnen J, Klumperman J, Kits KS, Lodder H, van der Schors RC, van Elk R, Sorgedrager B, Brejc K, Sixma TK and Geraerts WP. (2001). A glia-derived acetylcholine-binding protein that modulates synaptic transmission. *Nature* **411**: 261-8.

Soding J. (2005). Protein homology detection by HMM-HMM comparison. *Bioinformatics* **21**: 951-60.

Soding J, Biegert A and Lupas AN. (2005). The HHpred interactive server for protein homology detection and structure prediction. *Nucleic Acids Res* **33**: W244-8.

Steinlein OK. (2007). Genetic disorders caused by mutated acetylcholine receptors. *Life Sci* **80**: 2186-90.

Szarecka A, Xu Y and Tang P. (2007). Dynamics of heteropentameric nicotinic acetylcholine receptor: implications of the gating mechanism. *Proteins* **68**: 948-60.

Taly A, Corringer PJ, Grutter T, Prado de Carvalho L, Karplus M and Changeux JP. (2006). Implications of the quaternary twist allosteric model for the physiology and pathology of nicotinic acetylcholine receptors. *Proc Natl Acad Sci U S A* **103**: 16965-70.

Taly A, Corringer PJ, Guedin D, Lestage P and Changeux JP. (2009). Nicotinic receptors: allosteric transitions and therapeutic targets in the nervous system. *Nat Rev Drug Discov* **8**: 733-50.

Taly A, Delarue M, Grutter T, Nilges M, Le Novere N, Corringer PJ and Changeux JP. (2005). Normal mode analysis suggests a quaternary twist model for the nicotinic receptor gating mechanism. *Biophys J* **88**: 3954-65.

Teissere JA and Czajkowski C. (2001). A (β)-strand in the (gamma)2 subunit lines the benzodiazepine binding site of the GABA A receptor: structural rearrangements detected during channel gating. *J Neurosci* **21**: 4977-86.

Timmermann DB, Gronlien JH, Kohlhaas KL, Nielsen EO, Dam E, Jorgensen TD, Ahring PK, Peters D, Holst D, Chrsitensen JK, Malysz J, Briggs CA, Gopalakrishnan M and Olsen GM. (2007). An allosteric modulator of the α7 nicotinic acetylcholine

receptor possessing cognition-enhancing properties in vivo. *J Pharmacol Exp Ther* **323**: 294-307.

Toyoshima C and Unwin N. (1988). ION CHANNEL OF ACETYLCHOLINE-RECEPTOR RECONSTRUCTED FROM IMAGES OF POSTSYNAPTIC MEMBRANES. *Nature* **336**: 247-250.

Turnbull WB and Daranas AH. (2003). On the value of c: can low affinity systems be studied by isothermal titration calorimetry? *J Am Chem Soc* **125**: 14859-66.

Unwin N. (1993). NICOTINIC ACETYLCHOLINE-RECEPTOR AT 9-ANGSTROM RESOLUTION. *Journal of Molecular Biology* **229**: 1101-1124.

Unwin N. (1995). Acetylcholine receptor channel imaged in the open state. *Nature* **373**: 37-43.

Unwin N. (2005). Refined structure of the nicotinic acetylcholine receptor at 4A resolution. *J Mol Biol* **346**: 967-89.

Venkatachalan SP and Czajkowski C. (2008). A conserved salt bridge critical for GABAA receptor function and loop C dynamics. *Proc Natl Acad Sci U S A* **105**: 13604-9.

Vernino S, Amador M, Luetje CW, Patrick J and Dani JA. (1992). Calcium modulation and high calcium permeability of neuronal nicotinic acetylcholine receptors. *Neuron* **8**: 127-34.

Vernino S, Rogers M, Radcliffe KA and Dani JA. (1994). Quantitative measurement of calcium flux through muscle and neuronal nicotinic acetylcholine receptors. *J Neurosci* **14**: 5514-24.

Wang DW, Zhou RB and Yao YM. (2009a). Role of cholinergic anti-inflammatory pathway in regulating host response and its interventional strategy for inflammatory diseases. *Chin J Traumatol* **12**: 355-64.

Wang H, Yu M, Ochani M, Amella CA, Tanovic M, Susarla S, Li JH, Yang H, Ulloa L, Al-Abed Y, Czura CJ and Tracey KJ. (2003). Nicotinic acetylcholine receptor α7 subunit is an essential regulator of inflammation. *Nature* **421**: 384-8.

Wang HL, Toghraee R, Papke D, Cheng XL, McCammon JA, Ravaioli U and Sine SM. (2009b). Single-channel current through nicotinic receptor produced by closure of binding site C-loop. *Biophys J* **96**: 3582-90.

Wilkins ME, Hosie AM and Smart TG. (2005). Proton modulation of recombinant GABA(A) receptors: influence of GABA concentration and the beta subunit TM2-TM3 domain. *J Physiol* **567**: 365-77.

Williams BM, Temburni MK, Levey MS, Bertrand S, Bertrand D and Jacob MH. (1998). The long internal loop of the α 3 subunit targets nAChRs to subdomains within individual synapses on neurons in vivo. *Nat Neurosci* **1**: 557-62.

Wilson G and Karlin A. (2001). Acetylcholine receptor channel structure in the resting, open, and desensitized states probed with the substituted-cysteine-accessibility method. *Proc Natl Acad Sci U S A* **98**: 1241-8.

Wintersteiner O and Dutcher JD. (1943). Curare Alkaloids from Chondodendron Tomentosum. *Science* **97**: 467-470.

Woolf NJ. (1991). Cholinergic systems in mammalian brain and spinal cord. *Prog Neurobiol* **37**: 475-524.

Wu J, Liu Q, Yu K, Hu J, Kuo YP, Segerberg M, St John PA and Lukas RJ. (2006). Roles of nicotinic acetylcholine receptor beta subunits in function of human alpha4-containing nicotinic receptors. *J Physiol* **576**: 103-18.

Xiu X, Hanek AP, Wang J, Lester HA and Dougherty DA. (2005). A unified view of the role of electrostatic interactions in modulating the gating of Cys loop receptors. *J Biol Chem* **280**: 41655-66.

Xiu X, Puskar NL, Shanata JA, Lester HA and Dougherty DA. (2009). Nicotine binding to brain receptors requires a strong cation-pi interaction. *Nature* **458**: 534-7.

Xu J, Zhu Y and Heinemann SF. (2006). Identification of sequence motifs that target neuronal nicotinic receptors to dendrites and axons. *J Neurosci* **26**: 9780-93.

Yi M, Tjong H and Zhou HX. (2008). Spontaneous conformational change and toxin binding in α7 acetylcholine receptor: insight into channel activation and inhibition. *Proc Natl Acad Sci U S A* **105**: 8280-5.

Young GT, Zwart R, Walker AS, Sher E and Millar NS. (2008). Potentiation of α7 nicotinic acetylcholine receptors via an allosteric transmembrane site. *Proc Natl Acad Sci U S A* **105**: 14686-91.

Zanetti L, Picciotto MR and Zoli M. (2007). Differential effects of nicotinic antagonists perfused into the nucleus accumbens or the ventral tegmental area on cocaine-induced dopamine release in the nucleus accumbens of mice. *Psychopharmacology (Berl)* **190**: 189-99.

Zhong W, Gallivan JP, Zhang Y, Li L, Lester HA and Dougherty DA. (1998). From ab initio quantum mechanics to molecular neurobiology: a cation-pi binding site in the nicotinic receptor. *Proc Natl Acad Sci U S A* **95**: 12088-93.

Zwart R and Vijverberg HP. (1998). Four pharmacologically distinct subtypes of alpha4beta2 nicotinic acetylcholine receptor expressed in Xenopus laevis oocytes. *Mol Pharmacol* **54**: 1124-31.